NASA TN D-1061

TECHNICAL NOTE

D-1061

GODDARD SPACE FLIGHT CENTER CONTRIBUTIONS TO THE 1961 KYOTO CONFERENCE ON COSMIC RAYS AND THE EARTH STORM

NATIONAL AERONAUTICS AND SPACE ADMINISTRATION
WASHINGTON
June 1962

D-1061

TABLE OF CONTENTS

	Page
Preface	i
"Magnetic Field Measurements with the Explorer X Satellite" J. P. Heppner, N. F. Ness, T. L. Skillman and C. S. Scearce	1
"Magnetic Field Fluctuations on the Earth and in Space" N. F. Ness, T. L. Skillman, C. S. Scearce and J. P. Heppner	21
"Whistler Signals Observed with the Vanguard III Satellite" J. C. Cain, I. R. Shapiro, J. D. Stolarik and J. P. Heppner	33
"Rocket Observations of Solar Protons on September 3, 1960" L. R. Davis, C. E. Fichtel, D. E. Guss and K. W. Ogilvie	41
"Rocket Observations of Solar Protons during the November 12, 1960 Event" K. W. Ogilvie, D. A. Bryant and L. R. Davis	47
"Heavy Nuclei in Solar Cosmic Rays" C. E. Fichtel and D. E. Guss	55
"The Flux and Energy Spectra of the Protons in the Inner Van Allen Belt" J. E. Naugle and D. A. Kniffen	63
"A Study of the Rigidity and Charge Dependence of Primary Cosmic Ray Temporal Variation" F. B. McDonald and W. R. Webber	73
"Present State of Knowledge of the Composition of the Primary Cosmic Radiation" C. J. Waddington	89

1R

D-1061

GODDARD SPACE FLIGHT CENTER CONTRIBUTIONS TO THE 1961 KYOTO CONFERENCE ON COSMIC RAYS AND THE EARTH STORM

PREFACE

The International Conference on Cosmic Rays and the Earth Storm was held at Kyoto, Japan, on September 4-15, 1961. This volume is a compilation of papers presented at this Conference by members of the Fields and Particles group of NASA's Goddard Space Flight Center.

Frank B. McDonald
Head, Fields and Particles Group
NASA Goddard Space Flight Center
Greenbelt, Maryland

D-1061

MAGNETIC FIELD MEASUREMENTS WITH THE EXPLORER X SATELLITE

by

J. P. Heppner, N. F. Ness*, T. L. Skillman, and C. S. Scearce

INTRODUCTION

The description to follow summarizes the results of a preliminary analysis of Explorer X magnetic field data. A more comprehensive and interpretative paper will be prepared in the near future for journal publication.

Explorer X (1961 κ), launched at 15:17 GMT, March 25, 1961, was instrumented with a rubidium vapor magnetometer and two flux-gate saturable-core magnetometers for field measurements, a plasma probe for measurement of the flux of low energy protons, and an optical aspect system for precise determination of the satellite's orientation relative to the sun.

Figure 1 illustrates the trajectory and satellite orientation in inertial coordinates. The satellite was intended to have an active battery life of about 55 hours, which would provide operation approximately to apogee. In practice, 53 hours of reliable operation were obtained, and this was followed by several hours of uncalibrated operation (not presented here) in which only certain types of data could be obtained as battery power diminished.

Observatory magnetograms show that the magnetic field in low and middle latitudes was typically quiet for at least a week preceding the flight. In the auroral zone magnetic activity was confined to bays of weak-to-moderate intensity. These conditions prevailed until 15:03 GMT, March 27, at which time a sudden commencement occurred. Solar activity prior to the flight was comparatively low and confined largely to Class 1 and 1- flares. This condition prevailed until 10:15 GMT, March 26, at which time a Class 3 flare occurred near the east limb of the sun. The sudden commencement is believed to be associated with this flare. Consequently, the environment of the satellite prior to 15:03 GMT, March 27, is thought to be typical of undisturbed conditions.

*National Academy of Science – NASA Post Doctoral Resident Research Associate.

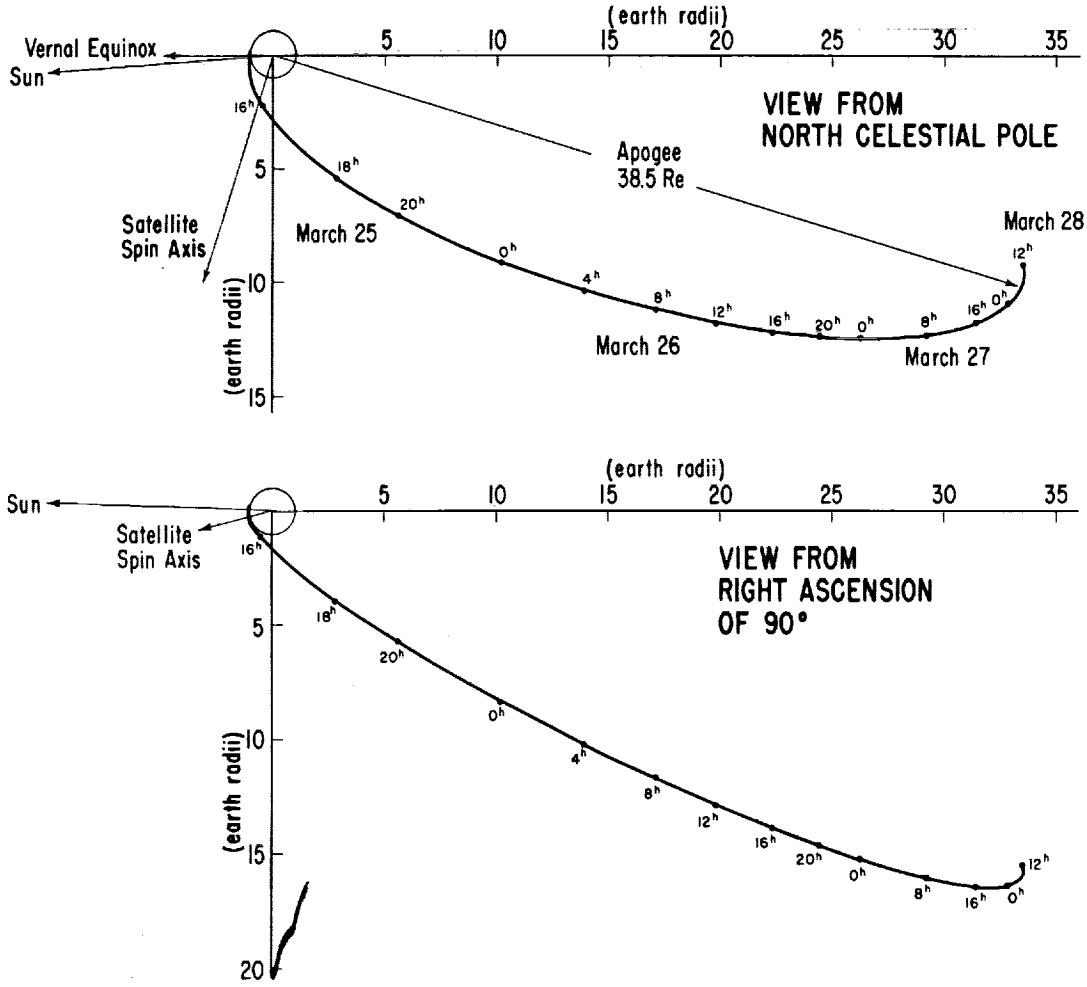

Figure 1 - Trajectory and orientation of Explorer X

MEASUREMENTS BETWEEN 1.8 AND 6.6 EARTH RADII

Figure 2 shows the difference between the total scalar field measured by the Rb-vapor magnetometer and the total scalar field given by the Finch and Leaton (Reference 1) representation of the geomagnetic field over the geocentric distance range of 11,100 to 42,000 km. (Note: a negative sign means the measured field is less intense than the computed reference field.) Field measurements are shown at 1-minute intervals. If the scale were enlarged to permit plotting in terms of seconds, the deviations from a smooth curve would be only slightly increased. These fluctuations of several gammas are a minor feature compared to the large differences between the measured and computed fields.

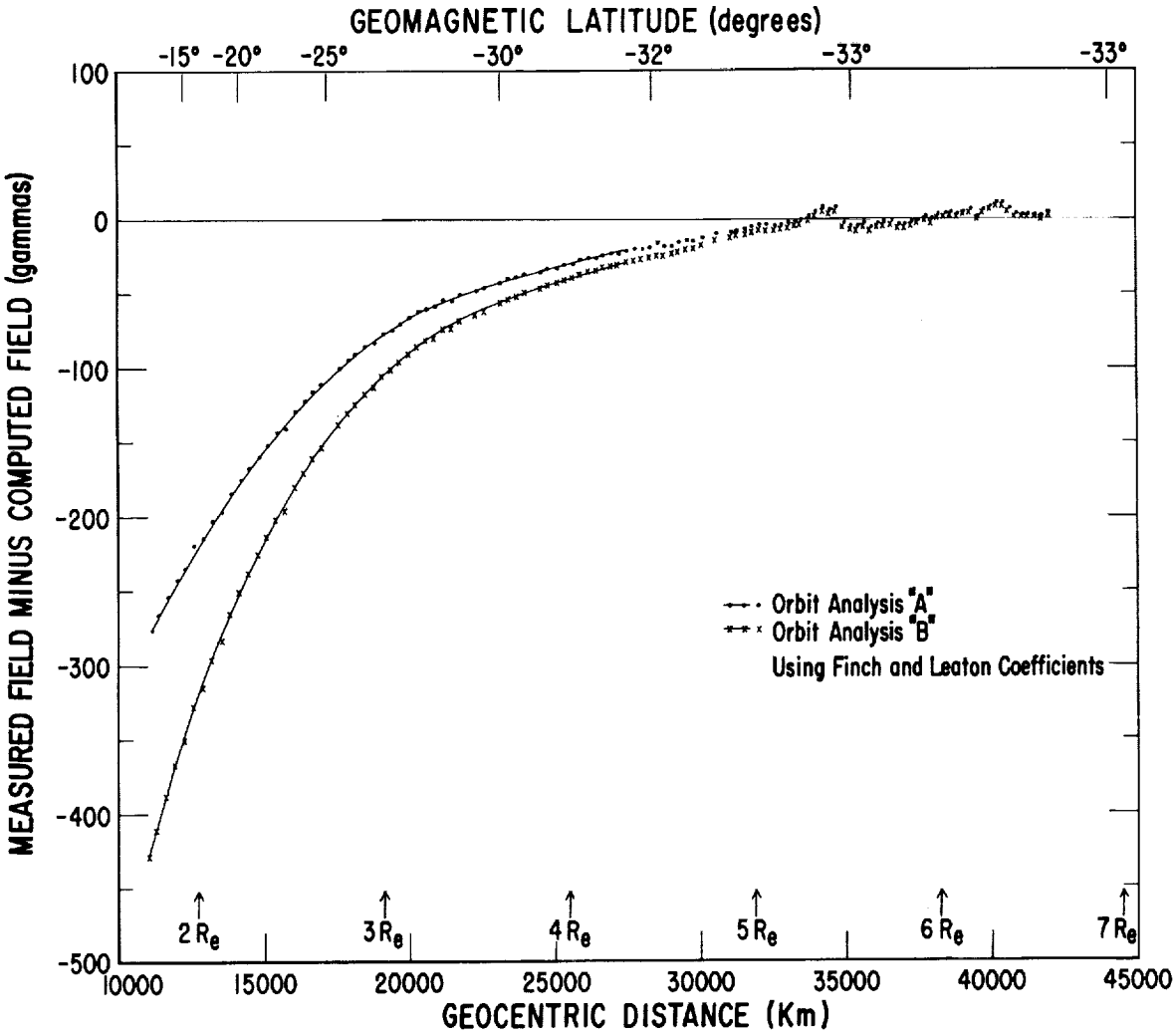

Figure 2 - The difference between the measured (Rb-vapor magnetometer) and the theoretical (Finch and Leaton) total scalar fields from 11,100 to 42,000 km

In interpreting measurements relative to a reference field, two sources of error have to be evaluated: (1) errors in the trajectory, or orbit, which cause the reference field to be calculated for a space location that is not identical with the satellite's location, and (2) the difference between the computed reference field and the true geomagnetic field which is unknown unless other absolute data is available. With regard to (1), a number of orbit determinations have been made in which different weights have been given to the various types of tracking data (Minitrack, Doppler, antenna pointing, etc.). The curve on Figure 2 labeled "orbit analysis B" uses the orbit giving the best fit to the tracking data. The curve labeled "orbit analysis A" uses the orbit that gives the smallest difference between the measured and computed fields. Thus, from orbit analyses it

appears improbable that the large field difference can be attributed to errors in the orbit. Next, the accuracy of the Finch and Leaton (m = 6, n = 6) reference field in representing the true geomagnetic main field near 2 earth radii (R_e) needs to be considered. The first measurement at 11,100 km was taken east of Ascension Island in the South Atlantic. As time progressed, the satellite moved toward and then over South Africa. The closest region where the accuracy of the Finch and Leaton field is independently known from Vanguard III measurements (References 2 and 3) is over South Africa at geocentric distances up to 10,000 km. If it is assumed that the Finch and Leaton field has a comparable accuracy in the region toward Ascension Island from South Africa, up to 50 gammas of the difference curves (Figure 2) below 2 R_e can be attributed to lack of accuracy in the computed field. The assumption receives some support from the fact that this represents an error of about 1 percent in the Finch and Leaton field which is typical of other areas of the earth as well. [Note: a reference field based on Jensen and Whitaker coefficients is not used here as it gives greater differences from the measured field and is also known to be more incorrect over this region of the earth (References 2 and 3). Above 3 R_e the difference between reference fields is negligible.] To attribute the difference curves of Figure 2 to errors in the computed field, the computed field near 2 R_e would have to be in error by 5 percent (Curve A) to 8 percent (Curve B). Thus it appears that only a small fraction of the difference in fields can be attributed to errors in the computed field.

These arguments lead to the conclusion that a field source located in the "slot" between the inner and outer radiation belts near the equator is necessary to explain the measurements. The extent of the field source proceeding outward to the field shell coincident with the maximum of the outer radiation belt cannot be uniquely defined solely from measurements along this trajectory.

The possibility that the reference field is grossly in error between Brazil and South Africa is being investigated by use of Project Magnet data. If this is found to be the case, a smaller field source having its maximum strength at a somewhat greater altitude between 1.8 and 3 R_e would still be required to explain the measurements. The fact that the percent difference increases to a maximum of 6 percent (Curve A) and 9 percent (Curve B) at 2.4 R_e and then decreases may also indicate that the source center is slightly above 1.8 R_e.

From 5 to 6.6 R_e (Figure 2) there is excellent agreement between the measured and computed fields. The region from 3 to 5 R_e is transitional between the two conditions.

At 6.6 R_e the Rb-vapor magnetometer became excessively hot as a result of contamination of the satellite's thermal surfaces during the launch phase. From 6.6 to 18 R_e it operated intermittently on a fast duty cycle; these data have been used to calibrate the flux-gate magnetometers in flight.

COORDINATE SYSTEM

The facts that the satellite was spin stabilized and the sun's position during each spin cycle was precisely given by the optical system made it convenient to define a coordinate system in terms of a plane containing the spin axis and the satellite-sun line as shown in Figure 3. The same coordinate system is convenient to use in interplanetary regions when the field is primarily radial from the sun with a "stream" or "garden hose" angle due to the sun's rotation (as depicted in various solar wind and magnetic bottle pictures of the solar field). As will be shown later, these angle conditions are frequently present; hence angle data are presented in this coordinate system in preference to ecliptic coordinates. In Figure 3 the spin axis points below the celestial equator at a declination of 15 degrees. When the angle ψ is 180 degrees and α is 112 degrees, the field

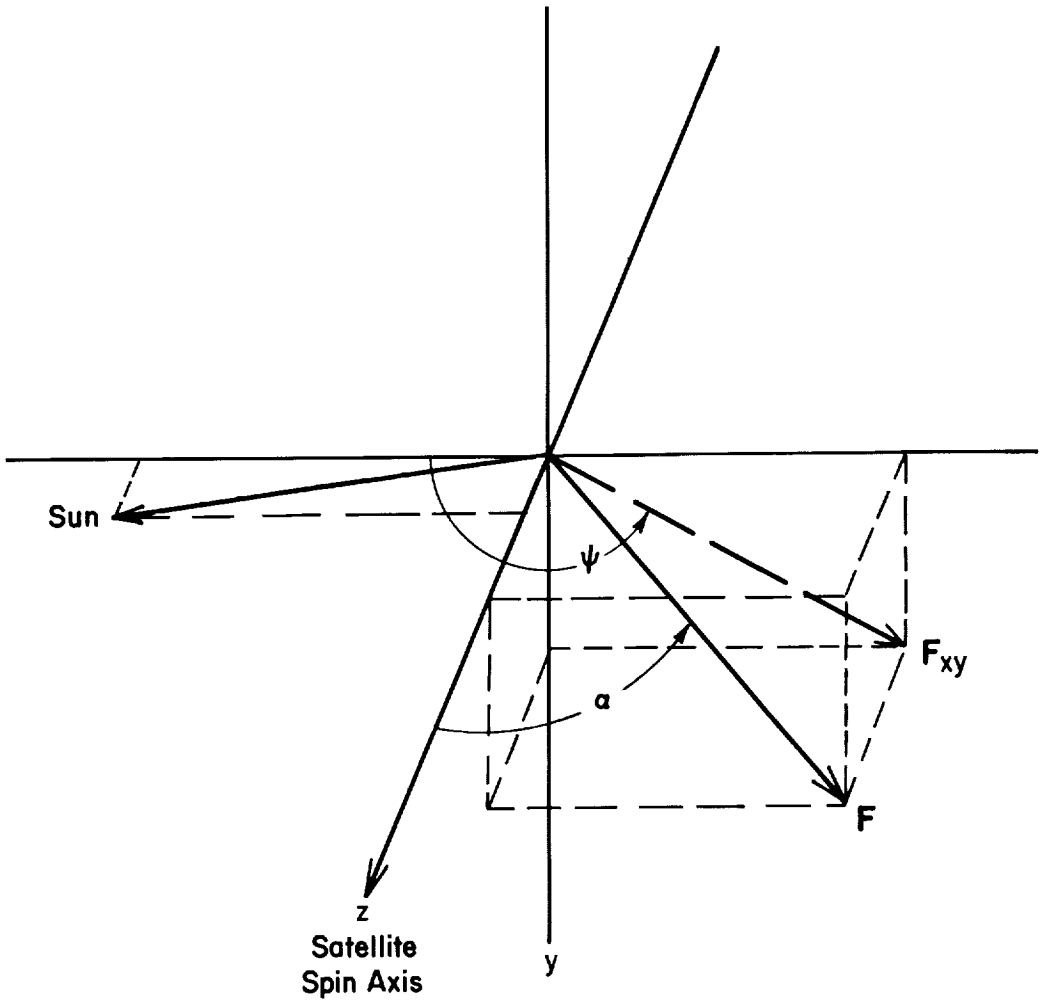

Figure 3 - Magnetic field angles in a coordinate system defined by the plane of the sun and the satellite spin axis

vector is directed away from the sun along the satellite-sun line. For ψ = 180 degrees and α < 112 degrees the "stream" angle is given by (112 - α) degrees. (Note: the term "stream" angle is used here in the same context as the angle $\theta = \tan^{-1}(\omega r/v)$ for a particle stream ejected radially from the sun with velocity v where ω is the sun's angular velocity and r is the distance from the sun.)

MEASUREMENTS BETWEEN 6.6 AND 11 R_e

As can be seen in Figure 4, the agreement between the measured and computed field intensities observed between 5 and 6.6 R_e continues out to 8 R_e, but an angular deviation

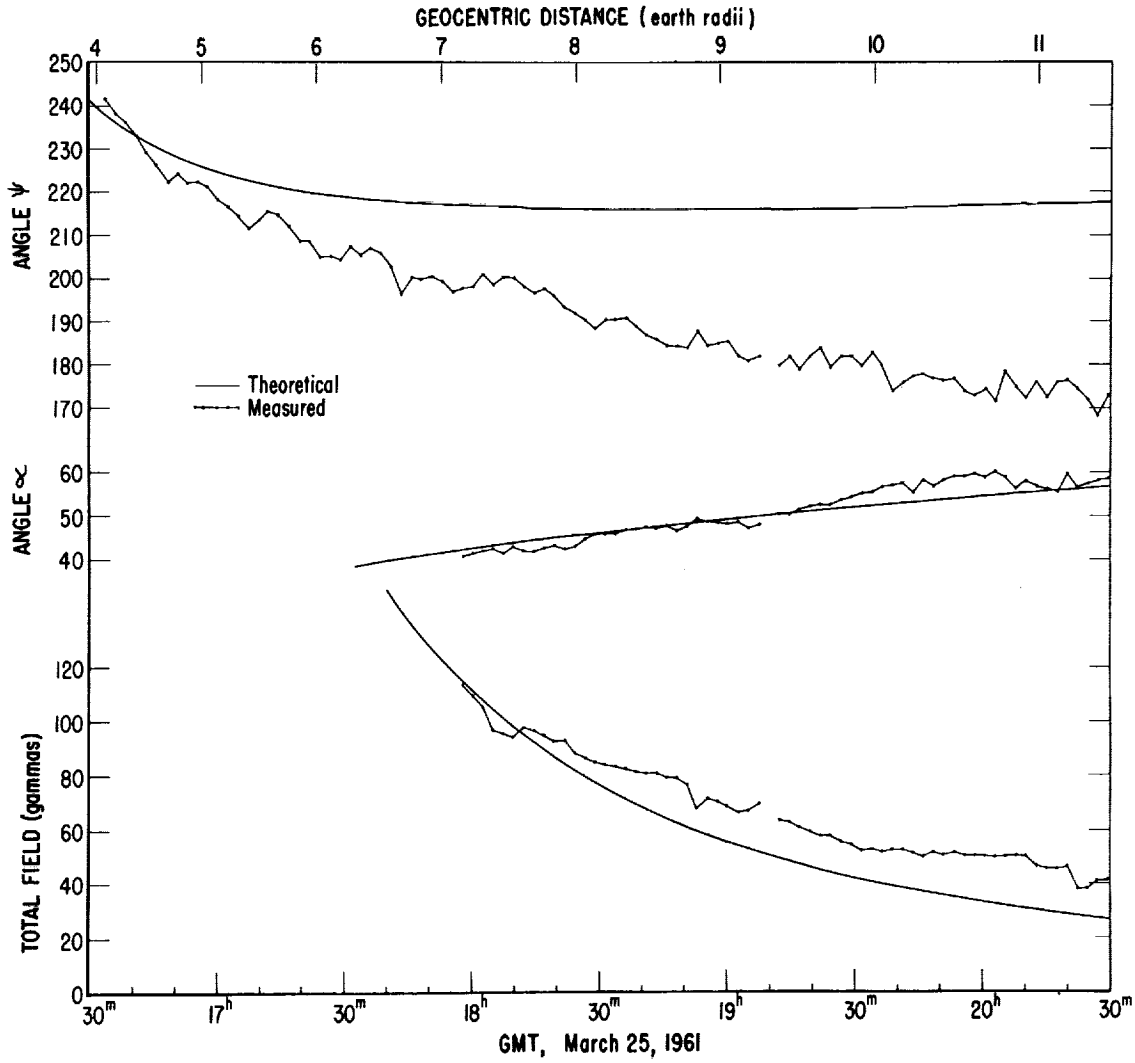

Figure 4 - Explorer X flight data

between the measured and computed fields is evident as low as 6 R_e. At 11 R_e the angle ψ becomes relatively stable between 170 and 180 degrees. The difference between the measured field and the Finch and Leaton "theoretical" field near 11 R_e is approximately equal to the field intensity that is observed at much greater distances. Thus, the measured field has the character of a superposition of the earth's field and the solar-interplanetary field. Whether this is truly a superposition or instead is the result of the earth's field being draped or bent back from the sunward side to the night side of the earth by the solar wind cannot be uniquely determined from the measurements. Another alternative is that the net field is the sum of the earth's field and a field from an equatorial ring current located near or beyond 10 R_e; but with this explanation, difficulty is encountered in explaining the measurements between 5 and 8 R_e.

MEASUREMENTS BETWEEN 11 AND 20 R_e

Between 11 and 19 R_e the field continues to have the appearance of a superposition of the earth's field and the solar-interplanetary field. The influence of the earth's field appears to become negligible at 19 R_e. Between 20 and 21.5 R_e (Figure 5) the field is stable and approximately radial from the sun with a "stream" angle of 30 to 40 degrees.

MEASUREMENTS BETWEEN 20 AND 27 R_e

At 05:30, March 26, the field changed character abruptly between flux-gate readings separated by 139 seconds. For the next 5 hours the field fluctuated greatly both in magnitude and direction. Multiple points occurring at the same time on Figure 6 represent the degree of variation within one 3-second interval of continuous measurement from one of the two flux gates (see Reference 4 for a detailed example of a rapid fluctuation). The sharp break at 05:30 is coincident with the first detection of solar plasma by the MIT plasma probe (Reference 5). The field was directed into the eastern hemisphere of the celestial sphere with predominantly a south declination during the period of fluctuation. It returned to a stable condition at 10:25 for a period of 1.5 hours.

MEASUREMENTS BETWEEN 27 AND 31 R_e

As the payload proceeded from 27 to 31 R_e, the field direction changed character at intervals of 1.5 to 2 hours as shown in Figure 7. On alternate steps the field returned to the nearly radial condition with a "stream" angle of 35 to 55 degrees. During the periods of $\psi > 180$ degrees, the field was directed between 90 and 180 degrees right ascension with predominantly a north declination. The field magnitude varied irregularly and did not show a pronounced change in character when the angles changed.

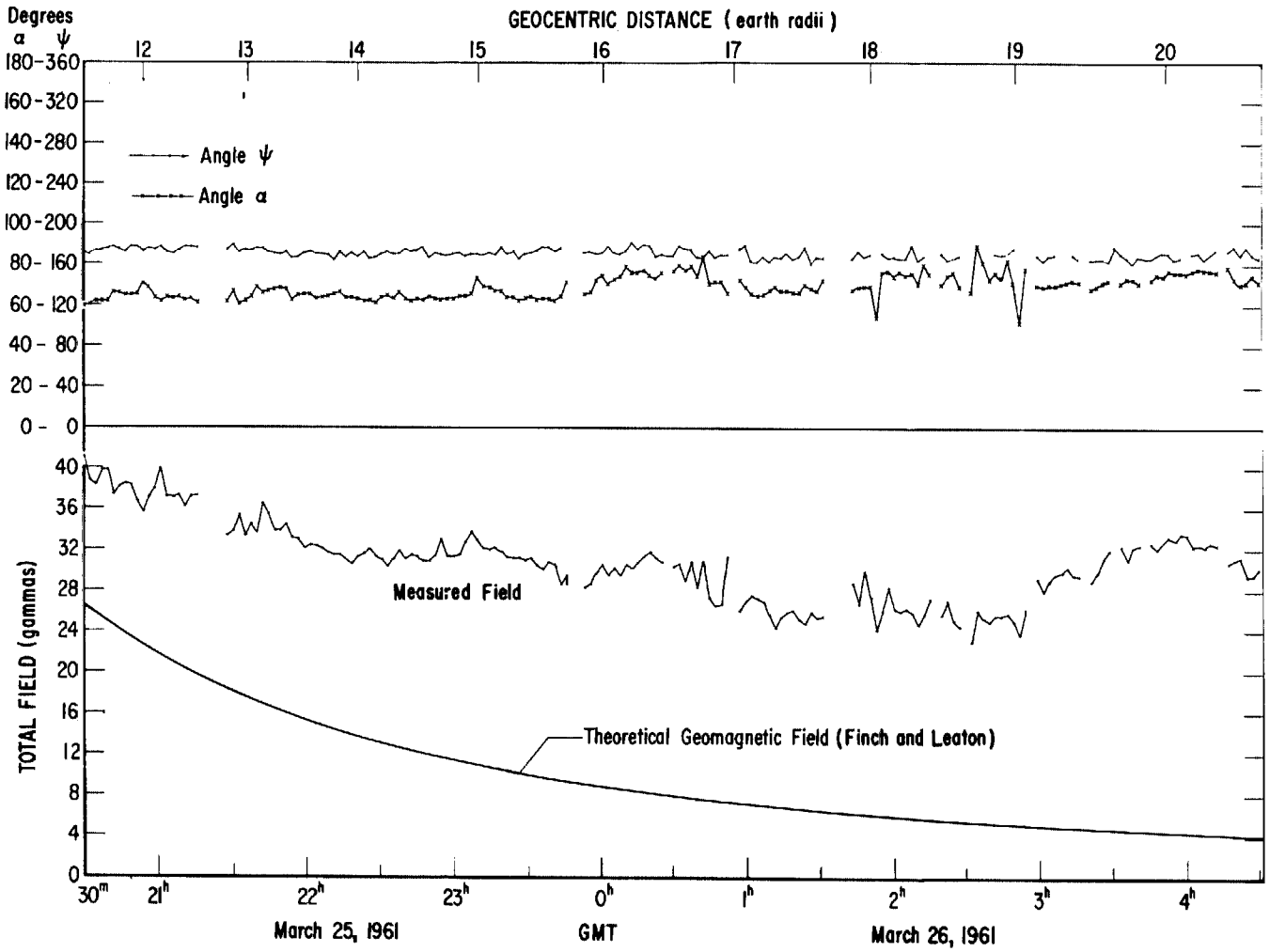

Figure 5 - Explorer X flight data

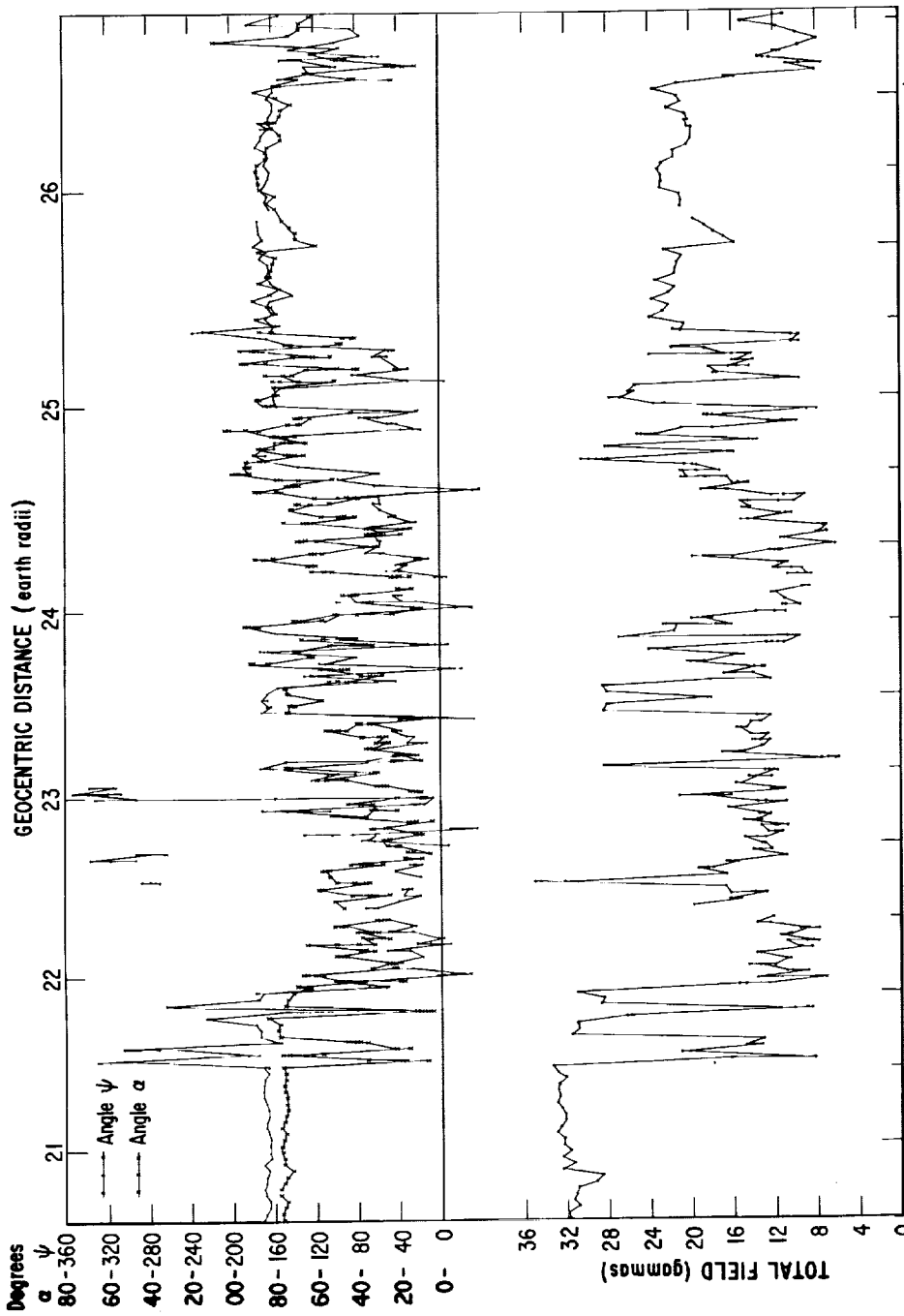

Figure 6 – Explorer X flight data

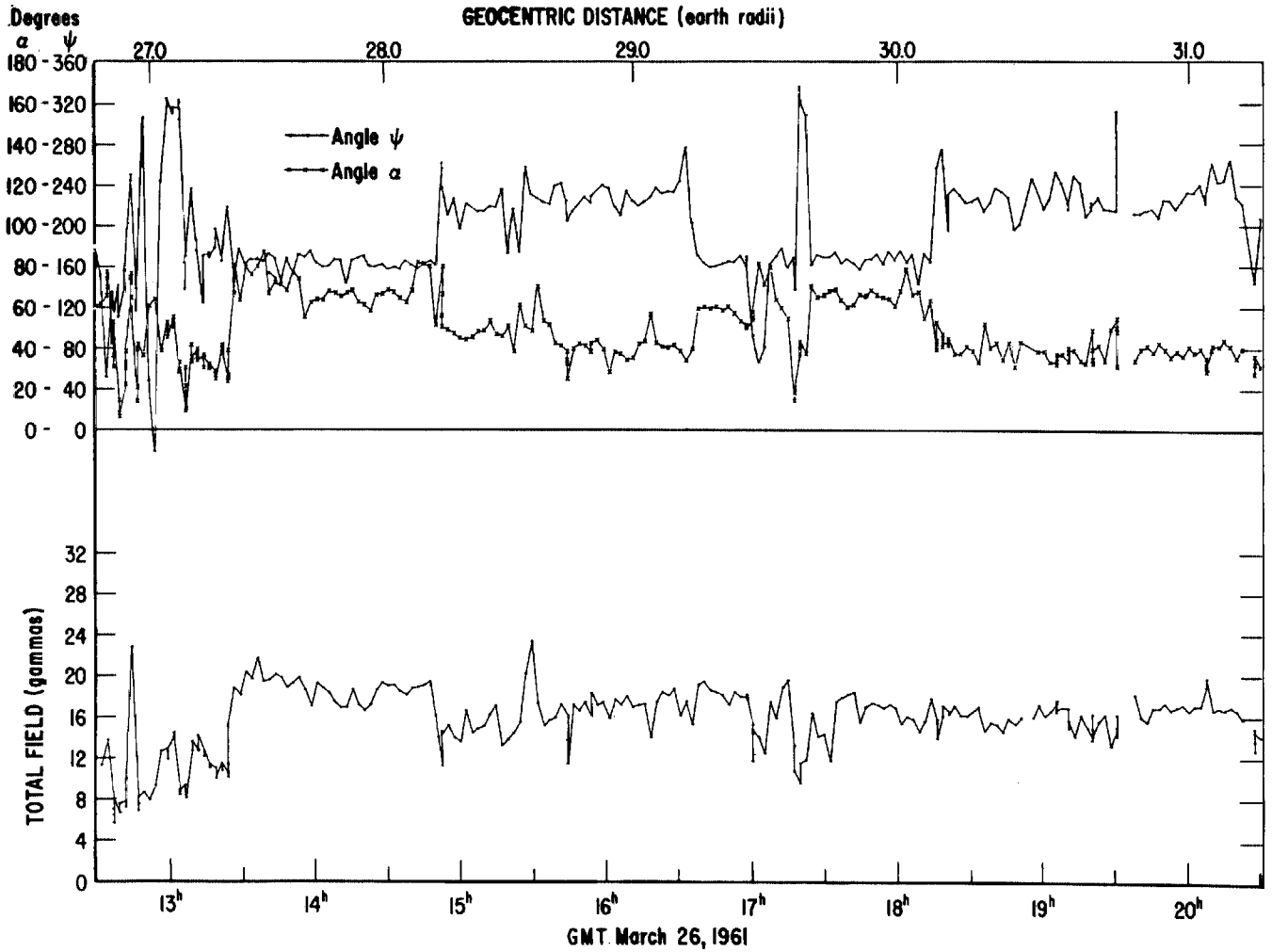

Figure 7 - Explorer X flight data

MEASUREMENTS BETWEEN 31 AND 34.5 R_e

Throughout the 8 hours shown on Figure 8 the field intensity fluctuated irregularly about mean values of 12 to 16 gammas. During the first 4 hours the field direction rotated slowly and irregularly about the spin axis of the satellite and was directed predominantly eastward in celestial coordinates.

MEASUREMENTS BETWEEN 34.5 AND 36.5 R_e

The field during the 8 hours shown in Figure 9 changed character at intervals of 1 to 2 hours in a manner somewhat similar to that seen in Figures 6 and 7. The intervals when the field intensity was high coincide with a field direction which was nearly radial from the sun with a "stream" angle of 25 to 55 degrees. The high intensity intervals also coincided with times when plasma was not detected by the plasma probe (Reference 5 and the final section here). In general, short period fluctuations of the field were also reduced in amplitude when the field intensity increased.

MEASUREMENTS BETWEEN 37 AND 38 R_e

After 13:00 and prior to the sudden commencement at 15:03 GMT, March 27, the field vector pointed primarily toward a region east and south of the sun (Figure 10). The rotation of the vector at about 14:40 does not have a recognizable association with the SC. However, on the basis of information on the plasma spectra (Reference 4) together with the increased field intensity after 15:03, it is believed that the increased field intensity at the satellite is associated with the SC. The field at the satellite increases gradually from 15:03 until 15:10 and then makes a greater change in both intensity and the angle α between 15:10 and 15:12. Thus, depending on which time is chosen for the SC at the satellite it occurred 0 to 7 minutes later at the satellite than on earth, with the largest change taking place 7 to 9 minutes after the SC at the earth's surface. Large angle changes in the field did not accompany the SC. However, after the SC, the field became more nearly directed toward the sun, particularly from 15:30 to 15:50 and 17:00 to 19:00.

The appearance of the SC at the earth's surface is illustrated by several magnetogram tracings in Figure 11. At low latitudes the SC was very distinct but the magnetic storm which followed was weak. This weakness of the main phase may be related to the fact that the storm producing flare was an east limb event. At College, Alaska, the SC produced an abrupt change of about 300 gammas in the horizontal component, accompanied instantaneously by very strong absorption on riometer records. According to H. Leinbach (personal communication) this feature appears identical to similar events in which balloon experiments have shown intense bremsstrahlung presumably from impacts of 50-kev electrons at greater altitudes (see Reference 5). The fact that the SC is not

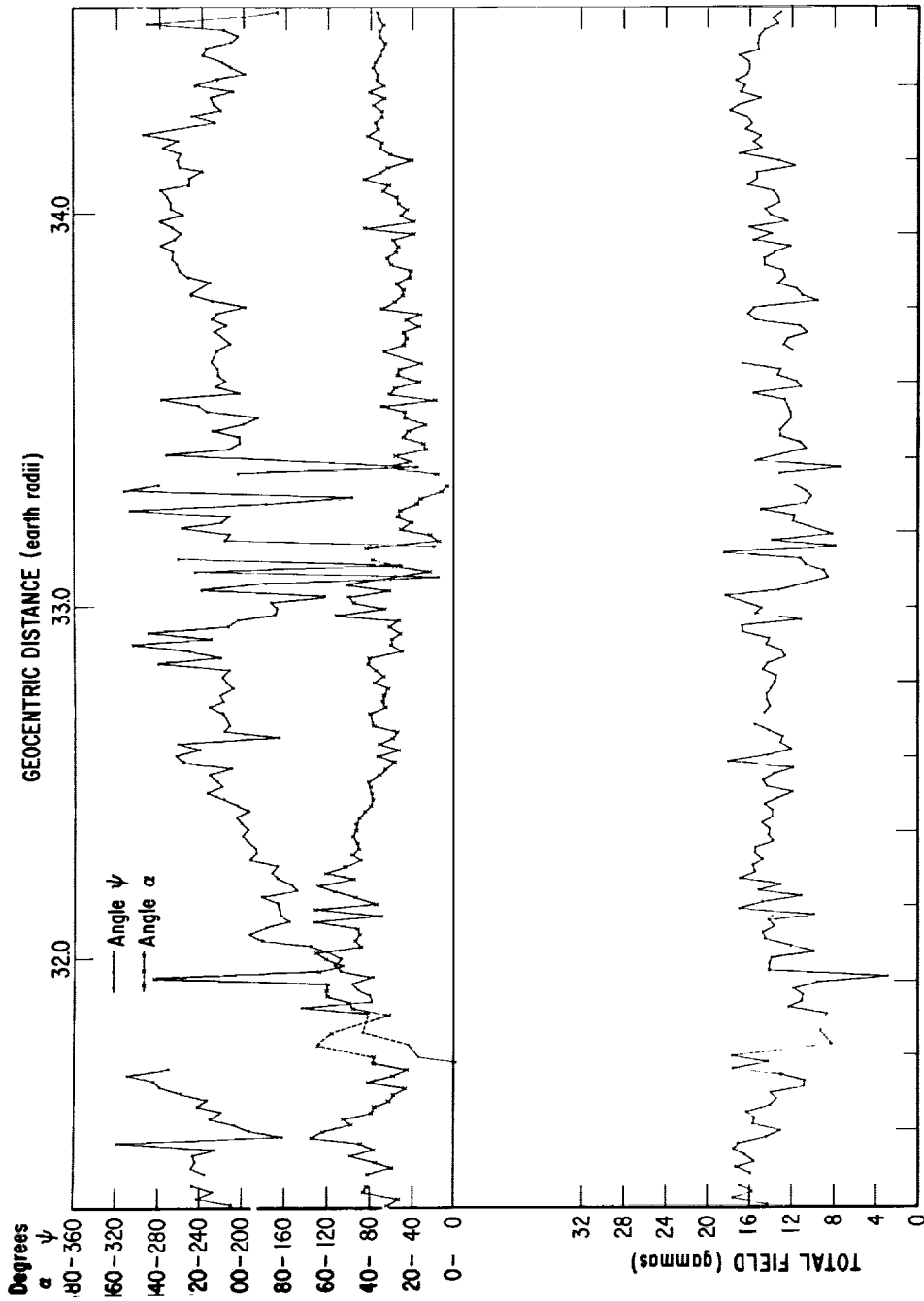

Figure 8 - Explorer X flight data

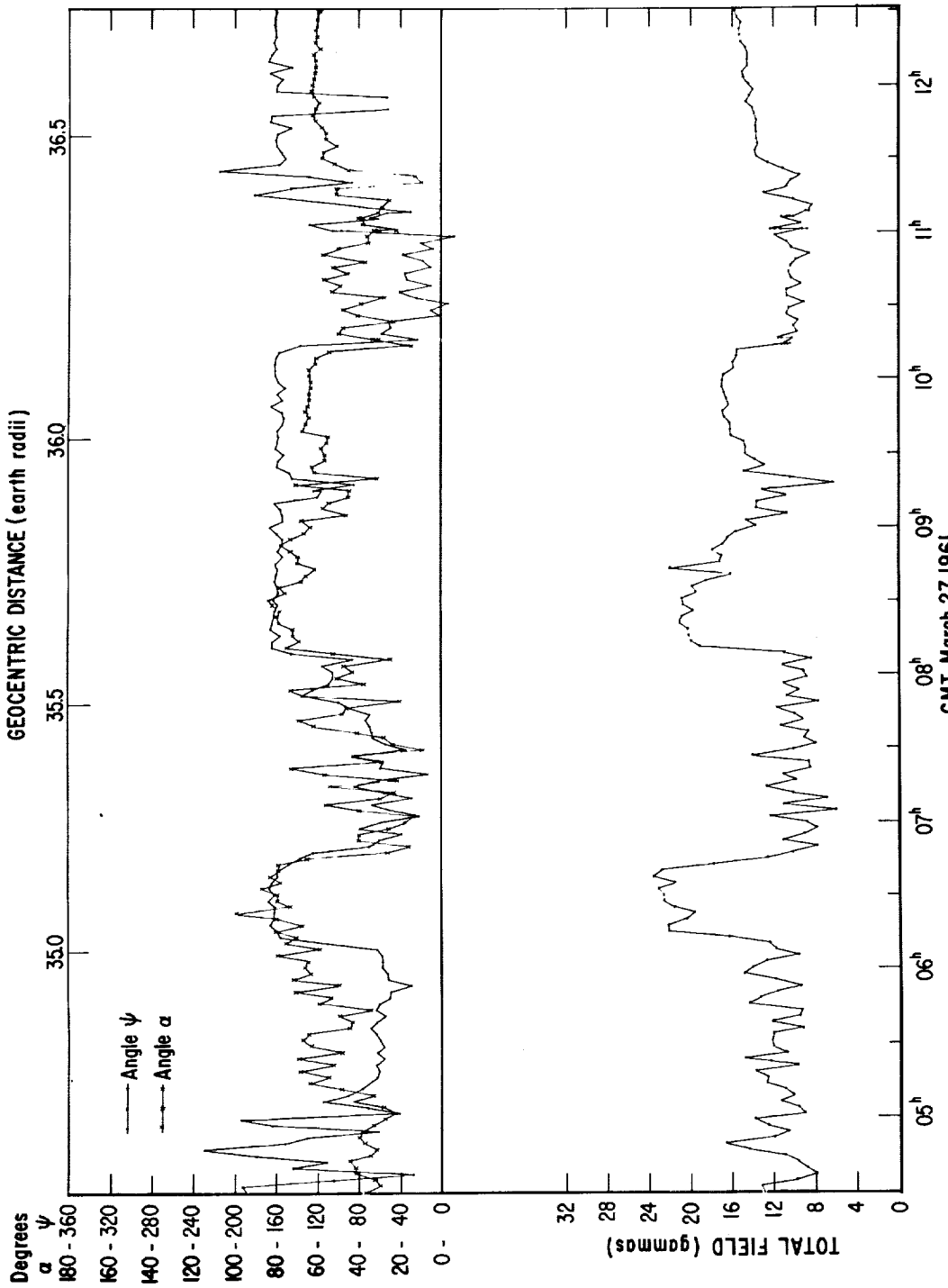

Figure 9 - Explorer X flight data

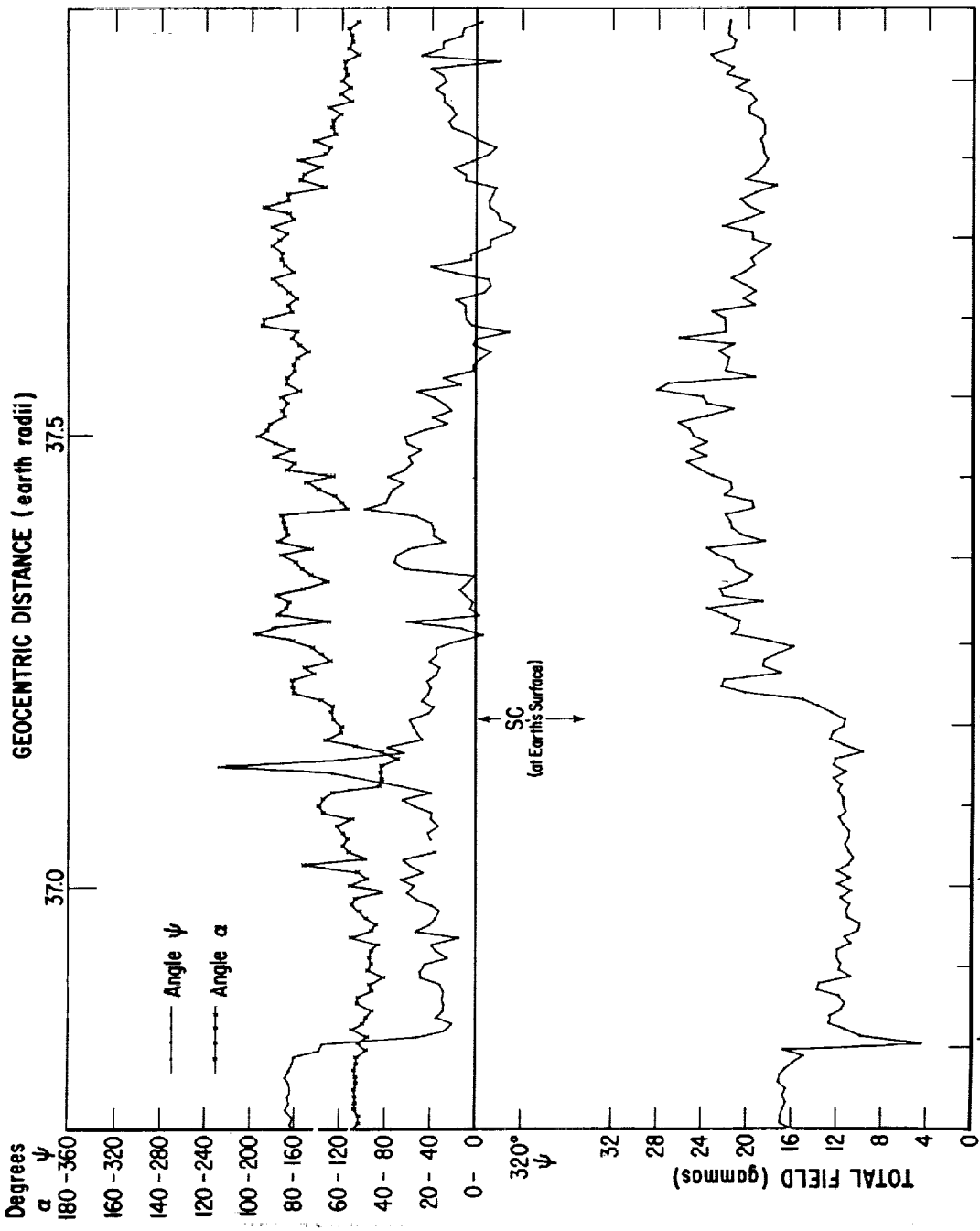

Figure 10 – Explorer X flight data

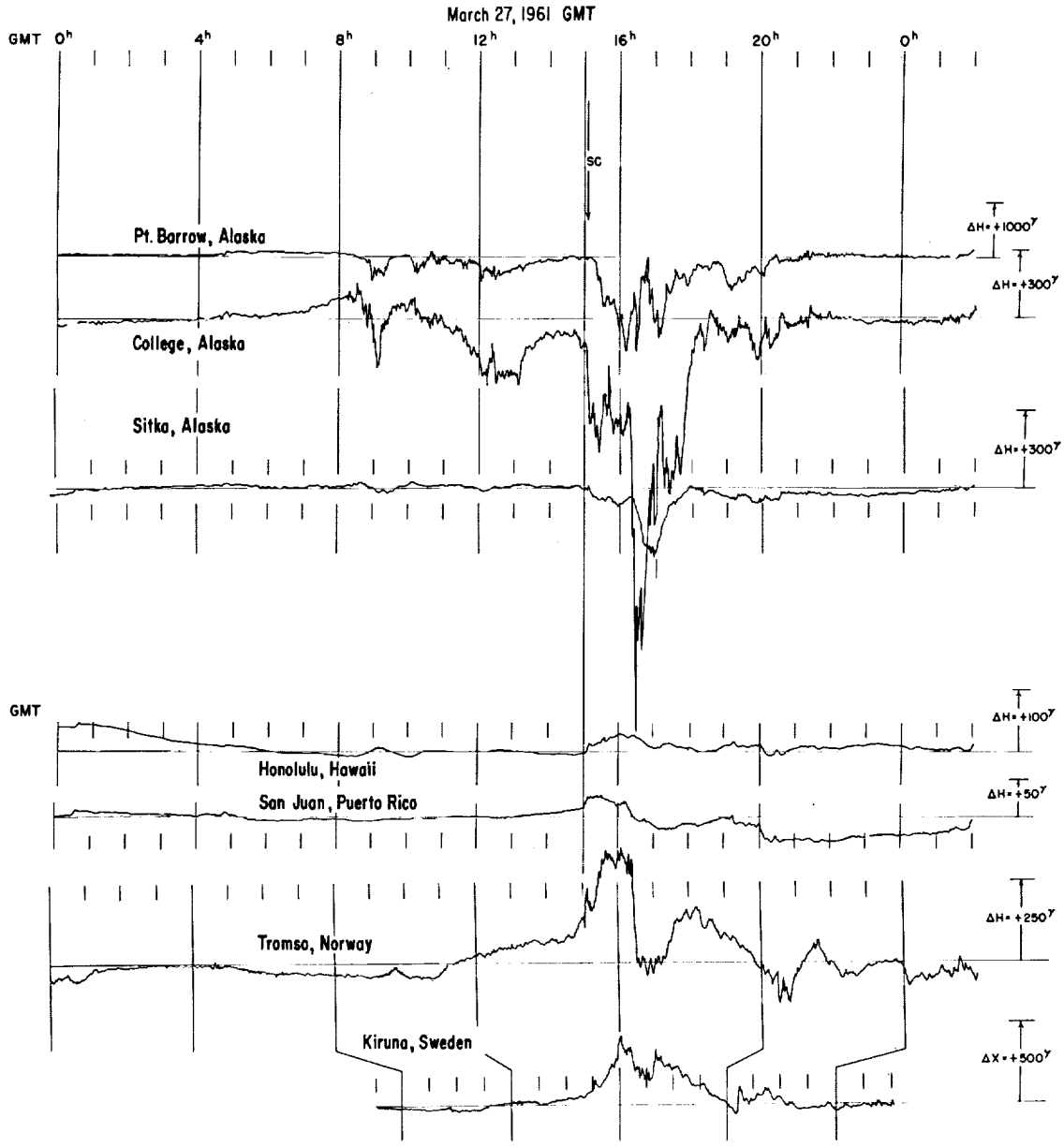

Figure 11 - Ground Station Magnetograms

apparent at Point Barrow, Alaska, at 15:03 and that only a small impulse occurred at Sitka indicates that the immediate effect was highly localized in the auroral zone. The satellite data indicate that (1) there is little if any delay associated with the SC reaching the earth's surface from outside the earth's field, and (2) other more pronounced field changes observed in space do not show visible effects on observatory magnetograms at low and middle latitudes. These features give support to the following ideas: First,

bremsstrahlung associated with SC's are created by particles entering directly from outside the earth's field rather than by dumping of electrons from the outer radiation belt. Second, SC's may represent the response of the ionosphere to sudden impacts in the auroral zone rather than a uniform compression of the earth's field by a solar stream.

CORRELATIONS WITH SOLAR AND MAGNETIC ACTIVITY

In addition to the SC event, correlations of abrupt changes in the character of the solar-interplanetary field and plasma with other solar-terrestrial events can reasonably be anticipated. For this purpose R. T. Hansen of the High Altitude Observatory, Boulder, Colorado, has compiled a solar history for the dates of interest. The most notable feature of this information is that minor flares (Class 1 and 1-) were observed at time intervals similar to the time intervals between major changes in the field at the satellite. However, attempts to make precise time correlation between particular flares and particular changes in the field character, assuming various time delays, have not yielded a positive result. Since a different velocity and path is probably associated with each source, this is not unexpected. For this type of correlation a long observation period and an extremely quiet solar period are probably required.

From examination of standard observatory magnetograms it is apparent that at times other than the SC time the field changes in space were not accompanied by simultaneous field changes at the earth's surface in low and middle latitudes. This lack of correlation may not, however, apply to high latitude stations. From the magnetograms that have been available for examination there is some possibility that correlations with bay activity in the auroral zone may exist. As an example (Figure 11), prior to the time of the SC the usual bay activity was present in the auroral zone. The changes at College, Alaska, near 09:00 and 13:00 might be related to the changes in space shown in Figures 9 and 10 at the same times. However, there are other changes which do not correlate and the coincidences can reasonably be attributed to chance until magnetograms distributed in longitude in the auroral zone are available for study.

EXPLORER X FIELD AND PLASMA CORRELATIONS

The correlations between the plasma measurements (Reference 6), and the magnetic field measurements (Reference 3) with Explorer X have been noted in each presentation. To illustrate these more effectively, several examples are shown in Figures 12, 13, and 14.

The curves of Figures 12 and 13 are typical of the behavior prior to the SC. The presence of plasma coincides with periods when the field intensity is relatively weak and the field direction is variable. This correlation exists even in fine detail. For example:

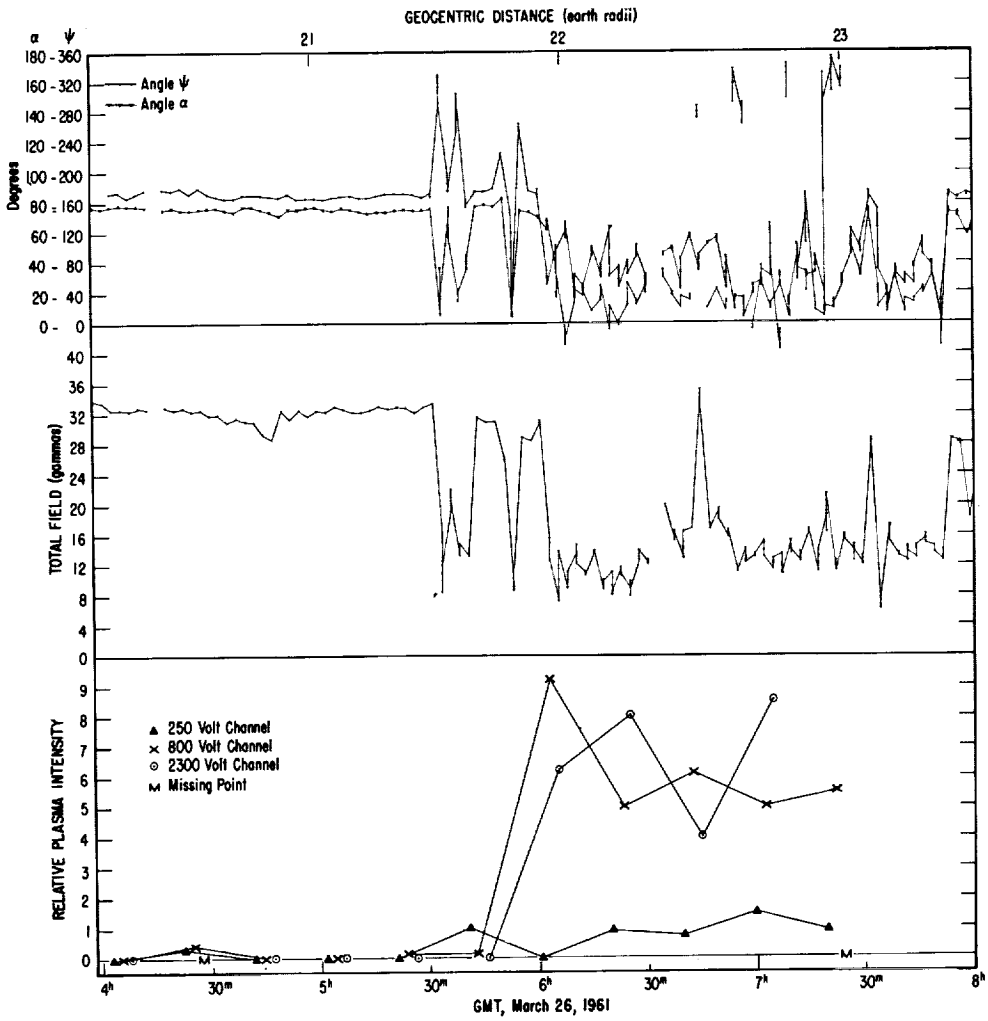

Figure 12 - Explorer X magnetic and plasma intensities

(1) near 05:40 (Figure 12) plasma was observed on the 250 volt channel when the field intensity dropped, but on the next reading the plasma was not observed and the field intensity was again high; (2) at 11:00 (Figure 13) plasma appeared during an otherwise stable field period at a time when the field fluctuated.

After the SC (Figure 14) both the plasma and the field intensities were high. The field direction was, however, quite different from the previous periods when the field intensity was high. Thus, whether or not the same correlation exists before and after the SC depends on whether the field direction or the field magnitude is most important in the correlation. The probable answer is that the absence of plasma correlates with the condition when the field has both high intensity and directional stability.

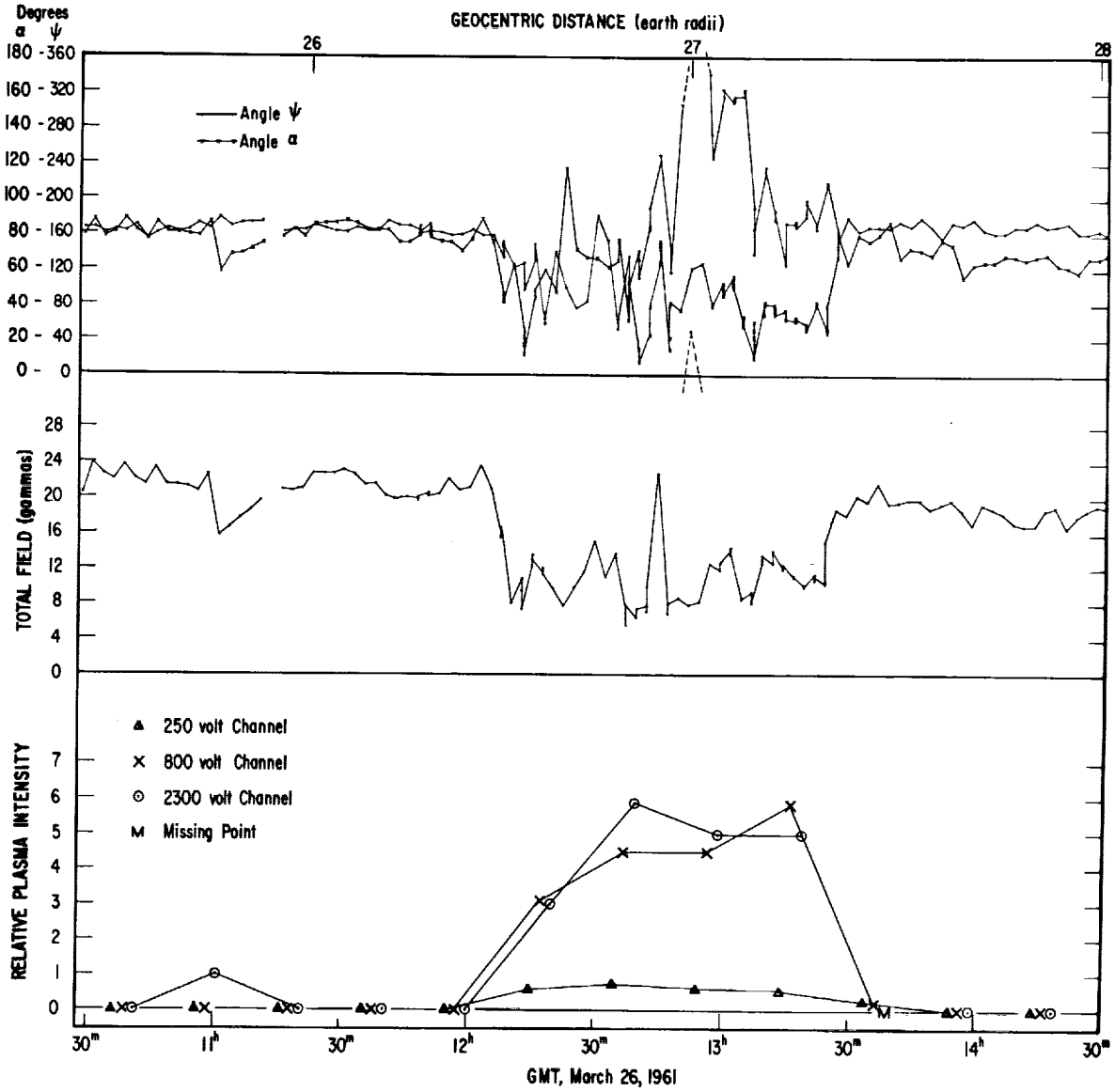

Figure 13 - Explorer X magnetic and plasma intensities

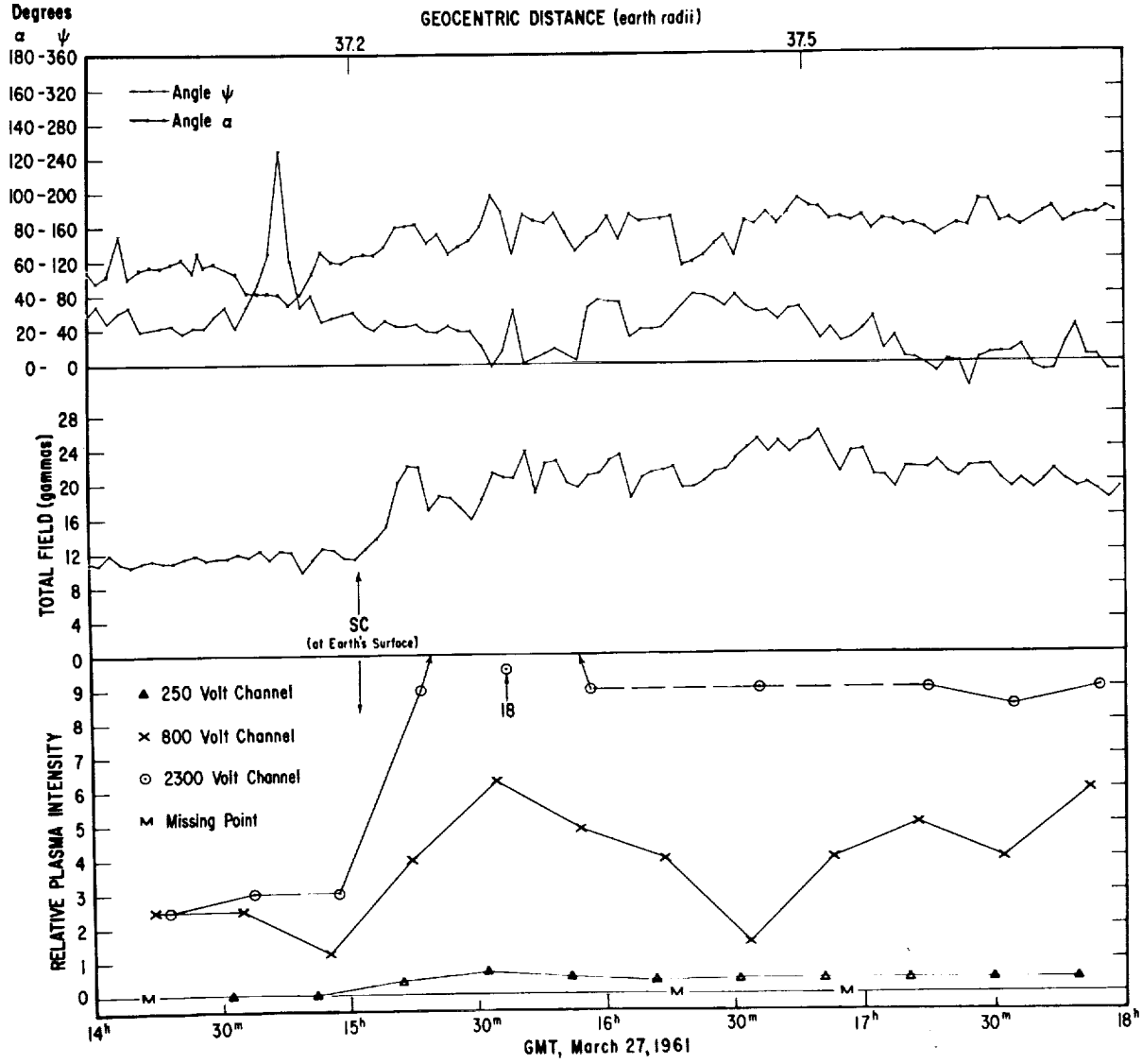

Figure 14 - Explorer X magnetic and plasma intensities

REFERENCES

1. Finch, H. F., and Leaton, B. R., "The Earth's Main Magnetic Field – Epoch 1955·0," Monthly Notices Roy. Astronom. Soc. Geophys. Suppl. 7(6):314-317, November 1957

2. Heppner, J. P., Stolarik, J. D., et al., "Project Vanguard Magnetic Field Instrumentation and Measurements," in: Space Res., Proc. 1st Int. Space Sci. Sym., Nice, January 1960, ed. by H. K. Bijl; Amsterdam: North-Holland Publ. Co., 1960, pp. 982-999; also NASA Technical Note D-486

3. Heppner, J. P., Cain, J. C., et al., "Satellite Magnetic Field Mapping," NASA Technical Note D-696, May 1961

4. Ness, N. F., Skillman, T. L., et al., "Magnetic Field Fluctuations on the Earth and in Space." This publication; also Proceedings of the International Conference on Cosmic Rays and the Earth Storm, Kyoto, Japan, September 1961, Suppl. J. Phys. Soc. Japan 17, 1962 (To be published)

5. Bridge, H. S., Dilworth, C., et al., "Direct Observations of the Interplanetary Plasma," in: Proceedings of the International Conference on Cosmic Rays and the Earth Storm, Kyoto, Japan, September 1961, Suppl. J. Phys. Soc. Japan 17, 1962 (To be published)

6. Brown, R. R., Hartz, T. R., et al., "Large-Scale Electron Bombardment of the Atmosphere at the Sudden Commencement of a Geomagnetic Storm," J. Geophys. Res. 66 (4):1035-1041, April 1961

D-1061

MAGNETIC FIELD FLUCTUATIONS ON THE EARTH AND IN SPACE

by

N. F. Ness*, T. L. Skillman, C. S. Scearce, and J. P. Heppner

Rubidium vapor magnetometers have recently been developed as practical instruments for the measurement of magnetic fields (References 1 and 2). These instruments are essentially atomic oscillators with a frequency directly proportional to the intensity of the magnetic field. Operating continuously and using intrinsic atomic properties, they permit rapid sampling of magnetic fields over a wide dynamic range with extremely high precision and accuracy. In addition, the information obtained with such a system is very amenable to electronic digital computer processing because of the unique manner in which the data are presented in the frequency domain. The first part of this paper treats terrestrial measurements of magnetic field fluctuations covering the period from March 24 to March 29, 1961 (at the Fredricksburg Magnetic Observatory) and the computed energy spectra of micropulsations. The remainder of the paper is devoted to a brief discussion of magnetic field fluctuations measured on the space probe Explorer X launched March 25, 1961, and correlations with the terrestrial measurements.

The ground station measurements were made with an Rb^{85} -vapor magnetometer originally designed for use in rocket borne experiments. Digitization of the magnetometer signal was accomplished by a technique using the magnetometer output as a gating signal for a paralleled high frequency (1 Mc) oscillator and counting circuit. This method preserves the inherent sensitivity of the instrument while allowing rapid sampling of the field strength. The count N from the counter was recorded automatically with a time reference precise to 0.1 second on digital tape compatible with IBM 729 tape units. In this method of counting and scaling, the magnetic field strength B is inversely proportional to the output count N as $B = n/4.67N$ gammas where n is the preset number of cycles of the magnetometer used for gating the counter. For the data obtained at the Fredricksburg Observatory the preset count n was adjusted so that a sample was obtained approximately once per second. The field strength recorded by this procedure is a time-average value with a sensitivity predicted from the least count random error

*National Academy of Science - NASA Post Doctoral Resident Research Associate.

in N of 1 unit. Thus, $\Delta B = \pm n/4.67N^2 = \pm B/N$, which, for this ground station, is approximately 0.056 gammas. The effect of this random least count is to set an apparent uniform instrumental noise level which appears in the computation of frequency spectra of magnetic field fluctuations.

For studying fluctuations of the earth's magnetic field, it is important to note that the Rb-vapor magnetometer detects only variations in the total field. This is to be contrasted with other instrumentation which is sensitive to component fluctuations and in certain cases the time derivative of such components. The Rb-vapor magnetometer senses total field variations with a uniform amplitude response over a broad frequency spectrum. Thus, it is particularly well qualified for determining frequency spectrum characteristics of magnetic field fluctuations. Let

R = the total field measured,

Z = the vertical component,

H = the horizontal component;

then
$$R = \sqrt{Z^2 + H^2} \cdot \tag{1}$$

Expanding R in a Taylor series, it is found that a variation δR in R correct to first order terms is given by

$$\delta R = \frac{Z}{R}\,\delta Z + \frac{H}{R}\,\delta H. \tag{2}$$

For most fluctuations, $\delta Z/Z_0$ and $\delta H/H_0$ are, in general, of the order of 10^{-4} or smaller so that Equation 2 can be replaced quite accurately by:

$$\delta R = \frac{Z_0}{R_0}\,\delta Z + \frac{H_0}{R_0}\,\delta H \cdot \tag{3}$$

It is seen that the measurement of total field variation is sensitive to variations in both vertical and horizontal components. The relative proportion of each component detected depends upon the inclination of the earth's field at the ground station. At the Fredricksburg Magnetic Observatory this inclination is 71 degrees, so that

$$\delta R = 0.95\,\delta Z + 0.33\,\delta H \cdot \tag{4}$$

In general, $\delta Z/\delta H < 1$; but the manner in which the total field variation is dependent upon inclination tends to compensate this ratio so that, at this station, approximately equivalent magnitudes for each component are detected.

Analyses of the small-scale (0.01-10 gammas) low-frequency (0.001-1.0 cps) fluctuations of the earth's magnetic and electric fields referred to as micropulsations have emphasized the morphological features and behavior of quantities directly or indirectly dependent on the micropulsation amplitudes (References 3, 4, and 5). The observational data suggest that micropulsations represent the oscillation of the outer atmosphere of the earth (References 6, 7, and 8). The conditions of this oscillating system change as a result of various causes, so that a precise study of the sources responsible for exciting these oscillations is confused by changes in the system and hence in its dynamical properties. The approach in the present study has been motivated by the consideration that the observed micropulsations represent the output of a system whose transfer function (frequency characteristics) is not constant. Thus, although the input to the system (the sources) may be identical, differences associated with system changes are observed at the output.

The resonant frequencies (eigen modes of oscillation) of the system are independent of the source characteristics and depend only on the distribution of physical parameters within the system. However, the relative amplitudes and phases of each eigen mode excited by a particular source is dependent on the source characteristics. It is possible that a detailed study and analysis of the frequency spectra of micropulsations with regard primarily to the existence and identification of distinct modes, rather than to relative amplitudes, will allow a determination of the model which best represents the oscillating system. Once this model has been accurately established it will be possible to study in detail the numerous distinct sources which exist as evidenced from the micropulsation observational data. The determination of the best model is a very important but difficult step in our understanding of the earth's immediate environment in space.

Mathematically, the field fluctuations represent an output which is the convolution of the impulse response of the system with the time behavior of the source. Thus, the output spectrum is given by the product of the Fourier transform of the impulse response and the frequency characteristics of the source. If the impulse response can be determined by investigating its frequency characteristics, it may be possible to deconvolve an observed time response to determine the nature of the source. It is apparent that there must be a strong interplay between the time and frequency domains in this method of analysis. Figure 1 summarizes in a block diagram these concepts and the mathematical foundation for this approach to the analysis. It should be noted that restrictions of linearity and superposition must be imposed on the system's response characteristics if the final analysis is to be valid. The justification for this assumption requires both a theoretical study of the detailed characteristics of the oscillations and measurements of the magnetic field fluctuations observed within the system.

The present study includes the results of frequency spectra computations using the data obtained with the Rb-vapor magnetometer at Fredericksburg, Virginia. The

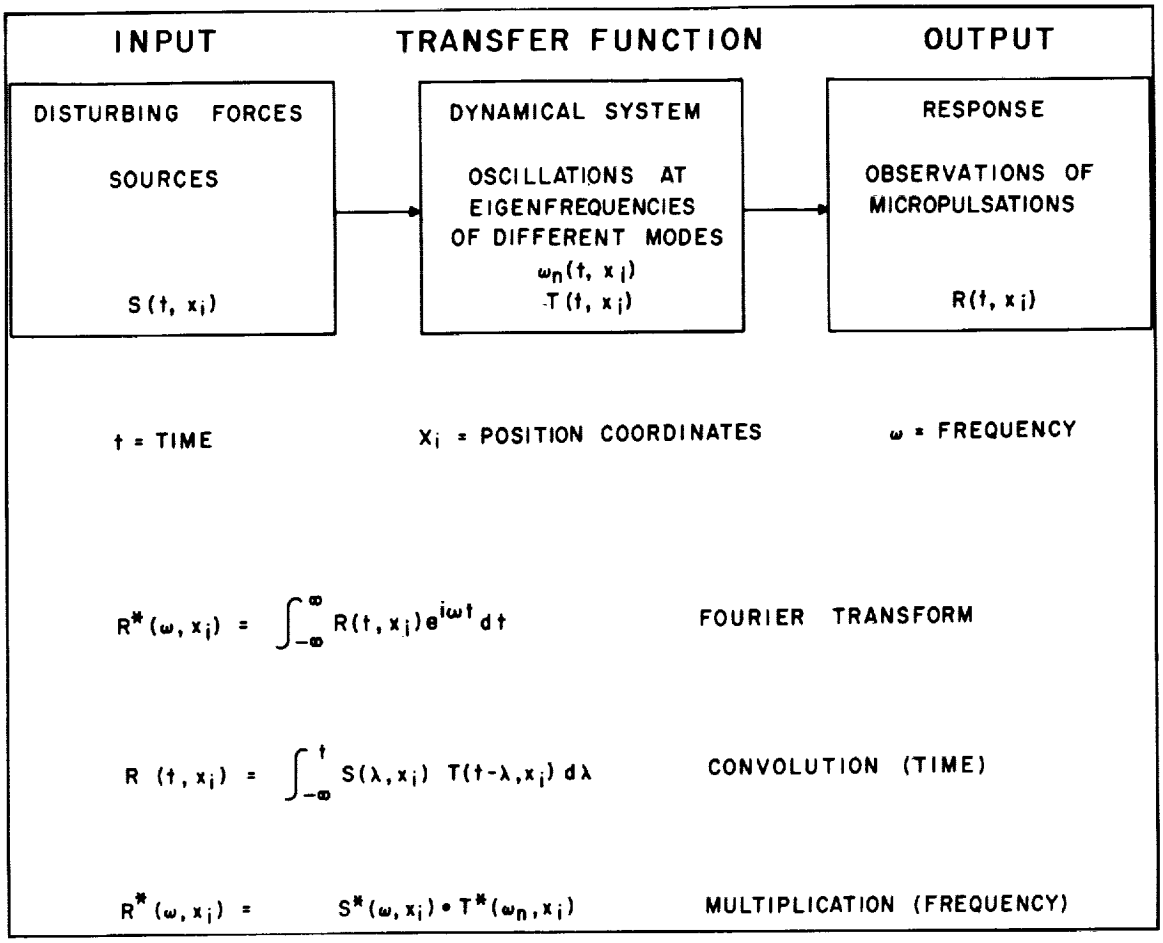

Figure 1 - Block diagram for micropulsation analysis

determination of the frequency spectra was made by using an IBM 7090 digital computer programmed to evaluate the power spectrum of a time series by the method outlined in Reference 9. This computational procedure predicts the average energy per unit bandwidth as measured in gamma^2/cps. Conversion to amplitude spectra is accomplished by determining the bandwidth of distinct spectral peaks. An advantage of this approach is that it allows a statistical evaluation of the significance of any spectral peak. Since the data were sampled once per second, the folding frequency or highest frequency capable of being uniquely determined is 0.5 cps. The counting technique yields a digital data value which represents a time average of the magnetic field. The averaging function or more properly the filtering function in this case is the diffraction function so that the problem of aliasing of frequency components is not present in this analysis. A problem does exist in the possible contamination of low-energy high-frequency peaks by high-energy low-frequency peaks. This has been eliminated by filtering the digital data with a numerical high-pass filter possessing a low frequency cutoff of 0.017 cps.

The study of the time variations of the micropulsation energy spectrum has been accomplished by segmenting the 5 days of data into consecutive 20-minute intervals beginning on the hour. The data were then numerically high-pass filtered and the power spectrum computed. Figure 2 shows the results of such analyses on six representative 20-minute intervals. A strong and statistically significant spectral peak is observed, with a period ranging from 6 to 12 seconds. The spectra all approach a uniformly constant value at higher frequencies which is consistent with the noise level predicted from the least-count analysis. When the spectral peak is above 0.1 cps certain additional peaks of lesser energy are observed in the spectrum at still lower frequencies. The approximate Q estimated from the width of the spectral peak varies between 4 and 8. This low value indicates that the dissipation of energy in these oscillations may be an important factor to consider in the theoretical determination of periods for any model system.

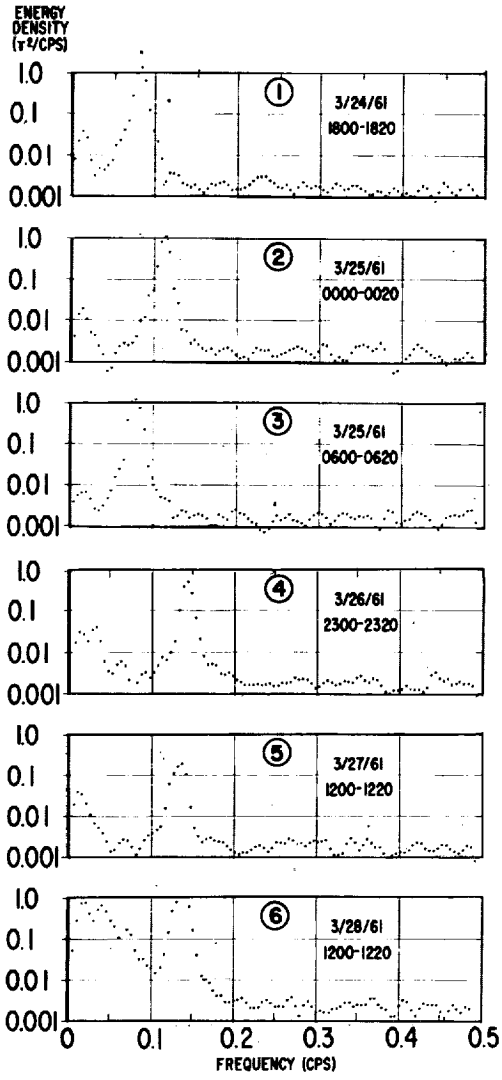

Figure 2 - Individual micropulsation spectra at Fredericksburg, Virginia

A composite summary of the behavior of the frequency and amplitude of the spectral peak with approximately a 10-second period is presented in Figure 3 with time indicated as UT. A striking point immediately noted is that considerably more structure and systematic behavior is apparent in the variation of the frequency at which the peak is observed than in the amplitude. There is a regular diurnal and semi-diurnal modulation of the frequency that repeats over the entire interval of 5 days. There does not appear to be a clear pattern to the amplitude behavior, although it must be realized that in this context the average amplitude is computed over a 20-minute interval, not for each distinct event. The six spectra corresponding to those in Figure 2 are indicated by the circled digits.

During the period covered by this data, a Class 3 solar flare occurred on March 26 at 1015 UT and an accompanying sudden commencement magnetic storm on March 27 at 1503 UT. Prior to the flare activity the oscillating system was modified, and there resulted a shift in the entire spectrum to higher frequencies; this included the introduction

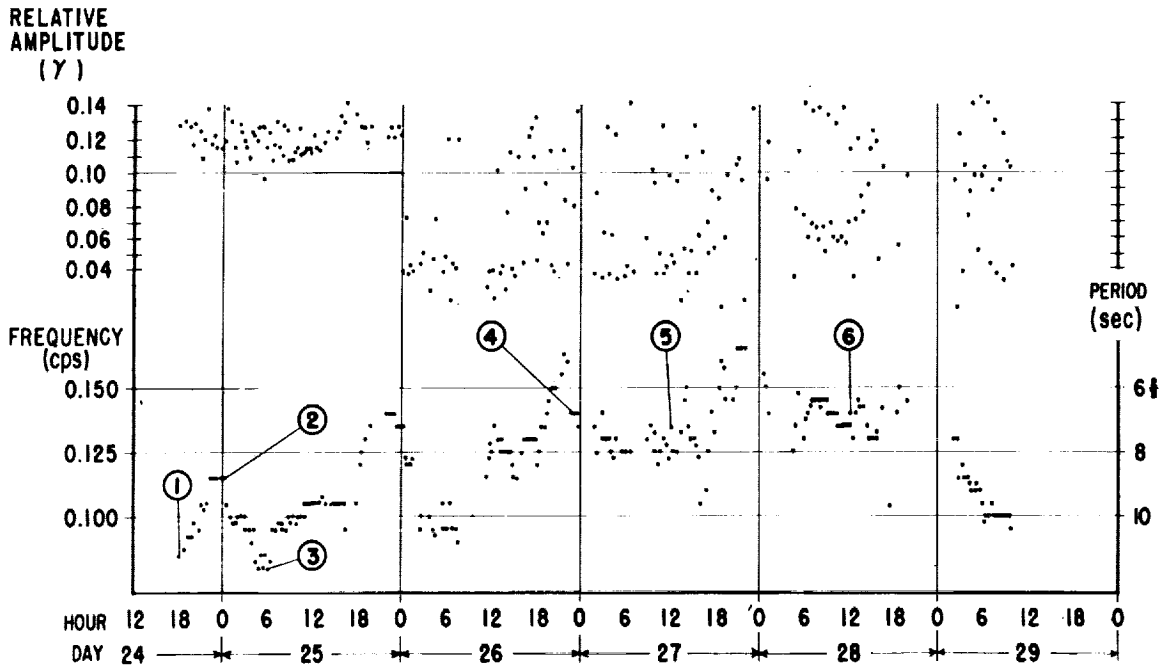

Figure 3 - Summary of variations in amplitude and frequency of the spectral peaks in Figure 2.

of other previously dormant modes. Previous investigators (References 10 and 11) have observed a diurnal variation in the periods of micropulsations. The results of this study strongly suggest that the variation of micropulsation period is continuous, rather than that different types of oscillations are involved; this agrees with the quantitative studies by Duncan (Reference 12). The upward shift in frequency of the micropulsation spectra at times of magnetic activity has been observed by Kato and Watanabe (Reference 11) and by Maple (Reference 13). Both of these features of the time variation of micropulsation spectra support the analysis based on the concept of a time-varying transfer function representing the oscillating system of the earth's outer atmosphere. Additional data related to this hypothesis with reference to magnetic field fluctuations in space will be presented in the following paragraphs. In conclusion, the experimental evidence indicates that the determination of the transfer function is a very important step for the future study of micropulsations.

These ground station measurements of the magnetic field of the earth were made simultaneously with space borne measurements of the magnetic field as detected by the satellite Explorer X (Reference 14). Figure 4 illustrates the magnetic field measured by flux-gate magnetometers during that portion of the flight covering and preceding the solar flare on March 26. The quantities measured were the total field F, the polar angle α and the azimuthal angle ψ relative to the spacecraft spin axis coordinates necessary to define the vector field. A change in behavior of the field in space is noted around 0600 on March 26: the field changed from relatively strong (32 gammas) and stable to weak

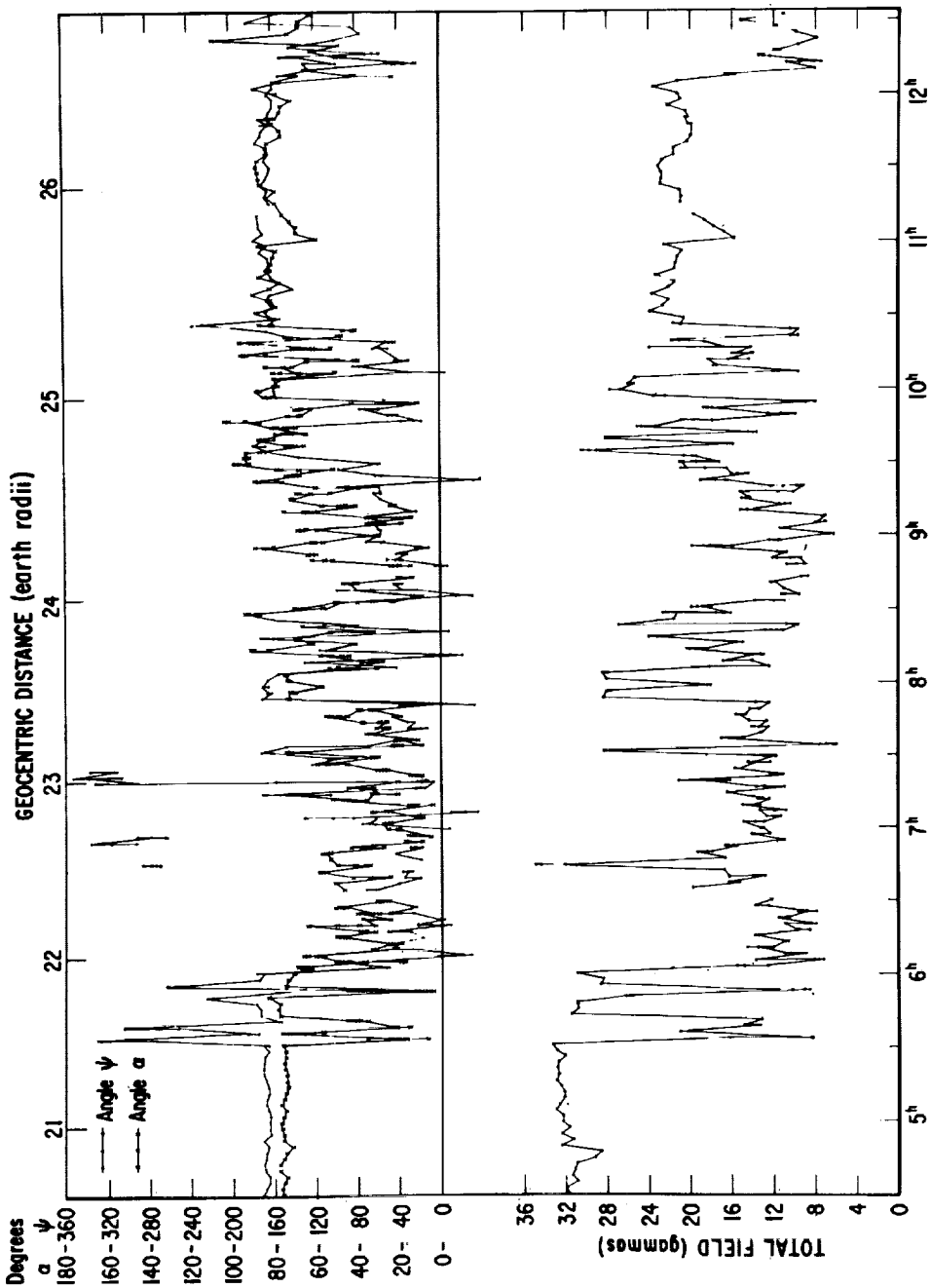

Figure 4 – Explorer X magnetic field measurements, March 26, 1961

(12 gammas), rapidly varying in orientation, and disordered. This time preceded the flare by some 4 hours and is coincident with a shift in the terrestrial micropulsation spectrum. The conditions in the outer atmosphere preceding the flare activity were modified, as is reflected in the micropulsation data and the field variations in space. Additional data and conclusions on the character of the field in space are presented in Reference 14 covering the entire flight interval.

The two flux-gate magnetometers were calibrated in flight with an Rb-vapor magnetometer. They were programmed to yield continuous field readings over consecutive intervals of 2.7 seconds every 2 minutes 25 seconds. Since these instruments are vector sensing elements and the probe spin-stabilized, the raw field measured varies periodically in time. Superimposed upon the spin modulation of the field are the temporal and spatial variations of the field. Digital sampling of these flux-gate data was made at 4-millisecond intervals and subsequent digital data processing yielded the values of F, α, and ψ as a function of time. Figures 5 and 6 show the raw data and the digital results for a representative sample of the field measurements which illustrate the manner in which the magnetic field fluctuated in space. This interval followed shortly after the significant change in the character of the magnetic field in space at 0600 on March 26.

As is readily evident from the raw data at the top of Figure 5, the field was undergoing rapid variations. The analysis indicated at the bottom of the figure, coincident in time with the data above, shows that the magnitude of the field did not change appreciably. However, the angles α and ψ did vary and combine to make it appear that the disturbing field vector was perpendicular to the steady field and rotated once around the steady field in a very short period of time. This mode of propagation could be interpreted as a classical Alfvén wave for the observed disturbance.

In Figure 6 the behavior of the field in the interval immediately following that in Figure 5 is presented. Here the raw data for flux-gate B show that the field changes, although in a different manner than for flux-gate A. The analysis of the data yields the contrasting result that over this interval the orientation of the field remained approximately constant while the magnitude changed appreciably over a short time interval (1 second). In brief summary, on the basis of the flight data there does appear to be a suggestion that preceding a magnitude change in the field there is an orientation change. The continuing detailed digital analysis will substantiate this conclusion. On the basis of these data, however, the measurement and interpretation of vector magnetic field fluctuations in space appears imperative. Precise correlations with terrestrial fluctuations on a time base may be possible once the details of the transfer function describing the outer atmosphere have been established.

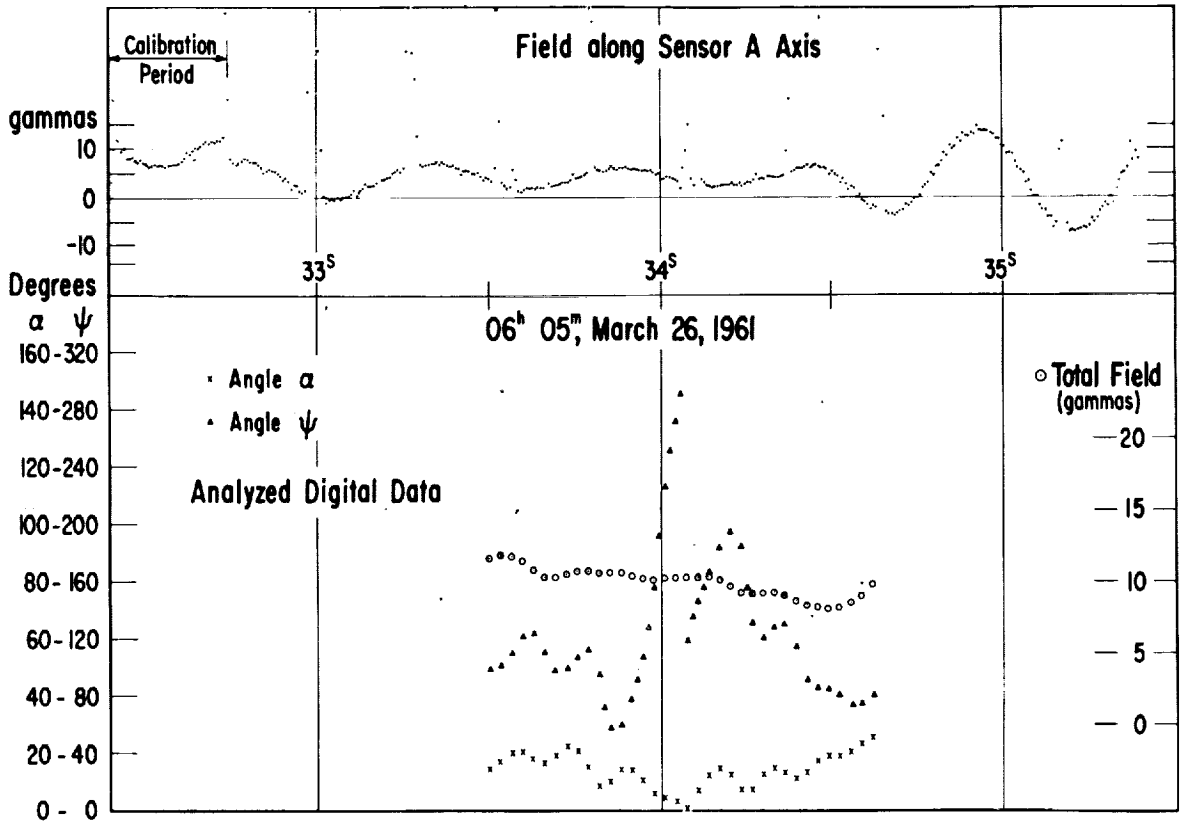

Figure 5 - Detailed fluctuations of magnetic field as measured by Flux-gate A

ACKNOWLEDGMENTS

The authors wish to acknowledge the invaluable assistance of Mr. Joseph Seek, Mr. Guy Marcot, and Mr. Edwin Cutler in this research and to express appreciation for the cooperation of the staff of the USCGS Magnetic Observatory at Fredericksburg, Virginia.

REFERENCES

1. Skillman, T. L., and Bender, P. L., "Measurement of the Earth's Magnetic Field with a Rubidium Vapor Magnetometer," J. Geophys. Res. 63(3):513-515, September 1958

2. Bloom, A. L., "Principles of Operation of the Rubidium Vapor Magnetometer," Applied Optics 1(1), January 1962 (To be published)

3. Kato, Y., and Watanabe, T., "A Survey of Observational Knowledge of the Geomagnetic Pulsation," Sci. Reports Tohoku Univ. Ser. 5, 8(3):157-185, March 1957

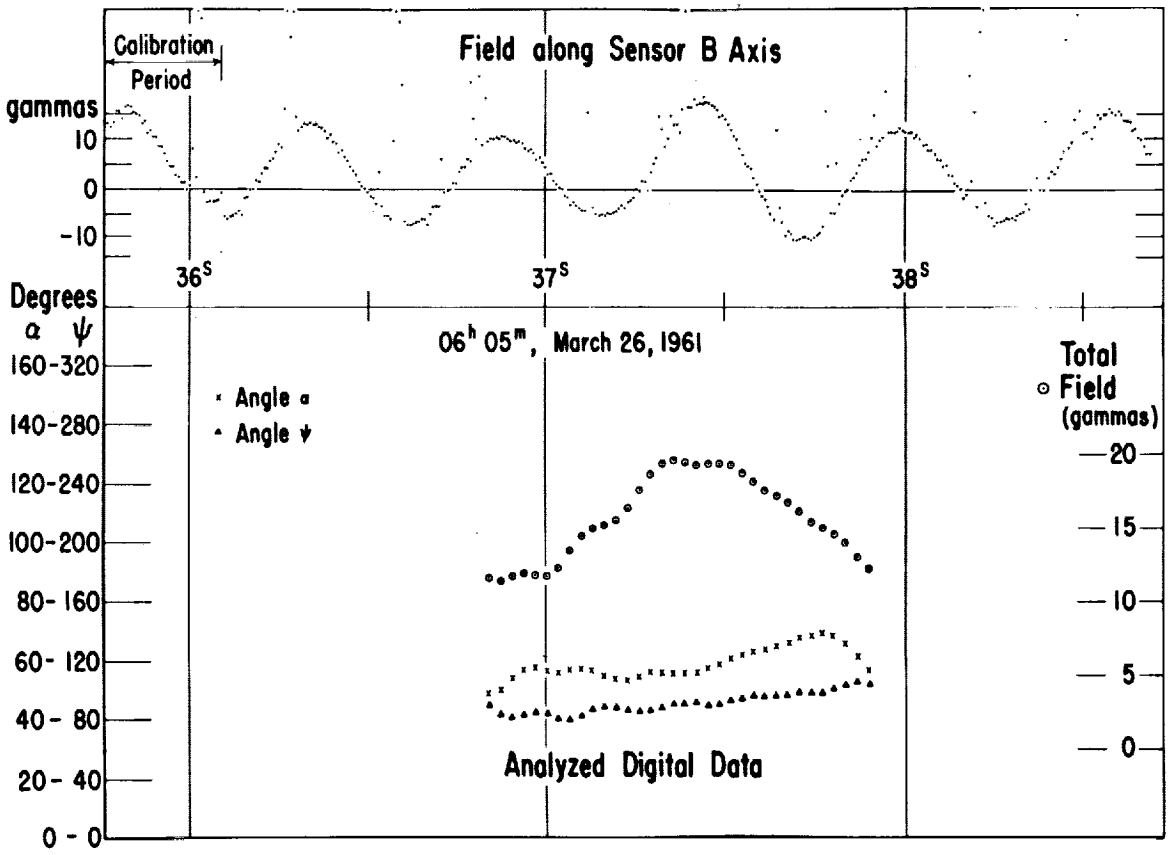

Figure 6 - Detailed fluctuations of magnetic field as measured by Flux-gate B

4. Benioff, H., "Observations of Geomagnetic Fluctuations in the Period Range 0.3 to 120 Seconds," J. Geophys. Res. 65(5):1413-1422, May 1960

5. Troitskaya, V. A., "Pulsation of the Earth's Electromagnetic Field with Periods of 1 to 15 Seconds and Their Connection with Phenomena in the High Atmosphere," J. Geophys. Res. 66(1):5-18, January 1961

6. Dungey, J. W., "Electrodynamics of the Outer Atmosphere," Ionosphere Res. Lab. Penn. State Univ. Sci. Rept. No. 69, September 15, 1954

7. Kato, Y., and Akasofu, S., "Outer Atmospheric Oscillation and Geomagnetic Micropulsation," Sci. Reports Tohoku Univ. Ser. 5, 7(3):103-124, March 1956

8. Obayashi, T., and Jacobs, J. A., "Geomagnetic Pulsations and the Earth's Outer Atmosphere," Geophys. J. 1(1):53-63, March 1958

9. Blackman, R. B. and Tukey, J. W., "The Measurement of Power Spectra," New York: Dover, 1959

10. Kato, Y., and Saito, T., "Preliminary Studies on the Daily Behaviour of Rapid Pulsation," J. Geomag. Geoelect. 10(4):221-225, 1959

11. Kato, Y., and Watanabe, T., "Studies on Geomagnetic Storm in Relation to Geomagnetic Pulsation," J. Geophys. Res. 63(4):741-756, December 1958

12. Duncan, R. A., "Some Studies of Geomagnetic Micropulsations," J. Geophys. Res. 66(7):2087-2094, July 1961

13. Maple, E., "Geomagnetic Oscillations at Middle Latitudes," J. Geophys. Res. 64(10):1395-1404, October 1959

14. Heppner, J. P., Ness, N. F., et al., "Magnetic Field Measurements with the Explorer X Satellite," This publication; also Proc. Int. Conf. on Cosmic Rays and the Earth Storm, Kyoto, Japan, September 1961, Suppl. J. Phys. Soc. Japan 17, 1962 (To be published)

D-1061

WHISTLER SIGNALS OBSERVED WITH THE VANGUARD III SATELLITE

by
J. C. Cain, I. R. Shapiro, J. D. Stolarik, and J. P. Heppner

Although the main information obtained from the proton precessional magnetometer in the Vanguard III Satellite (1959 η) was measurements of the geomagnetic field (References 1 and 2), its sensing coil also served as a magnetic antenna for detecting audio-frequency electromagnetic waves. Detection was possible only during each 2-second period following an interrogation on command from the NASA Minitrack stations. During this interval the coil output was connected to an audio-band high-gain amplifier for transmission of the proton precession signal. There were approximately 4000 such transmissions during the 85 days of active satellite life, September 18 to December 12, 1959. The tracking stations were so located that magnetic data were obtained mainly over western South America, the West Indies, part of the southeastern United States, a region south of California, and central Australia. A few readings were also taken over southern Africa. Within these regions the orbital inclination of 33.5 degrees gives a geomagnetic latitude range of ± 45 degrees. The perigee and apogee altitudes were 510 and 3750 km, respectively.

The results presented here bring up to date an earlier preliminary analysis (Reference 1) in which about 100 magnetometer transmissions containing whistlers were considered. Since the first analysis the signal reduction procedure was changed from one of searching for whistlers to one of systematically handling all transmissions in time sequence. This process has particularly changed the statistics obtained on whistler occurrence rate as a function of magnetic activity. Thus, the previous report that the rate of occurrence was greater during periods of magnetic storms can no longer be considered valid, and exact statistical tests cannot be made until the systematic handling of all signals is complete. To date, 379 whistlers have been counted on 160 frequency-time spectrograms known to contain whistlers. Despite the lack of random sampling noted above, comparisons indicate that the number of whistler occurrences per unit time observed by the satellite is at least comparable to the number observed at the earth's surface in middle latitudes, and certainly much greater than the number observed on the ground in very low latitudes.

Since the data sampling has not been biased with regard to day or night selection, the diurnal dependence of the number of occurrences is fairly reliable. It was previously reported (Reference 3) that about 90 percent of the whistlers occurred between 6 p.m. and 6 a.m. local time. The most recent figure obtained is 83 percent. Figure 1 shows the distribution of 2-second intervals containing whistlers as a function of local time for a sample of 133 such intervals. The diurnal dependence is believed to be the result of having much stronger absorption in the lower ionosphere during daylight hours than during the night. This belief is consistent with the 18-kc measurements made with the Lofti (1961 η_1) satellite (Reference 4) in which it was found that the ionospheric attenuation of 18-kc transmission was negligible at night.

The whistlers observed by Vanguard III typically show less dispersion than is observed on the earth's surface. This supports the assumption that the observed signals are "fractional hop" whistlers propagating from lightning strokes near the earth's surface to the satellite along geomagnetic lines of force. The dispersions measured to date range from 1.0 to 68.2 $\text{sec}^{\frac{1}{2}}$.

Figure 2 is an example of a spectrogram made from a Vanguard III magnetometer transmission. The heavy, horizontal line is the proton precessional signal, f(cps) = 4257.6 H (Gauss). The values of D shown are the whistler dispersions from the well-

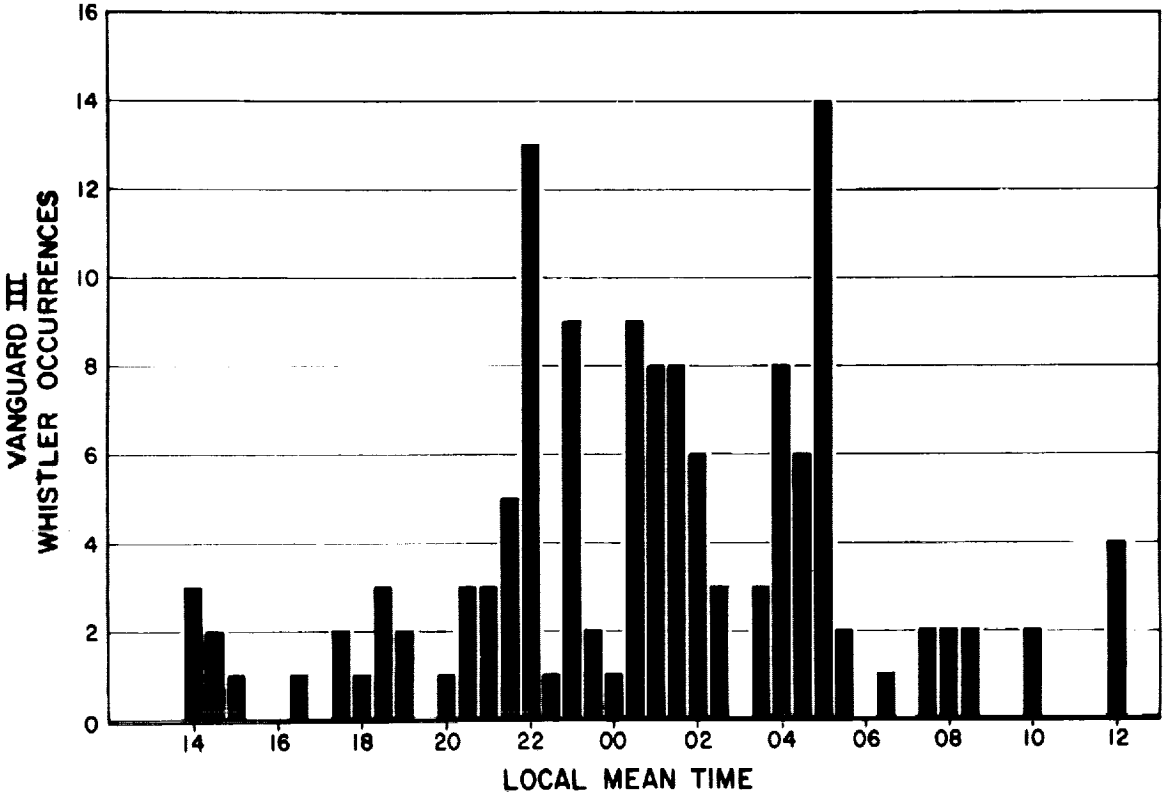

Figure 1 - The distribution of 2-second intervals containing whistlers as a function of local time for a sample of 133 intervals

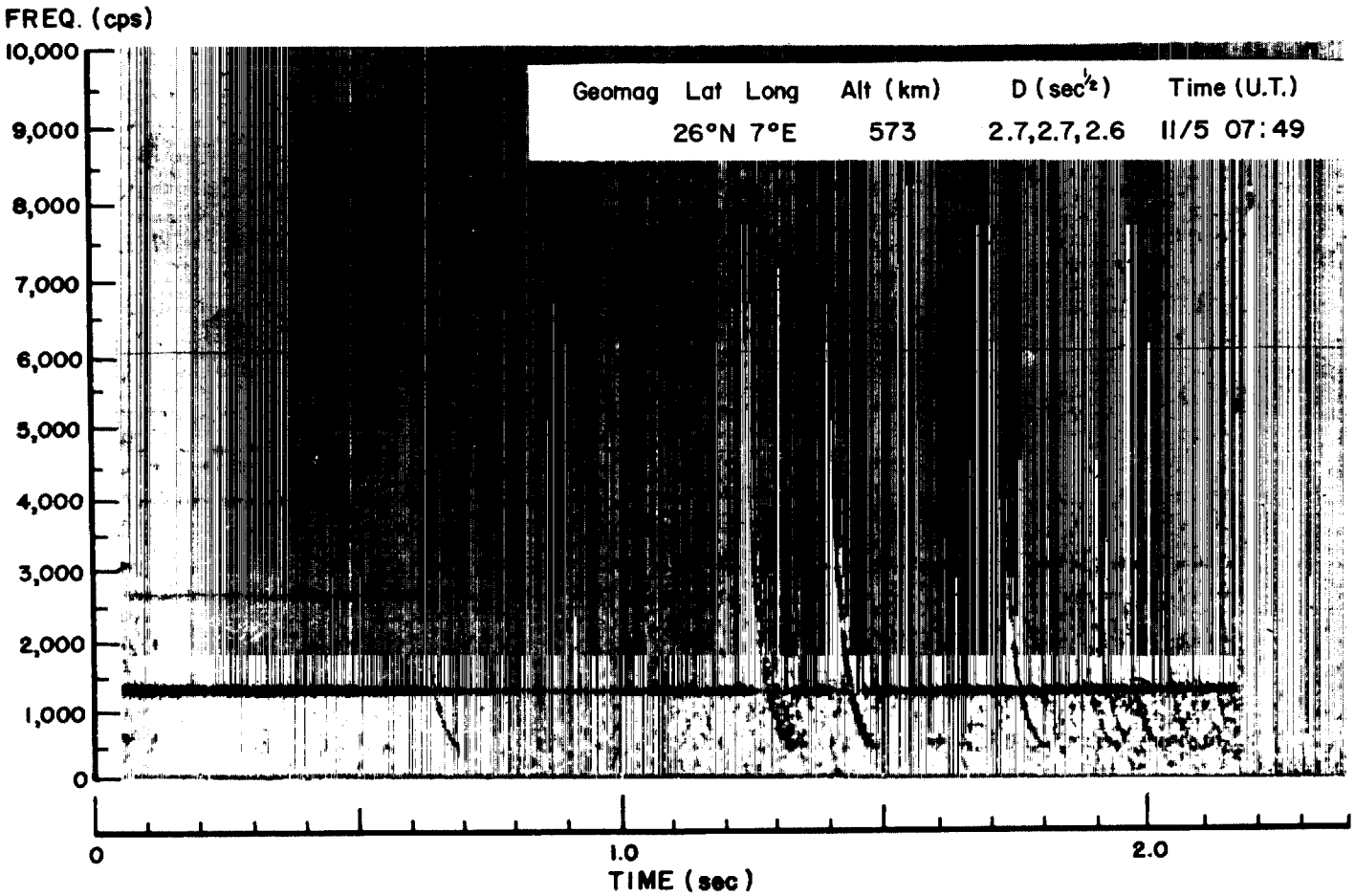

Figure 2 - Spectrogram made from a Vanguard III magnetometer transmission

known approximation (Reference 5) $D = dt/df^{-\frac{1}{2}}$ where f is in cycles per second. This example shows a whistler group typical of a multiple-flash type with the small dispersions indicating a single transmission through the ionosphere. Multiple-flash groups appear to be prevalent near the equator, and in one case 20 distinct whistlers were recorded within one 2-second interval.

Figure 3 illustrates the locations of the satellite for a sample of 203 whistlers. These are shown with 150 values to avoid duplication of a given dispersion at approximately the same location. The letters P and A refer to the heights of perigee and apogee. With the exception of three points shown at 40°S and five points near 35°N and 1500 km, all points shown fall in the geographic longitude range 60°W to 80°W. Upon detailed examination it is seen that the majority of the dispersion values follow a pattern in which the dispersion increases with distance along the field line from the earth's surface. From only these values, ignoring others for the present, it is apparent that it should be possible to obtain average electron densities in various strips above the F region and extending through most of the inner radiation belt. This is one of the objectives in using these measurements that will be pursued as a greater density of points becomes available and the selection of points becomes more exact. Preliminary to these determinations, a study is being conducted to test the agreement between observed dispersions and theoretical dispersions. The latter are calculated by integrating electron densities and field intensities over the field line path between the earth's surface and the satellite by using the simplified equation (Reference 6)

$$D = \frac{1}{2C} \int_{path} \frac{f_p}{\sqrt{f_H}} \, \delta S \ .$$

Electron densities for this calculation are taken from charts supplied by J. W. Wright of CRPL in which electron densities are extrapolated above the F2 layer between latitudes 15° and 50°N, near longitude 75°W, following the method outlined in Reference 7. Table 1 illustrates the extent of the agreement.

The differences between the calculated and measured dispersions given in Table 1 can be attributed to the lack of exactness in the assumption that the source was located on the same field line as the satellite; errors in the extrapolated electron densities; longitudinal differences between the ionospheric sounding stations and satellite positions; and the differences between ionospheric chart times and the times of whistler observations. However, the agreement is sufficiently good to give confidence that reasonably good average electron densities will be attainable in regions above F2 from this study as more data become available.

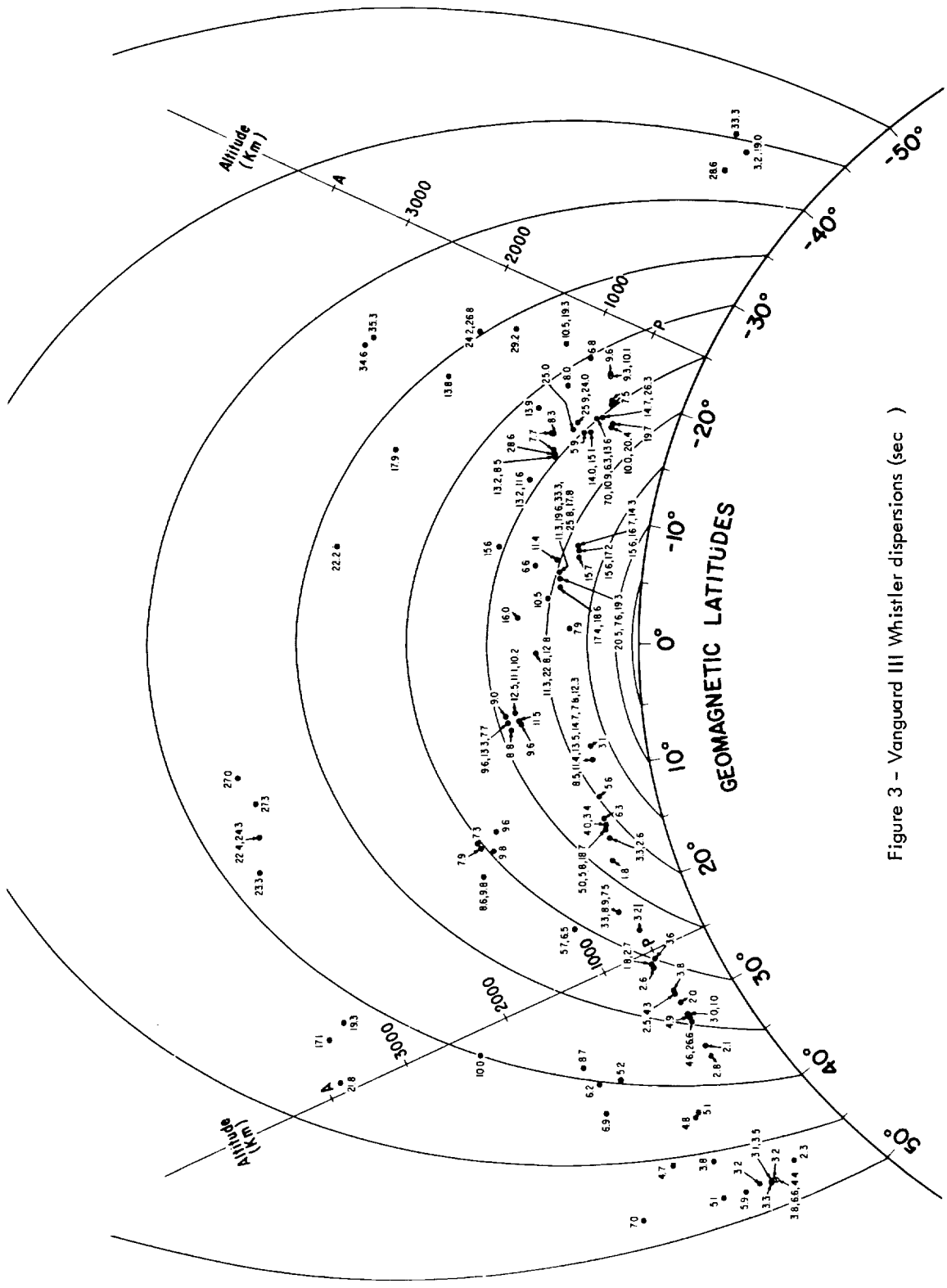

Figure 3 - Vanguard III Whistler dispersions (sec)

Table 1

Comparison of Calculated and Measured Dispersions

Date	Whistler Time (GMT)	Chart Time (GMT)	Satellite Geographic Location			Dispersion (sec)	
			Lat.	Long.	Alt. (km)	Calculated	Measured
Sept. 19	05:23	05:30	20.0°N	61.5°W	517	3.0	4.6,4.8,4.4
Sept. 22	04:57	05:00	17.5°N	62.8°W	519	2.9	2.5,4.3,4.3
Oct. 06	17:00	17:00	10.9°N	80.1°W	3551	16.3	17.1
Nov. 05	07:49	07:45	14.6°N	62.0°W	573	3.5	1.8,2.7,2.7,2.6
Nov. 25	07:06	07:00	33.3°N	76.1°W	587	1.4	2.3
Nov. 28	02:05	02:00	20.4°N	62.0°W	1552	5.3	6.2,6.1
Nov. 29	08:51	09:00	22.1°N	61.1°N	537	1.4	2.1
Dec. 02	06:02	06:00	33.4°N	78.2°W	850	2.7	3.2
Dec. 05	05:36	05:30	32.7°N	75.2°W	962	2.7	3.2

The dispersions on Figure 3 which do not fit an obvious pattern can temporarily be placed in two classes: (1) those which could possibly be explained as being due to a source in the opposite hemisphere from neighboring points, and (2) those for which there is not an obvious explanation. Explanation for those in class (1) can be sought in terms of peculiar propagation paths but it is not obvious that such explanations will be adequate for all cases.

Precise data are not available on signal amplitudes because no inflight calibrations of the amplitude response of the instrument were provided. Measurements of the relative amplitudes between the whistler and proton precession signal on a particular record cannot be used to compute the absolute whistler amplitude because the angles between the coil axis, the magnetic field, and the whistler wave normal were not known. However, approximate estimates can be based on the maximum proton signal strengths and the detection limitations of the instrument. The 600-turn 6-millihenry coil and amplifier, with a voltage gain of about 10^7, had a maximum response at a frequency of 1 kc. At 0.35 and 4 kc the sensitivity was down by a factor of 10, and at 10 kc it was down by a factor more than 100 relative to that at 1 kc. A computation reveals that nearly all of the observed whistlers correspond to VLF waves whose H components lie between about 0.001 and 5 gammas (1 gamma = 10^{-9} weber/m^2). It is thought that most of those examined have an amplitude between 0.01 and 0.5 gamma, with a few signals exceeding 1 gamma. The fact that frequencies as high as 10 kc are observed supports this belief.

The high occurrence rate of whistlers with significant signal strength near the equator suggests that whistlers may be important in the acceleration and diffusion of electrons in the inner Van Allen radiation belt. Although the possible importance of

electromagnetic waves has been emphasized by various investigators (References 8, 9, 10, and 11); the theory is not yet adequate to permit conclusions beyond the assumption that the whistlers will have some diffusive effect.

REFERENCES

1. Heppner, J. P., Stolarik, J. D., et al., "Project Vanguard Magnetic Field Instrumentation and Measurements," in: Space Res., Proc. 1st Int. Space Sci. Sym., Nice, January 1960, ed. by H. K. Bijl, Amsterdam: North-Holland Publ. Co., 1960, pp. 982-999

2. Heppner, J. P., Cain, J. C., et al., "Satellite Magnetic Field Mapping," NASA Technical Note D-696, May 1961

3. Cain, J. C., Shapiro, I. R., et al., "A Note on Whistlers Observed Above the Ionosphere," J. Geophys. Res. 66(9):2677-2680, September 1961

4. Bearce, L. S., and Young, C. E., "Penetration of the Ionosphere by Very Low Frequency Radio Signals: Some Initial Results of the LOFTI I Experiment," Paper presented at the URSI-IRE Joint Meeting, Washington, D. C., May 1961

5. Storey, L. R. O., "An Investigation of Whistling Atmospherics," Phil. Trans. Roy. Soc. 246A(908):113-141, July 9, 1953

6. Helliwell, R. A. and Morgan, M. G., "Atmospheric Whistlers," Proc. IRE 47(2):200-208, February 1959

7. Wright, J. W., Wescott, L. R., and Brown, D. J., "Mean Electron Density Variations of the Quiet Ionosphere," U. S. Nat. Bur. Standards Technical Note 40-3, May 1959

8. Alfvén, H., "Momentum Spectrum of the Van Allen Radiation," Phys. Res. Letters 3(10):459-460, November 15, 1959

9. Herlofson, N., "Diffusion of Particles in the Earth's Radiation Belts," Phys. Res. Letters 5(9):414-416, November 1, 1960

10. Helliwell, R. A., and Bell, T. F., "A New Mechanism for Accelerating Electrons in the Outer Atmosphere, J. Geophys. Res. 65(6):1839-1842, June 1960

11. Kellogg, P. J., "Electrons of the Van Allen Radiation," J. Geophys. Res. 65(9):2705-2713, September 1960

ROCKET OBSERVATIONS OF SOLAR PROTONS ON SEPTEMBER 3, 1960

by

L. R. Davis, C. E. Fichtel, D. E. Guss,* and K. W. Ogilvie*

To obtain a more detailed picture of the character of solar particle beams in the range of energies between 2 and 250 Mev, sounding rockets have been used to carry charged-particle detectors well above the earth's atmosphere during several of these events. The rockets were launched from Churchill, Manitoba, Canada (geomagnetic coordinates 60.7°N, 324.4°E), where the earth's magnetic field does not prevent the entry of low-energy particles. A typical flight trajectory for the Nike-Cajun sounding rocket is shown in Figure 1. Each rocket carried a Geiger counter, a scintillation detector, nuclear emulsions, and a magnetometer to provide rocket aspect as a function of time.

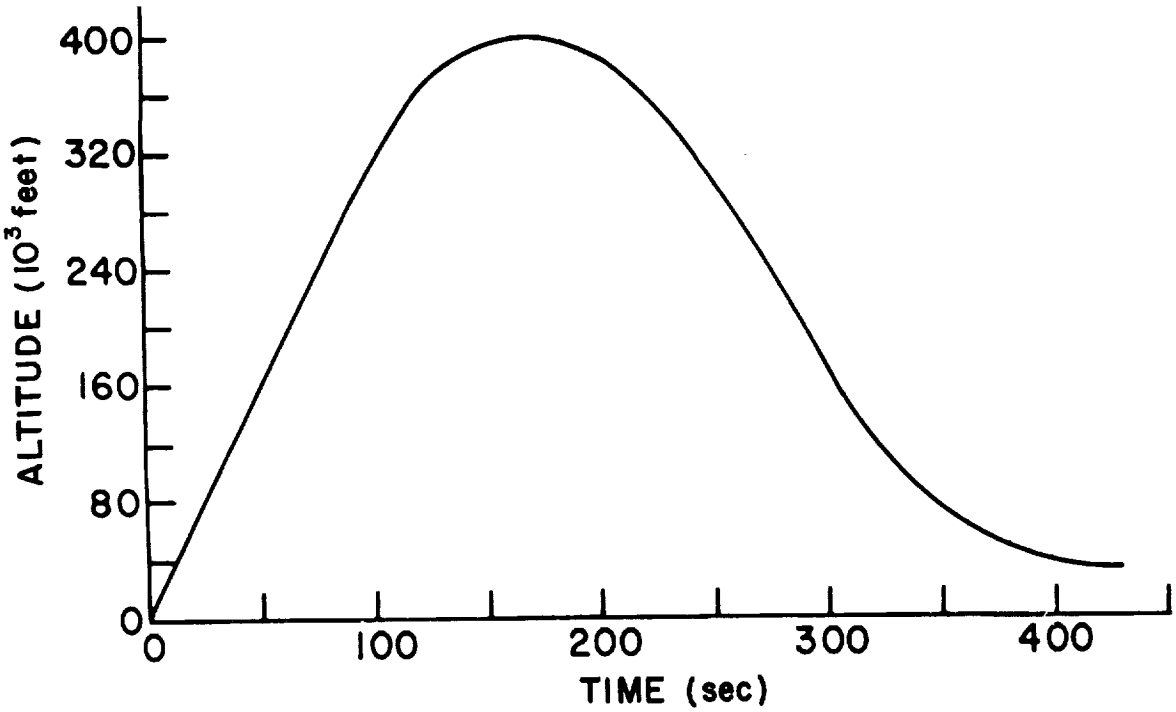

Figure 1 - Nike-Cajun trajectory for the Solar cosmic ray experiment

*National Academy of Science – NASA Post Doctoral Resident Research Associate.

Beginning on June 6, 1960, a 24-hour-a-day stand-by for a solar particle beam was begun at the Rocket Research Facility at Churchill. Arrangements had been made with several solar observatories and riometer stations to send immediate notification of a major solar flare or polar cap absorption event. When the experiment was concluded at the end of November, ten firings had been made into four solar particle beams, and four other firings for comparison purposes had been made during quiet periods and periods of auroral absorption.

During the solar particle event, which began on September 3, 1960, and is generally credited to a solar flare of Class 3 (solar coordinates 20°N, 87°E) occurring at 0040 U. T. on September 3, two rockets were shot. The exact firing times are given in Table 1. Reduction and interpretation of the scintillation counter results for these two firings is not complete, but the Geiger counter and emulsion results are reduced and will be presented here. The counter data were reduced by Davis and Ogilvie, and the emulsion data by Guss and Fichtel. The results are presented together because they refer to the same event and the same conclusions can be drawn from both.

Table 1

Rocket Firing Data for the September 3 Event

Rocket	Firing Time (U. T.)	Max. Altitude (km)	Emulsions Recovered
NASA 1019	1408	130	Yes
NASA 1020	1730	130	No

The Geiger counter used was an Anton 302, placed with its axis parallel to that of the rocket and mounted close to its wall on one side. The solid angle to the front, of almost 2π steradians, was shielded by the equivalent of 0.65 gm/cm^2 of aluminum; and the solid angle to the rear was shielded by a variable but larger amount. Outside the atmosphere, the regular precessional motion of the rocket places a variable amount of absorber between the protons and the sensitive volume. Assuming an isotropic distribution in the upper hemisphere, two points on the integral energy spectrum of the particles may be obtained from the counting rates observed with the Geiger counter pointing first up and then down. The angular distribution of the Geiger counter rates is consistent with the assumption of isotropy in the upper hemisphere. The only particles that have been considered approaching the apparatus from below are those which mirror so close below it that their range allows them to make the journey back up again. This correction increases the effective solid angle by about 10 percent. Another flux value may be found by summing up contributions to the solid angle, when the apparatus is at a depth of

approximately 10 gm/cm on the way up. The appropriate energy is found by weighting the contribution of each sector by the reciprocal of the proton energy which can just penetrate to it.

The flux values in Table 2 show that at 1730 U. T. the flux in the energy region from 22 to 67 Mev was the same as at 1408 U. T., but a reduction had occurred in the 200-Mev region. This absence of change in intensity of the low energy protons is consistent with the Churchill riometer observations which, as can also be seen in Table 2, showed no change in absorption during the firing period. The decrease in intensity of the higher energy protons is in general agreement with the sea-level neutron monitor observations at Deep River, Canada, which showed a slow decrease during the firing period.

Table 2

Proton Flux Measurements During Polar Cap Absorption Event on September 1960

Energy (Mev)	Integral Flux $\left(\frac{\text{particles}}{\text{cm}^2 \text{ ster sec}}\right)$	Time (U. T.)	Churchill 30-Mc Riometer Absorption (db)
22	18.5 ± 1	1408	1.4
67	7.3 ± 0.5		
177	3.8 ± 1.0		
22	19.7 ± 1	1730	1.4
67	6.5 ± 1		
220	1.3 ± 0.6		

The emulsion section of the payload consisted of a cylindrical stack 1 inch thick and 4 inches in diameter, of 600μ-thick Ilford G-5 nuclear emulsions with the plane of the emulsions perpendicular to the rocket axis. The stack was shielded from the ambient radiation by 0.175 gm/cm^2 of aluminum and 0.013 gm/cm^2 of reflective aluminum foil and Mylar.

To obtain the proton energy spectrum, the emulsions were scanned so that all tracks from protons with kinetic energies between 13 and 250 Mev within a given solid angle would be recorded. The proton energies were determined from range measurements in the energy interval between 13 and 90 Mev and from grain density measurements in the energy interval between 90 and 250 Mev. In the latter interval it is not possible to determine the direction of motion of the particles, and a penetration correction must be made for those particles which cross the scan line by first traversing the emulsion.

The analysis of the Geiger counter data from this flight is consistent with the assumption that the solar beam particles were isotropic over slightly more than the upper hemisphere and zero over the remainder of the lower hemisphere; therefore, this was assumed in obtaining the unidirectional fluxes from the emulsion data. With this assumption, the observed spectrum was corrected in the following way for ascent, descent, and the ionization loss in the atmosphere of mirrored particles, to yield the integral spectrum under zero atmosphere. The observed differential spectrum was corrected for background and approximately corrected for penetration. An integral spectrum was then formed by normalizing to the flux at 250 Mev observed by Winckler et al. (Reference 1) at the same time at balloon altitudes. Because of the relatively small flux of protons with energies greater than 250 Mev, a change of the integral flux at that point would not appreciably alter the shape of the integral spectrum at lower energies, as may be seen from Figure 2. The resulting spectrum was taken as a first approximation to the integral spectrum at the top of the atmosphere. With this the spectra at various absorber depths were computed, and the contributions (including penetration) at each absorber depth were added to give a spectrum which was compared to the observed spectrum. From this comparison, a better estimate of the spectrum at zero atmosphere was made and the procedure was repeated until agreement was reached.

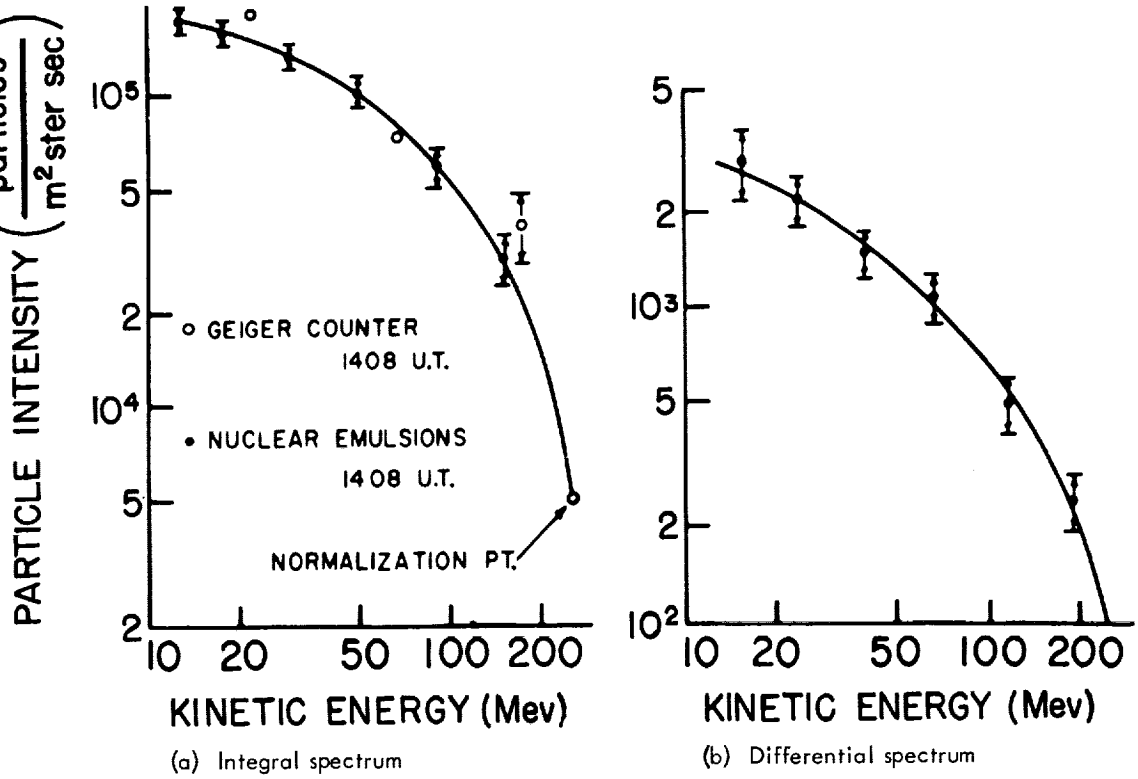

(a) Integral spectrum (b) Differential spectrum

Figure 2 - Proton energy spectrum from solar particle beam of September 3, 1960

The integral energy spectrum (a) and the differential energy spectrum (b) for protons at zero atmosphere, found from the emulsion data, are shown in Figure 2. The errors on the emulsion points include the uncertainty of the ascent correction as well as the statistical uncertainty associated with each point. Also shown are the points obtained at the same time by means of the Geiger counter. These were calculated completely independently of the emulsion flux values and spectral slope, and represent good agreement with them.

The results are important in that they are the first direct measurement showing that protons below 100 Mev in energy and, indeed, down to at least 13 Mev, are present in solar beams. The extreme flattening of the spectrum at the lower energies may be due to a rather unique feature of this event. Winckler et al. (Reference 1) have compared the build-up in intensity of the solar protons on September 3 as measured by sea-level neutron monitors and balloon equipment flown at Minneapolis with the same data as measured at Churchill. This comparison shows that the maximum intensity occurred hours after the flare, and the delay was greater the lower the proton energy. This they interpret as being caused by the passage of the solar protons through a magnetic cloud from a previous flare. The lowest energy protons they could detect, 125 Mev, reached a maximum intensity about 10 hours after the flare. The rocket proton spectrum is consistent with this picture in showing that over 13 hours after the flare there was a deficiency of 13 to 50 Mev protons. By comparison, the more recent rocket measurements (Reference 2) made during the events of November 12 and 15, 1960, when the propagation conditions were cleaner, show proton spectra extending down to 5 Mev and lower with little or no flattening below 100 Mev.

REFERENCES

1. Winckler, J. R., Bhavsar, P. D., et al., "Delayed Propagation of Solar Cosmic Rays on September 3, 1960," Phys. Rev. Letters 6(9):488-491, May 1, 1961

2. Ogilvie, K. W., Bryant, D. A., and Davis, L. R., "Rocket Observations of Solar Protons During the November 12, 1960 Event," this publication and Proc. Internat. Conf. on Cosmic Rays and the Earth Storm, Kyoto, Japan, September 1961, Suppl. J. Phys. Soc. Japan 17, 1962 (To be published)

ROCKET OBSERVATIONS OF SOLAR PROTONS DURING THE NOVEMBER 12, 1960 EVENT

by
K. W. Ogilvie,* D. A. Bryant,* and L. R. Davis

Three Nike-Cajun rockets were fired from Churchill, Canada, during the solar proton event of November 12, 1960. The Geiger counter and scintillation counter instruments were carried to a height of 130 km, and were above 90 km for a period exceeding 150 sec. The rocket also carried nuclear emulsions. The times of firing and other details are given in Table 1.

Table 1

Rocket Firing Data for the November 12 Event

Rocket	Firing Time (U. T.)	Time from Flare	Churchill 30-Mc Riometer Absorption (db)	Emulsions Recovered
NASA 1024	1840/12th	5 hr 27 min	12.6	Yes
NASA 1015	2332/12th	10 hr 19 min	4.6 (night)	No
NASA 1016	1603/13th	26 hr 50 min	14.9	Yes

The first shot occurred towards the end of the period, when the neutron monitor rate was approximately constant after its initial increase. The second shot occurred some time after the second increase, when the rate was decreasing steadily. The third was made when the neutron monitor rate had decreased almost to normal. From the response of the detectors we can find the spectra of the protons incident at the top of the atmosphere at these three times. Thus, we have a spectrum of the protons which diffuse out of the trapping region as it approaches the earth (Table 1, Rocket 1024) and of those contained

*National Academy of Science - NASA Post Doctoral Resident Research Associate.

in the trapping region at two later times. We can also find the angular distribution of the protons at the top of the atmosphere.

Figure 1 shows the magnetic zenith angular distribution found for Flights 1024 and 1016 for the CsI scintillation counter (sensitive from 1.8 to 160 Mev). This shows the assumption of isotropy to be well fulfilled in the upper hemisphere, for angles between 25 degrees and about 90 degrees. The falloff outside the upper hemisphere is not sharp, owing to the ± 15 degrees opening angle of the detector. The flux at angles greater than about 110 degrees is due to particles scattering below the apparatus, and also those being reflected by the magnetic field and returning from below. The angular distribution for the ZnS scintillator (Figure 2) shows more variation. Isotropy just above the atmosphere does not, of course, mean isotropy in space away from the earth's magnetic field.

The integral proton energy spectra found by analysis of the first three flight records are shown in Figure 3. The shapes of the spectra are generally similar, with a gradual lessening of slope in the region down to a few Mev, and an increase in flux at even lower energies.

In the diagram of the spectra, the point marked "Explorer VII" indicates the flux value given by Lin (Reference 1), divided by 4π, obtained from the Explorer VII results. The satellite was at an altitude of 877 km, 44°N latitude, and 300° longitude at the

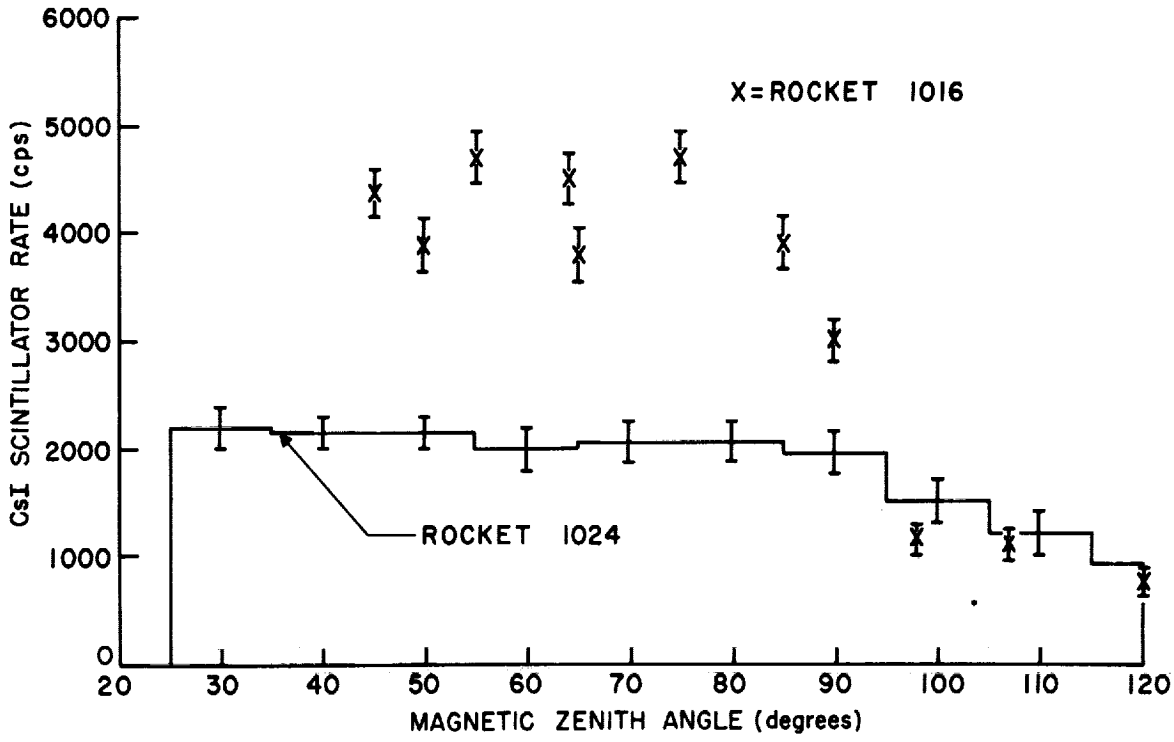

Figure 1 - Angular dependence of the CsI scintillator rates

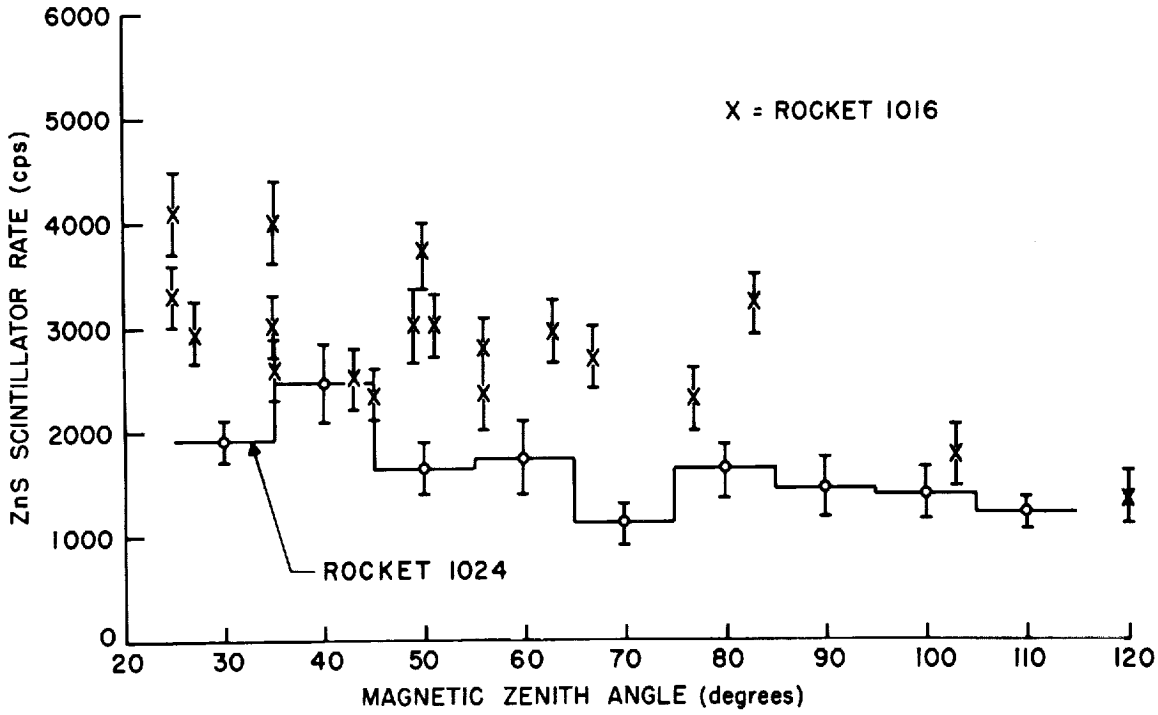

Figure 2 - Angular dependence of the ZnS scintillator rates

time of the firing of Rocket 1015; the magnetic field line passing through this point crosses the equator at about three earth radii. The point marked "Winckler" is derived from the observations of Winckler's group at Churchill during the event.

Balloon observations have previously indicated power-law spectra with exponents in the range 4-5, above about 100 Mev (Reference 2). It is now clear that extrapolation of the balloon spectra to low energies is not a satisfactory procedure. The intensity found by balloon measurements at the time of the firing of Rocket 1015 do, however, agree with the rocket measurements at the corresponding energy.

The analyses of the scintillation counter results in the energy region above 2 Mev were made by assuming a power-law spectrum and introducing a cutoff at low energies when necessary. This procedure gives the best straight-line fit to the data, and comparison with the completely independent emulsion results obtained by Fichtel and the Geiger counter results shows good agreement. It is thus possible that these cutoffs represent the magnetic thresholds at Churchill at the times of firing of the rockets. The Quenby and Webber cutoff for Churchill is 5.8 Mev.

We must now consider the rising portion of the spectrum below 0.4 Mev. Auroral absorption was not shown in the Churchill riometer at the time of any of the shots, but at the firing times of Rockets 1024 and 1016, the instrument was almost off scale and not

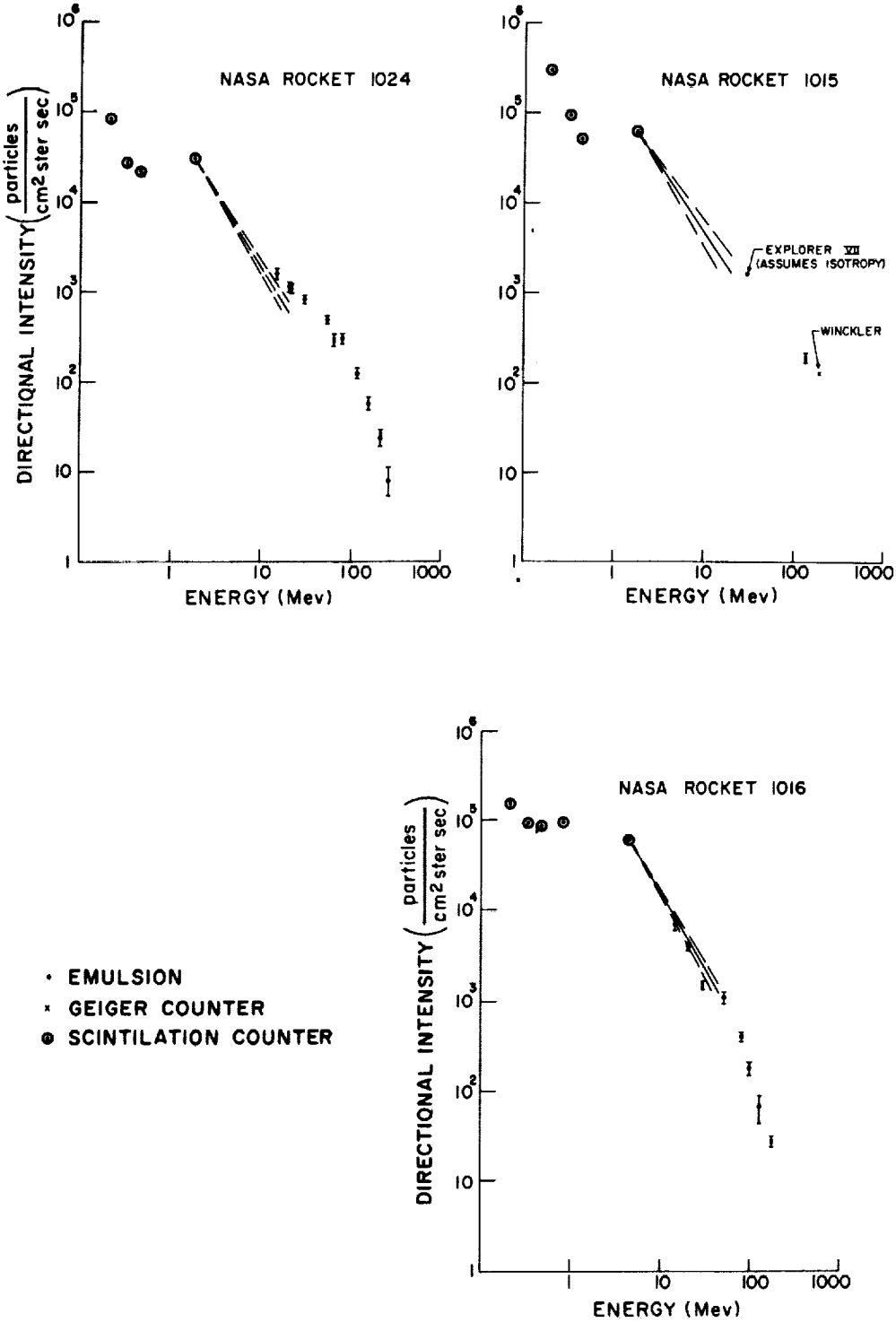

Figure 3 - Proton spectra measured during the November 12, 1960 event

very sensitive. Proton intensities of similar order of magnitude and similar spectrum have been observed in and near auroras by Davis et al. (Reference 3), McIlwain (Reference 4) and recently by McDiarmid et al. (Reference 5).

Figure 4 shows the neutron monitor rate (Reference 6), the Fort Churchill riometer absorption, the intensity at three energies, and ΔJ, the excess of intensity at 200 Kev over that at 2 Mev, plotted against time.

If a day/night ratio of 3:1 (Reid, private communication) is assumed, then the riometer absorption and the intensity of particles with energies greater than 10 Mev* correlate well. Comparison of the intensities at the three energies shows the rapid steepening of the spectrum towards high energies which has been previously noted by many observers. The figure also shows that the riometer absorption is predominantly produced by particles in the range between 10 and 100 Mev.

The value of ΔJ underwent a large increase between the times of Rocket 1024 and Rocket 1015, when the earth was supposed to be entering the trapping region, and a considerable decrease again by the time of firing of Rocket 1016.

This experiment cannot clearly determine whether the additional very low energy particles represent a simple extension of the spectrum of particles from the sun, in which case the cutoffs observed do not correspond to threshold rigidities, or whether they are a separate phenomenon. If they are, the implication is that we are observing the high energy tail of the distribution of protons responsible for the magnetic disturbances, and that these are not excluded by the threshold. The rocket observations cited (References 3, 4, and 5) strongly suggest that these protons are present in some quantity for a high proportion of the time at Churchill.

Supporting the idea that the additional low energy particles are associated with the magnetic storm is the fact that at 0.2 Mev the rectilinear travel time from the sun is 7 hours, so that such particles emitted by the flare could not have been observed by Rocket 1024. By the time of Rocket 1015, when a very large intensity of such particles was observed, the particle path length would have to have exceeded the direct path length by less than 50 percent. This is an interesting contrast to the behavior of the intensity at 10 Mev, which was still rising at 26 hours after the flare, more than twenty times greater than the time for rectilinear passage from the sun.

Again, because of the complicated nature of the event, the possibility cannot be excluded that the lowest energy particles were produced by the flare, probably of importance 3+ and accompanied by sudden ionospheric disturbance of duration 4-1/2 hours and type IV radio emission, which occurred at 0316 U. T. on November 11. This flare did not produce a neutron monitor increase or an effect on the riometer.

*Extrapolated from 22 Mev.

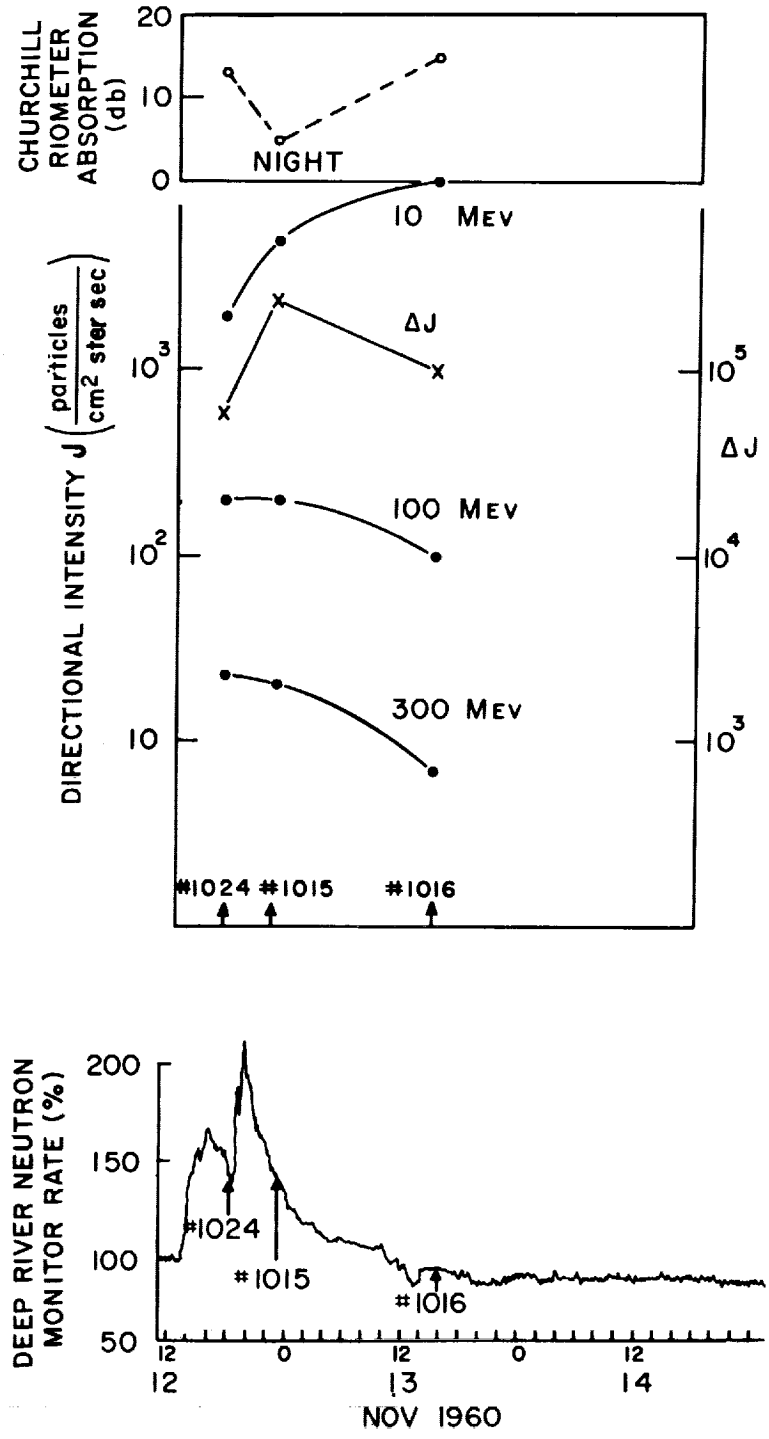

Figure 4 - Time variation of riometer absorption, particle intensities, and neutron monitor rate during November 12, 1960

To summarize the conclusions from these rocket flights:

(1) The spectra of protons at all times has a generally similar form and cannot be adequately represented near the earth by an extrapolation of the power law appropriate at balloon altitudes. This does not mean that the spectra observed here are appropriate at large distances from the earth.

(2) The particles are isotropic in the upper hemisphere just above the atmosphere.

(3) The observed low energy particles are either the high energy part of the magnetic storm distribution; or, less likely, are the results of the modification of the initial spectrum by the expansion of the solar plasma cloud in which the trapping occurs; or a combination of both. The most reasonable interpretation is that the observed cutoffs represent the magnetic thresholds at the time, that the low energy particles enter the field by another mechanism, and that the shape of the spectrum above the cutoff is influenced by the expansion of the trapping region.

A full account of these experiments will be published in the Journal of Geophysical Research.

REFERENCES

1. Lin, Wei Ching, "Observation of Galactic and Solar Cosmic Rays from October 13, 1959 to February 17, 1961 with Explorer VII (Satellite 1959 Iota)," State Univ. of Iowa SUI-61-16, August 1961 (Thesis submitted for M.S. degree)

2. Winckler, J. R., "Balloon Study of High-Altitude Radiations during the International Geophysical Year," J. Geophys. Res. 65(5):1331-1359, May 1960

3. Davis, L. R., Berg, O. E., and Meredith, L. H., "Direct Measurements of Particle Fluxes in and Near Auroras," in: Space Research: Proc. 1st Internat. Space Sci. Sympos., Nice, January 1960, ed. by H. K. Bijl, Amsterdam: North-Holland Pub. Co., 1960, pp. 721-735

4. McIlwain, C. E., "Direct Measurement of Particles Producing Visible Auroras," J. Geophys. Res. 65(9):2727-2747, September 1960

5. McDiarmid, I. B., Rose, E. D., and Budzinski, E., "Direct Measurement of Charged Particles Associated with Auroral Zone Radio Absorption," Can. J. Phys. (To be published)

6. Steljes, J. F., Carmichael, H., and McCracken, K. G., "Characteristics and Fine Structure of the Large Cosmic-Ray Fluctuations in November 1960," J. Geophys. Res. 66(5):1363-1377, May 1961

HEAVY NUCLEI IN SOLAR COSMIC RAYS

by
C. E. Fichtel and D. E. Guss*

D-1061

INTRODUCTION

Many properties of solar cosmic ray events have been studied by means of ground-level monitors, balloon-borne equipment, and satellites. In order to obtain more detailed information on the characteristics of the low energy portion of these phenomena, Nike-Cajun sounding rockets were used to carry nuclear emulsions and other equipment above the earth's atmosphere in several solar cosmic ray events. The rockets were launched from Churchill, Manitoba, Canada, geomagnetic latitude 60.7°N, at which point the magnetic field of the earth does not prevent the entry of low energy particles. This paper is particularly concerned with the detection of heavy nuclei in the three solar cosmic ray events studied and an examination of their properties.

EXPERIMENTAL PROCEDURE

In order to determine whether or not heavy particles were present in the solar particle beam under consideration, a complete scan of the periphery of the 4-inch-diameter nuclear emulsion disks was made for delta-ray tracks which had residual observable ranges in the emulsion of 700 microns or more and were within a specified solid angle. After the elimination of tracks which could be identified as those of slow alpha particles, the remaining tracks fell into two groups; those which had residual ranges of the order of several millimeters or less, and those which had residual ranges of many centimeters or more. In each case the number in the latter group was found, within statistics, to be consistent with the expected cosmic-ray background of 15 to 20 particles/m^2-ster-sec seen at balloon altitudes during the same period in the solar cycle.

Since the amount of material above a normal balloon flight is equivalent in stopping power to one or two centimeters of emulsion, the heavy particles in the former group (those with ranges less than one centimeter) would not have reached balloon altitudes. Hence, it is necessary to determine whether or not a significant fraction of the particles

*National Academy of Science–NASA Post Doctoral Resident Research Associate

in this group represent the normal cosmic-ray low-energy heavy spectrum. There was an identical firing on June 6, 1960, with the same Nike-Cajun payload system, to obtain background data for the subsequent shots. In an equivalent scan of the nuclear emulsion plates flown on June 6 there were no heavy particles with residual ranges less than one centimeter. On the basis of this finding, the calculated probability that the flux of heavy nuclei exceeded 3 particles/cm^2-ster-sec in this range interval during the time of the June firing is less than approximately 0.05. Since no major decline in solar activity or increase in cosmic-ray intensity was detected during the period from June to November, 1960, the flux of galactic cosmic-ray heavy nuclei with potential ranges in nuclear emulsion of less than one centimeter during the September flights may be assumed to be essentially zero, or a few particles/m^2-ster-sec at most.

The particles of interest, then, are those which had the short ranges, since, on the basis of the foregoing discussion, these are the true solar particles. In order to determine the charge of the nuclei the delta-ray method was used, since it gives a more reliable estimate of the charge than the thin-down or effective-track-width measurements. The variation of the delta-ray density with range was found to agree well with Mott's formula, with m/E_m equal to 13. This equation has previously been shown to be a good representation of the experimentally observed delta-ray distribution (References 1 and 2). Discussions of further details of charge identification, charge calibration, and the expected distributions due to errors may be found in References 2 and 3.

RESULTS

After the charge, range, and thereby the rigidity and energy of each particle had been determined, a comparison of the heavy particle flux to the proton flux was made. The particles of medium charge, $6 \leq Z \leq 9$, were chosen for this purpose because they are the most abundant and they are not widely separated in charge and mass. Table 1 gives the flux of solar cosmic ray medium particles at the time indicated in the event and also the ratio of these nuclei to singly charged nuclei above the same rigidity cutoff, the same energy/nucleon cutoff, and the same energy charge cutoff. There was a lower limit on the range of the heavy nuclei of about 0.5 gm/cm^2 because of the thin skin of the rocket and the minimum track length accepted for inclusion in the analysis. It is apparent that the three medium fluxes listed in the table represent three different orders of magnitude in intensity. The medium-to-proton ratio is seen to vary appreciably from event to event for the same rigidity cutoff, but is found to be much more nearly the same for the same energy/nucleon cutoff.

However, an examination of the energy and rigidity spectra of the heavy nuclei in comparison with the proton spectra in the same intervals (Figures 1 and 2) reveals that the heavy nuclei in the three events do not have the same energy/nucleon spectrum as

Table 1

Fluxes of Medium Nuclei ($6 \leq Z \leq 9$) and Medium-to-Proton Ratios

Time of Flare	0040 UT 9/3/60	1322 UT 11/12/60	0200 UT 11/15/60
Time of Measurement	1408 UT 9/3/60	1840 UT 11/12/60	1951 UT 11/16/60
Medium Particle Flux at $E/N \geq 42.7$ Mev (particles/ m^2-ster-sec)	19 ± 4	1530 ± 210	258 ± 40
M/p (same rigidity interval)	$(0.7 \pm 0.3) \times 10^{-3}$	$(2.3 \pm .5) \times 10^{-3}$	$(12^{+7}_{-5}) \times 10^{-3}$
M/p (same E/Z interval)	$(0.3 \pm 0.1) \times 10^{-3}$	$(0.61 \pm 0.12) \times 10^{-3}$	$(1.3 \pm 0.4) \times 10^{-3}$
M/p (same E/N interval)	$(0.17 \pm 0.05) \times 10^{-3}$	$(0.25 \pm 0.05) \times 10^{-3}$	$(0.42 \pm 0.13) \times 10^{-3}$

the protons. Although the information is unfortunately limited by the necessarily poor statistics resulting from the short flight time, there does seem to be reasonably good agreement between the differential rigidity spectra of the protons and the heavy nuclei. If we compare the differential flux in the same energy/charge intervals, the agreement is much better than for the same energy/nucleon intervals but not quite as good as for the same rigidity intervals, although within present statistics it cannot be said that there is definite disagreement. If we assume partial ionization, and consider the same energy per ionized charge interval, we then approach a comparison which is similar to the same-rigidity one.

We shall now examine the charge distribution to observe the more general features. Within the medium nuclei group, carbon and oxygen nuclei are more abundant than the odd charges. Table 2 shows the relative abundances of the carbon, nitrogen, and oxygen nuclei, taking the sum of all the nuclei observed in the three events together as a basis. There are no statistically significant variations from this average in individual events, however. The number of nuclei classified as nitrogen can only be taken as an upper limit because of the limitations on the charge determination, and there is no positive evidence for fluorine. A few heavier nuclei ($Z \geq 10$) were detected. Their flux was an order of magnitude smaller than the medium nuclei flux for the same range cutoff, but the heavy-to-medium ratio varied appreciably from event to event. This is due partially to statistics, but probably also to the different character of the events, and especially the different energy spectra. Only an upper limit can be set for the abundance of the light nuclei. This limit is given in Table 2, and indicates that the heavy nuclei have gone through no more

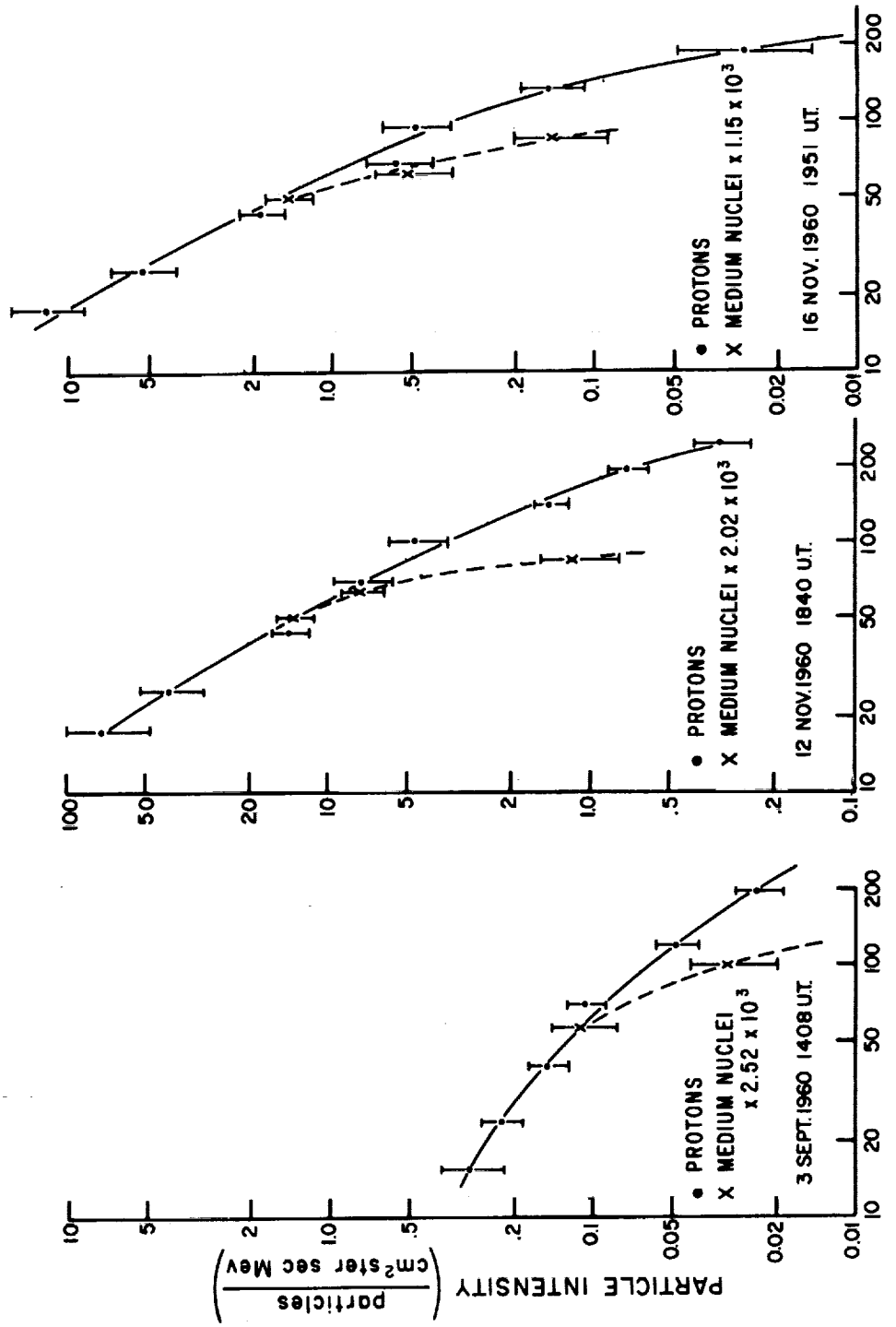

Figure 1 – Comparison of differential energy nucleon spectra for protons and medium nuclei

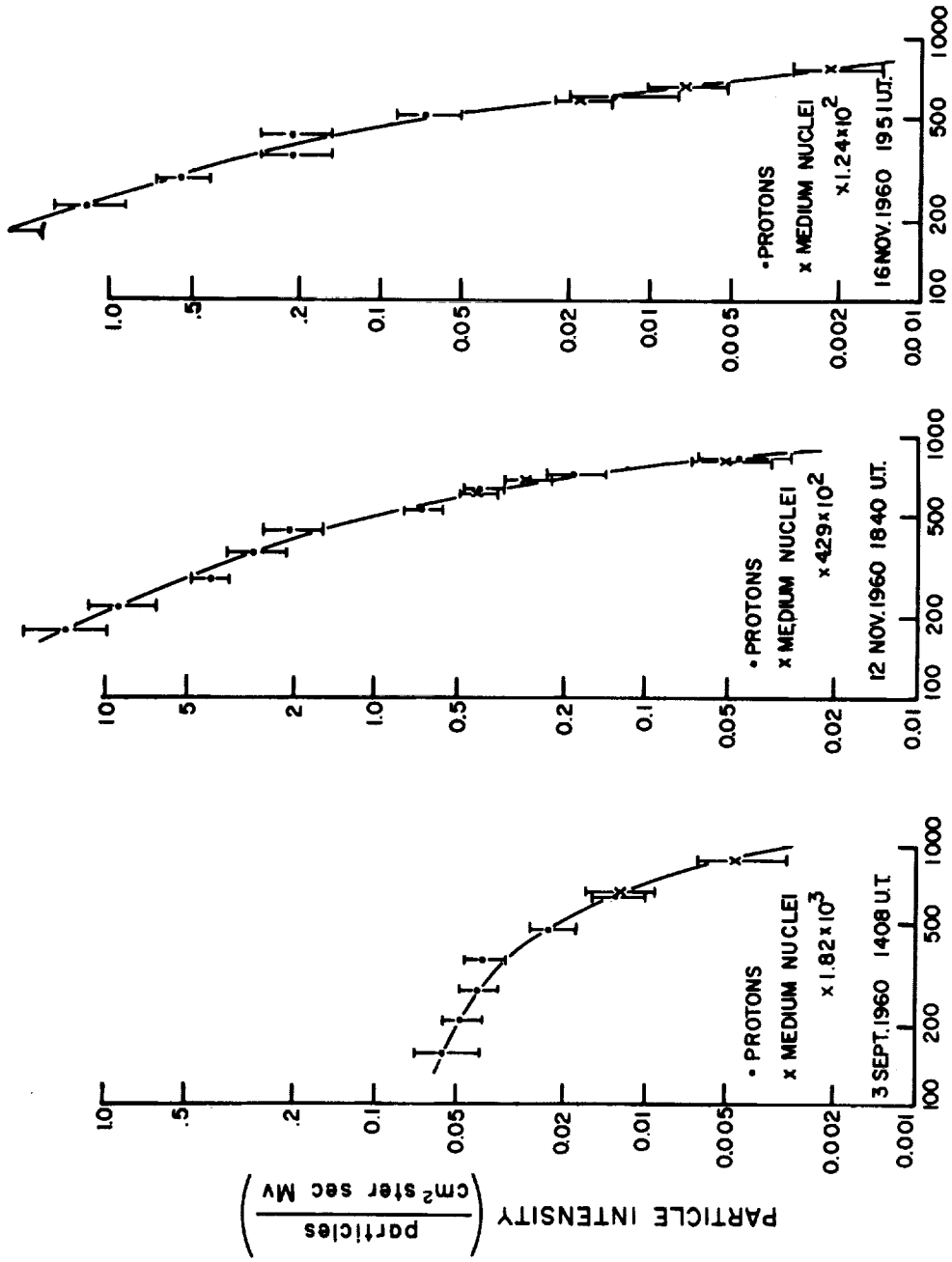

Figure 2 – Comparison of different rigidity spectra for protons and medium nuclei

Table 2

Comparison of Charge Composition of Solar Cosmic Rays, Galactic Cosmic Rays, and the Sun

Source	Abundances (Relative to Carbon)				
	H	Be,B	C	N	O
Galactic Cosmic Rays (Same Rigidity Interval)	2.6×10^3	5	10	$5\lesssim$	6
Sun	20×10^3	10^{-5}	10	2	18
Solar Cosmic Rays (Same Rigidity Interval)	$(2.6 \text{ to } 50) \times 10^3$	$0.5\lesssim$	10	$6\lesssim$	19

than a fraction of a gm/cm² before reaching the emulsion. (There was 0.19 gm/cm² between the emulsion and the ambient radiation in the rocket.) The significance of these results will be discussed in the next section.

DISCUSSION

The detection of heavy nuclei in each of the three solar cosmic ray events investigated with sounding rockets, and the fact that their abundance was an increasing function of the size of the event as measured by the proton flux, indicate that the sun or its surroundings is capable of accelerating heavy ions to tens of Mev per nucleon or higher and probably does so in every major cosmic ray event.

Since carbon, nitrogen, and oxygen have the same charge-to-mass ratio, nearly the same charge, and even similar partial ionization states, their relative abundances should reflect those of that part of the sun from which they came, and indeed Table 2 shows that they do agree with spectroscopic evidence. (Some of the more recent results and a summary of other data can be found in Reference 4.) In fact, the carbon-to-oxygen ratio in the sun is much more uncertain than that in the solar cosmic rays, as determined in this experiment. The observed absence of light nuclei is reasonable on the basis of (1) their very low abundance in the sun where, as a group, they are less abundant than hydrogen by a factor of 10^{-9} or more (Reference 4), and (2) the fact that the solar cosmic rays would not be expected to have gone through even as much as 0.1 gm/cm² in getting to the top of the earth's atmosphere, unless they had done so in an unlikely type of acceleration phase. If we consider the ratio of medium nuclei M to those which have charges of 12 or more,* H , at the same range cutoff in the emulsion, we find that the ratio is always

*The group $Z \geq 12$ was chosen rather than $Z \geq 10$ because there is no special evidence to indicate what the abundance of Ne in the sun is.

equal to or less than that deduced from spectral observation of the sun. This result is reasonable since heavier nuclei of a given energy per nucleon have shorter ranges than medium nuclei, and most models of the acceleration process do not predict favorable acceleration for these larger nuclei even if they are fully ionized — which they may not be.

In summary, the information available thus far indicates that the charge distribution of the heavy nuclei is in agreement with that observed in the sun together with reasonable acceleration and transit models, but is quite different from the galactic cosmic ray spectrum in at least three ways: the light-to-medium ratio, the carbon-to-oxygen ratio which is the inverse of that observed in galactic cosmic rays, and the H/M ratio.

Two interesting features of the medium-to-proton ratios indicate that probably no simple explanation for the characteristics of the heavy component will be found which will apply to all events. These are the large variations of the medium-to-proton ratio from event to event and the fact that, although the differences are much smaller for the same energy/nucleon intervals as opposed to the same rigidity intervals, the heavy nuclei seem to have the same rigidity spectrum as the protons and not the same energy/nucleon spectrum. The variations may be due either to the acceleration phase, the transit and modulation phase of the solar cosmic ray event, or both. In the acceleration phase, they may be due to favorable or unfavorable acceleration of the heavy nuclei, partial ionization, or differences in the source composition. In the second phase, several effects might cause variations. For example, initially similar spectra in each event might then be acted upon by different rigidity-dependent and velocity-dependent diffusion mechanisms. There is now appreciable evidence from the proton results to indicate that the transit phenomena are extremely complex and vary appreciably from event to event.

REFERENCES

1. Tamai, E., "Heavy Nuclei in the Primary Cosmic Rays over Minnesota," Phys. Rev. 117(5):1345-1351, March 1, 1960

2. Aizu, H., Fujimoto, Y., et al., "Heavy Nuclei in the Primary Cosmic Radiation at Prince Albert, Canada. I. Carbon, Nitrogen, and Oxygen," Phys. Rev. 116(2):436-444, October 15, 1959

3. Fichtel, C. E., "The Multiply Charged Component of the Primary Cosmic Radiation at a Low Energy Cut-Off During Solar Maximum," Ph.D. Thesis, Washington Univ., St. Louis, Mo., 1960

4. Goldberg, L., Müller, E. A., and Aller, L. H., "The Abundances of the Elements in the Solar Atmosphere," Astrophys. J. Suppl. 5(45):1-138, November 1960

D-1061

THE FLUX AND ENERGY SPECTRA OF THE PROTONS IN THE INNER VAN ALLEN BELT

by
John E. Naugle* and D. A. Kniffen

On September 19, 1960, a research rocket with a special nose cone developed for the exposure and recovery of emulsions was flown into the northern edge of the inner Van Allen belt along a trajectory which closely corresponded to a magnetic meridian. The payload was designed to permit a 4-inch cylindrical emulsion container to be extended through the front of the nose cone, thereby reducing the amount of material surrounding this container to a minimum. Time resolution of the spectrum was obtained by exposing sections of the cylindrical emulsion stack to the ambient radiation through a port in the tungsten emulsion container. Figure 1 shows the experimental arrangement. The emulsion stack began rotating at lift-off of the rocket at a uniform rate of 0.221 degree/second. Rotating for a total of 1440 seconds, the stack turned through 318 degrees. The emulsion container was extended at an altitude of 173 and retracted at 1100 kilometers. The regions labelled 1 through 8 on the periphery of the stack were each behind the port for approximately 80 seconds. During the rest of the flight they were shielded by 30.6 gm/cm^2 of tungsten. Therefore, the track population in such regions is made up of particles which came in through the port during the 80-second exposure and a background of particles which passed through the tungsten during the remaining 600 seconds the payload was in the radiation belt. The portion of the stack labelled BG, which did not pass behind the port, was used to measure this background. Protons with energies of 8 Mev or more were able to penetrate the aluminum port and be detected, whereas only protons with energies of 145 Mev or more were recorded in the emulsion after passing through the tungsten shield.

Figure 2 is a meridian section containing the trajectory of the rocket payload. The numbered points along the trajectory indicate the locations at which the corresponding sections of the stack were behind the port. Also shown are the lines of magnetic force and the contours of constant counting rate from Explorers IV and VII (Reference 1).

*Now at NASA headquarters, Washington, D. C.

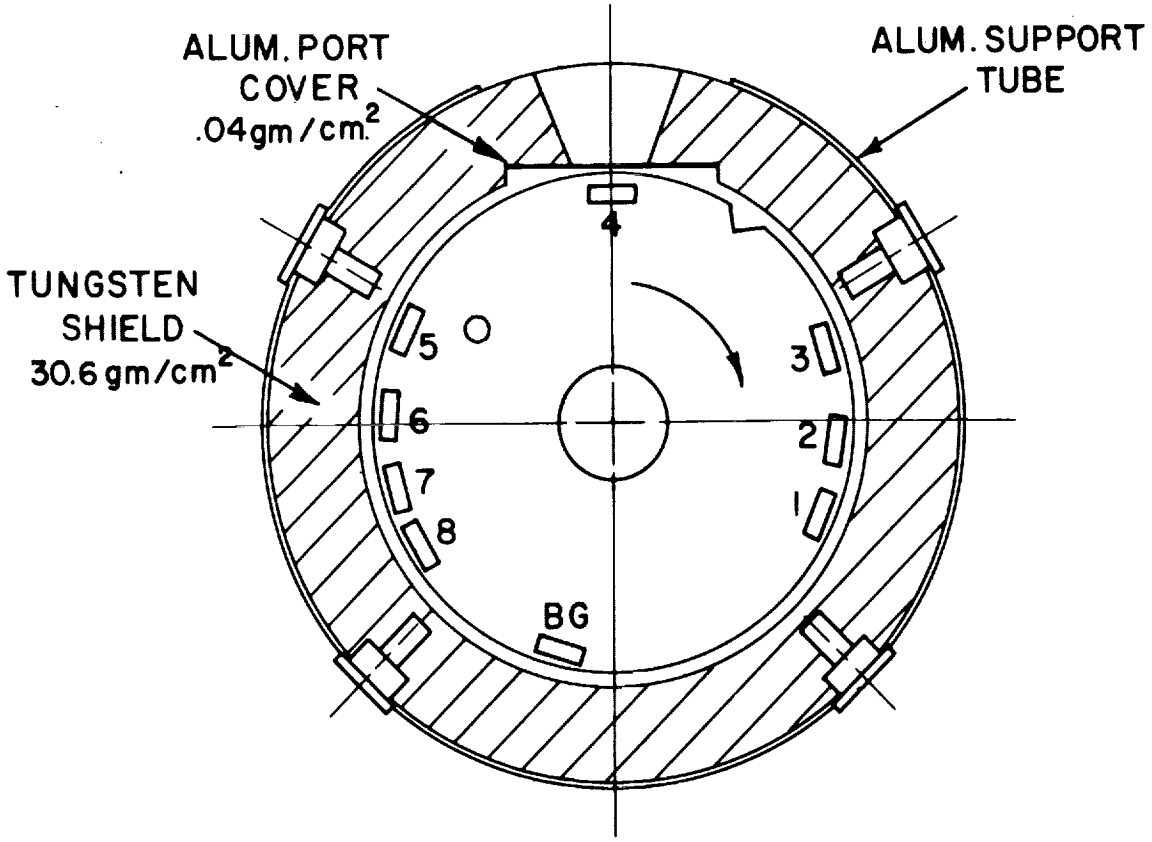

Figure 1 - Experimental arrangement

Table 1 lists the altitude, magnetic field, and geomagnetic latitude at the locations of the measurements. Values of the parameter L, used by McIlwain (private communication) to specify the magnetic shell on which the measurements were made, are also given in Table 1. The angle α_c is the pitch angle, at the equator, of a particle which mirrors at the lower edge of the belt. The angle α_c' is this pitch angle transformed to the location of the measurement. The angle α_0 is the value of the pitch angle of a particle at the equator which mirrors at the location of the measurement. Thus, at a given location only those particles whose pitch angles lie between α_0 and α_c at the equator are accessible to measurement.

The payload and fourth stage were spin-stabilized. After the rocket left the atmosphere, its spin axis remained fixed in inertial space until the payload was despun and separated from the fourth stage just prior to re-entry. By using the trajectory data and a geomagnetic field $\vec{B}$ calculated with the Finch and Leaton coefficients, the angle γ between $\vec{B}$ and the spin axis of the rocket has been calculated. Table I gives the value of this angle γ

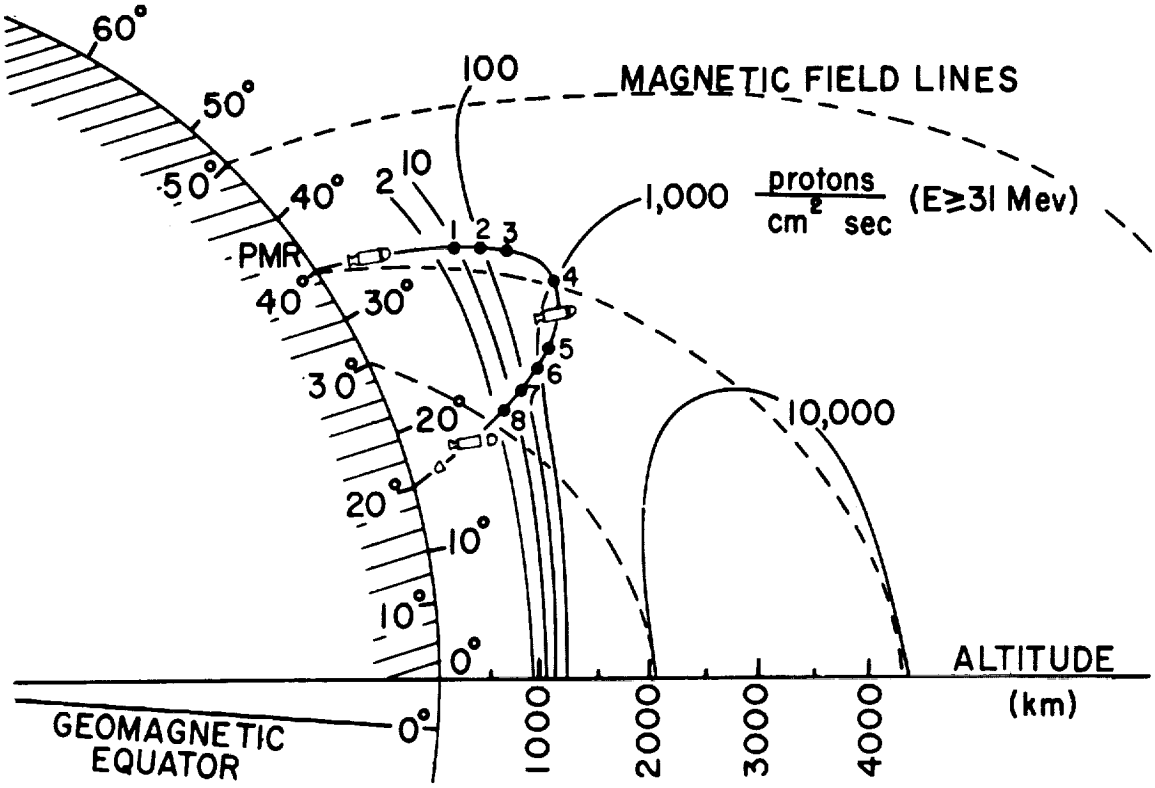

Figure 2 - Meridian section through the rocket trajectory. Dotted lines are magnetic lines of force. Solid lines are contours of constant omnidirectional proton intensity measured by the Iowa group. The numbered points are the locations along the trajectory at which the correspondingly numbered regions of the emulsion were behind the port.

Table 1

Parameters Involved in the Experiment

Location	Altitude (km)	B (Gauss)	λ (degrees)	L (earth radii)	γ (degrees)	α_c (degrees)	α_0' (degrees)	α_c' (degrees)
3	1600	0.231	33.8	1.793	25	26.7	29.0	67.2
4	1884	0.198	30.5	1.722	32	28.5	33.7	59.7
5	1600	0.209	26.5	1.543	40	35.2	39.7	65.2
6	1400	0.223	25.3	1.471	42	39.0	41.5	71.8

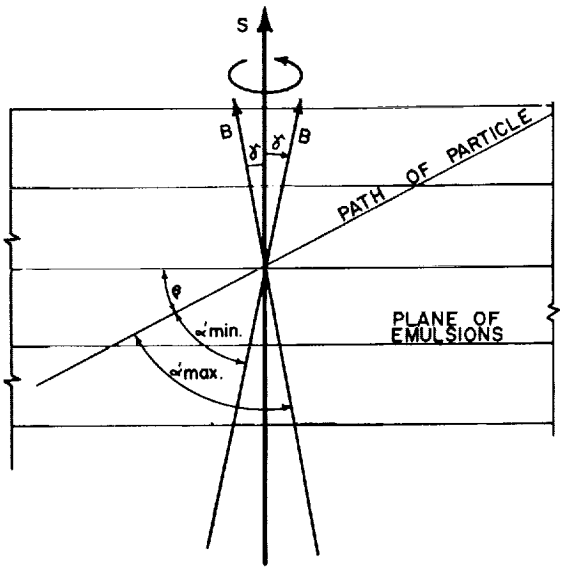

Figure 3 - Schematic diagram showing the relation between the dip angle of the track; the angle γ between the spin axis of the rocket and the magnetic field; and the pitch angle α' of the particle.

for each location. The plane of the emulsions was normal to the spin axis of the rocket.

Figure 3 shows the relation between γ, β (the angle between the track and the plane of the emulsion), and α (the pitch angle). A particle with a given dip angle β in the emulsion may have had a pitch angle α' between $(90° - \beta) \pm \gamma$, depending upon what time during a roll period it entered the emulsion. For large values of γ or β there is a portion of the roll period during which the corresponding value of α' is $\leq \alpha_c'$. The flux values were obtained by assuming that the unidirectional flux was isotropic for $\alpha_c' \leq \alpha' \leq 90°$ and was zero for $\alpha' < \alpha_c'$, and computing the fraction f of a roll period during which the acceptance cone was within the allowed cone of pitch angles. Since this involves a sizeable correction, the value of f is tabulated with the flux.

Line scans have been made at points 3, 4, 5, and 6 (Figure 1). Scans were made approximately 600 microns and 1200 microns from the edge of the emulsions. It was not possible to scan closer than 600 microns to the edge of the emulsion because of blackening. All tracks which, at the scan line, were within ± 45 degrees of the plane of the emulsion and within ± 25 degrees of a radius vector were recorded. The flux at points 1, 2, 7, and 8 was so low that it cannot be distinguished from the background. Therefore, no analysis has been made at these points.

The portion of the emulsion labelled BG, which was not exposed behind the port, was also scanned with the same criteria to obtain an integral flux averaged over the entire flight, and to obtain a background correction for the other sections of the stack.

Preliminary analysis showed that because of the high background it was not possible to detect tracks with blob densities of 30 blobs/100 microns or less (225 Mev protons) at 600 microns from the edge. The efficiency for particles with blob densities of 20 or more (400 Mev protons) at 1200 microns from the edge was found to be 100 percent. The blob density of a track of a particle at minimum ionization in these plates was about 14. Because of the high background and the low minimum blob density, particles at minimum ionization could not reliably be detected. Therefore, only tracks with blob densities greater than 20 have been used in all of the results reported here.

The integral, unidirectional flux $\overline{J(E_t - 400\ \text{Mev})}$ obtained is listed in Table 2, E_c is the energy required for a proton to reach the scan line, assuming that it came through the port. These fluxes have been corrected for the background and the effect of the roll of the rocket. Hence, they are absolute fluxes. The bar over J is to indicate that the flux has been averaged over a range of pitch angles from α_c' to 90 degrees.

In order to measure the differential energy spectrum, the track of every particle in the scan which had a blob density of at least 20 blobs/100 microns and a possible residual range in the emulsion at the scan line of at least 2.5 millimeters was followed until it ended, interacted, or left the stack. The energy and mass of each such particle was then determined from range, ionization, and scattering measurements. The background correction to the differential energy spectrum was made by measuring the density of tracks of a given energy at the scan line in the BG area and subtracting this density from that measured at the scan line at the point being studied. A small correction was also made for those particles which may have come through the edges of the port rather than through the aluminum window.

Rather large corrections to both the differential and integral fluxes were required because the vehicle was spinning and the average orientation of the emulsion relative to the magnetic field changed during the flight.

The differential spectra obtained at points 3, 4, 5 and 6 are shown in Figure 4. These spectra have been corrected for those particles which came in at the edge of the port and have been corrected for roll so that they represent the absolute differential, unidirectional flux $\overline{j(E)}$ averaged over values of α' from α_c' to 90 degrees. The spectra are superposed in Figure 5.

The integral fluxes for $E \geq 96$ and $E \geq 15$ Mev are tabulated in Table 2 and plotted as a function of L in Figure 6. In addition, the integral flux for $E \geq 31$ Mev has been calculated for comparison with the integral omnidirectional flux measured by the Iowa group. The omnidirectional flux J_0 tabulated in Table 2 was obtained by assuming that the observed unidirectional flux was isotropic and integrating over pitch angles from α_c' to 90 degrees. The omnidirectional flux J_0, the satellite data, and the corresponding values of L were kindly furnished by McIlwain (private communication). With the exception of point 6, the agreement with the satellite data is quite good. At point 6 the flux is changing rapidly with altitude and a slight error in altitude could account for the discrepancy.

Four things are apparent from the differential spectra:

(1) At the high latitudes, larger values of L, the slope of the spectrum below 40 Mev is very steep compared to predictions from galactic cosmic ray neutron albedo theory and to measurements at lower geomagnetic latitudes (References 2 and 3).

Table 2

Summary of Results

Location	f	E_c (Mev)	$\overline{J(\geq E_c)}$	E_c	$\overline{J(\alpha', \geq E_c)}$ $\left(\frac{\text{particles}}{\text{cm}^2 \text{ ster sec}}\right)$	E_c	$\overline{J(\alpha', \geq E_c)}$ $\left(\frac{\text{particles}}{\text{cm}^2 \text{ ster sec}}\right)$	$J_0(\geq 31)$ $\left(\frac{\text{particles}}{\text{cm}^2 \text{ ster sec}}\right)$	$J_0^*(\geq 31)$ $\left(\frac{\text{particles}}{\text{cm}^2 \text{ ster sec}}\right)$
3	0.59	17.0	100 ± 20	96	3.4 ± 1.3	31	42	210 ± 50	220
4	0.68	15.5	420 ± 50	96	49 ± 18	31	120	770 ± 140	1000
5	0.48	15.2	390 ± 40	96	200 ± 40	31	370	1480 ± 270	1290
6	0.38	14.2	210 ± 30	96	110 ± 20	31	190	750 ± 100	390
BG	0.58	150	15 ± 1						

J_0^* Omnidirectional flux of particles of energy $\geq$ 31 Mev measured by the Iowa group at the same point (private communication).

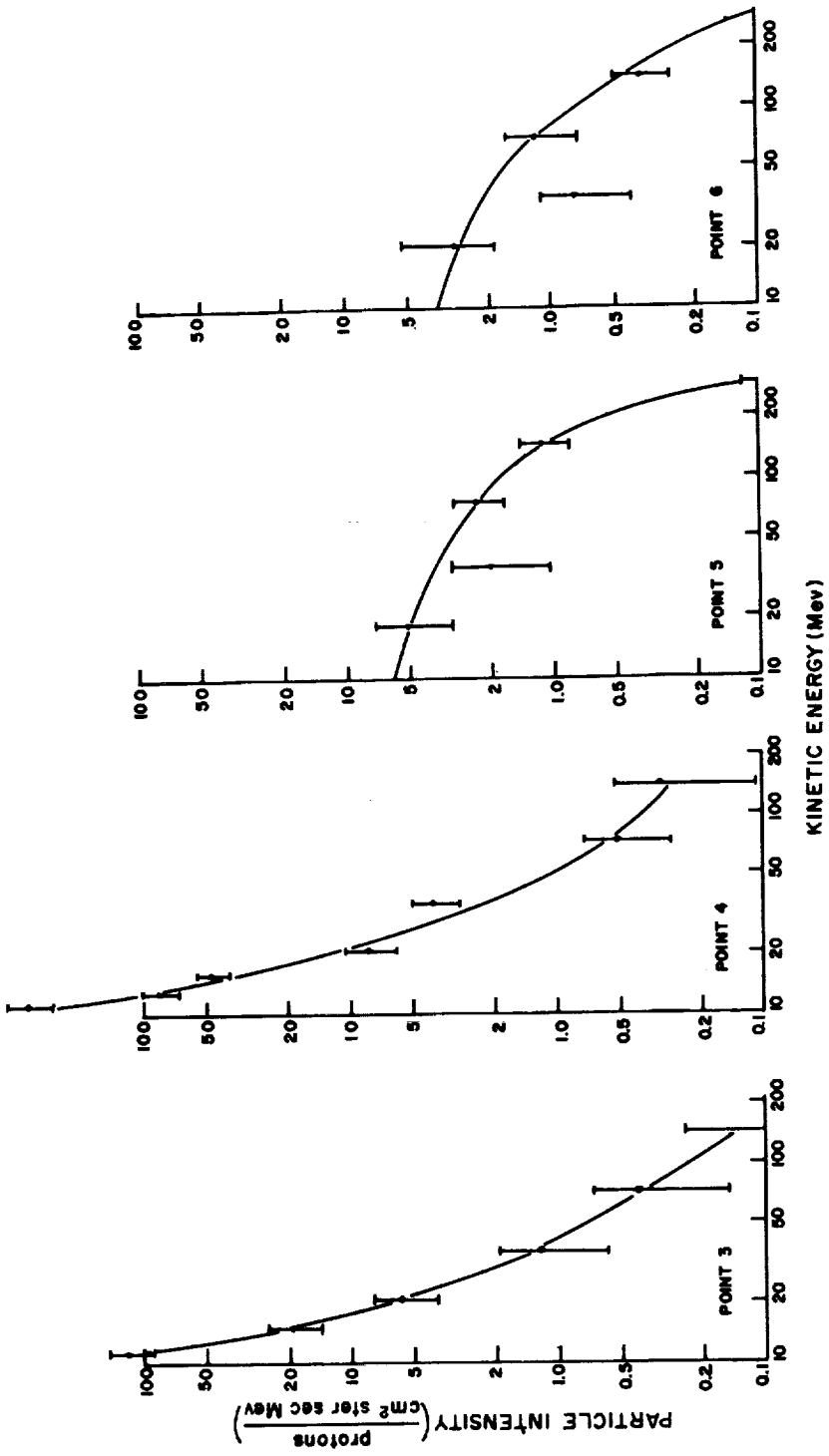

Figure 4 - Differential energy spectra obtained at the four locations

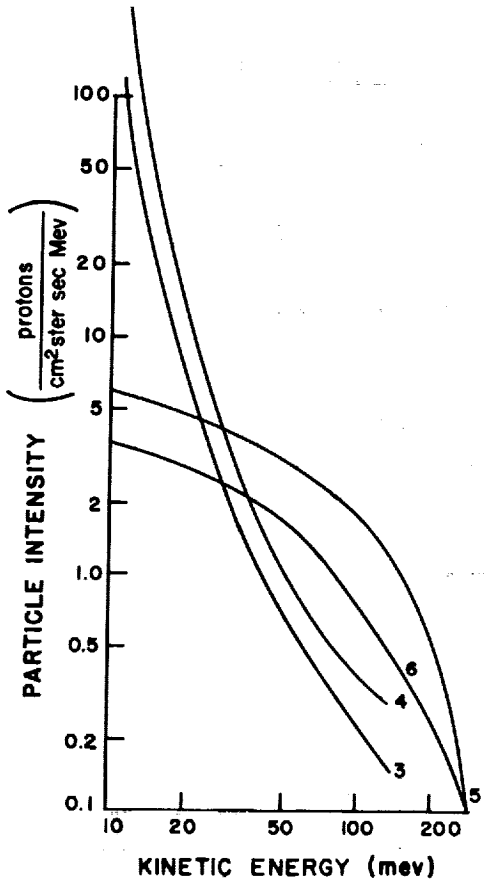

Figure 5 - The spectra superimposed for comparison

(2) The shape of the spectrum, and the unidirectional flux, change with latitude. Points 3 and 5 are at the same altitude and geomagnetic longitude.

(3) At a comparable position in the belt, point 5, the flux and shape of the spectrum agree with the previous data (References 2 and 3).

(4) The particles with $E \geq 96$ Mev decrease as L increases, that is, as we go to lines of force which cross the equator at higher altitudes. Figure 6 shows the variation of the integral flux $\overline{J(E_c)}$ with L for $15 \geq 15$ Mev and for $E \geq 96$ Mev. This plot shows quite clearly that, with higher values of L, not only is there a relative increase in the number of low energy particles, but there is also a relative decrease in the number of high energy particles.

The energy spectrum at low energies and its variation with position cannot be explained by the cosmic ray neutron albedo theory (References 4, 5 and 6). The large numbers of low energy protons at points 3 and 4 most probably result from the decay of neutrons produced in nuclear interactions of solar protons over the polar regions. Changes in the energy spectrum with time have been reported in References 4, 5 and 6, and have been cited as evidence for a component in the belt originating from solar protons. Lenchek and Singer (Reference 7) have discussed in detail the spatial distribution of trapped protons resulting from the interactions of solar flare protons.

The solar proton hypothesis does not explain the loss of the higher energy protons at high L values. Singer (Reference 8) has predicted a loss of high energy particles at higher L values due to the breakdown of the adiabatic invariance of the magnetic moment of the trapped particles. Dragt (Reference 9) and Wentzel (Reference 10) have calculated the effects of hydromagnetic waves on the trapped protons. Singer's theory predicts that the maximum energy which can be trapped varies inversely as the 4th power of the geocentric distance, whereas Dragt's theory predicts that the maximum energy proton which will be trapped varies inversely as the 11th power of the geocentric distance. The variation of the maximum energy which can be trapped has not been measured directly in this experiment. However, Figure 6 shows that the integral flux above 96 Mev falls off very rapidly $(\sim R^{-12})$ with increasing L values.

However, these mechanisms, while they explain the behavior of the spectrum at higher energies, do not explain the absence of low energy protons near the equator. Therefore, it appears that both the effects of solar protons and the loss of high energy particles contribute to and are required to explain the changes in the spectrum with position observed in this experiment.

SUMMARY

It has been shown that the energy spectrum varies in a systematic way depending on the magnetic shell in which the measurement is made. At high values of L (magnetic shells which pass through the outer edge of the inner belt) the spectrum is characterized by large numbers of low energy protons and a relative absence of high energy protons. On the magnetic shells with low values of L (those which pass through the lower edge of the inner belt) the spectrum is characterized by an absence of low energy protons and is flatter.

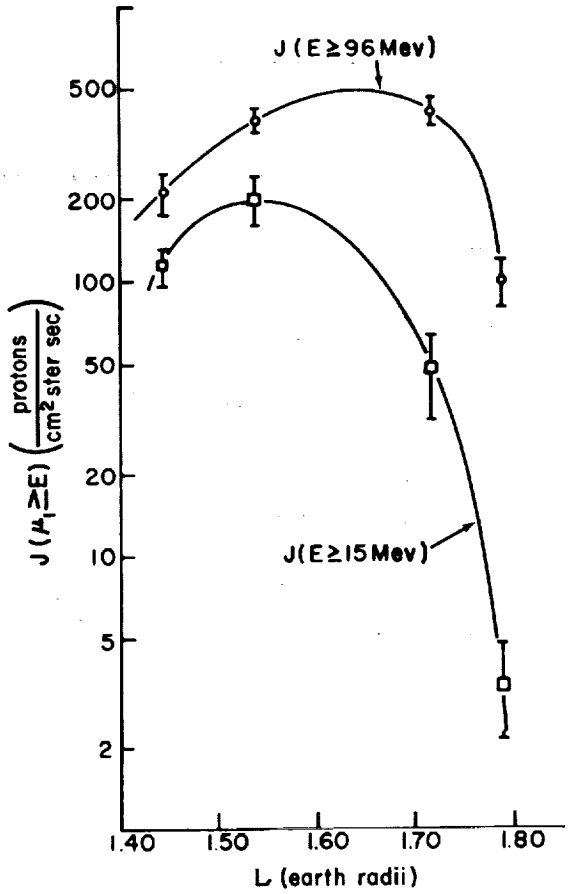

Figure 6 - Variation of the integral flux with L for two values of E, 15 and 96 Mev

REFERENCES

1. Yoshida, S., Ludwig, G. H., and Van Allen, J. A., "Distribution of Trapped Radiation in the Geomagnetic Field," J. Geophys. Res. 65(3):807-813, March 1960

2. Freden, S. C., and White, R. S., "Particle Fluxes in the Inner Radiation Belt," J. Geophys. Res. 65(5):1377-1383, May 1950

3. Armstrong, A. H., Harrison, et al., "Charged Particles in the Inner Van Allen Radiation Belt," J. Geophys. Res. 66(2):351-357, February 1961

4. Singer, S. F., "'Radiation Belt' and Trapped Cosmic-Ray Albedo," Phys. Res. Letters 1(5):171-173, September 1, 1958

5. Singer, S. F., "Trapped Albedo Theory of the Radiation Belt," Phys. Res. Letters 1(5):181-183, September, 1958

6. Hess, W. N., "Van Allen Belt Protons from Cosmic-Ray Neutron Leakage," Phys. Rev. Letters 3(1):11-13, July 1, 1959

7. Lenchek, A. M., Singer, S. F., and Wentworth, R. C., "Geomagnetically Trapped Electrons from Cosmic Ray Albedo Neutrons," J. Geophys. Res. 66(12):4027-4046, December 1961

8. Singer, S. F., "On the Nature and Origin of the Earth's Radiation Belts," in: Space Research; Proc. 1st Internat. Space Sci. Sympos., Nice, January 1960, ed. by H. K. Bijl, Amsterdam: North-Holland Publ. Co., 1960, pp. 797-820

9. Dragt, A. J., "Effect of Hydromagnetic Waves on the Lifetime of Van Allen Radiation Protons," J. Geophys. Res. 66(6):1641-1649, June 1961

10. Wentzel, D. G., "Hydromagnetic Waves and the Trapped Radiation. Part 2. Displacements of the Mirror Points," J. Geophys. Res. 66(2):363-369, February 1961

A STUDY OF THE RIGIDITY AND CHARGE DEPENDENCE OF PRIMARY COSMIC RAY TEMPORAL VARIATIONS*

by

Frank B. McDonald

Goddard Space Flight Center

and

William R. Webber

*Imperial College of Science and Technology, London***

HYDROGEN AND HELIUM COSMIC RAY TIME VARIATIONS

In order to study the cosmic ray temporal variations, the primary cosmic ray energy and charge composition should be monitored as a function of time over a significant portion of the solar cycle. In this first section the studies are limited to the hydrogen and helium component because of the great significance of their different charge-to-mass ratios in defining the form of the various types of modulation.

The experimental flight apparatus is a three element telescope containing a crystal scintillation counter, a lucite Cerenkov counter and a Geiger counter tray. The scintillation crystal and the Geiger counter tray are the defining elements of the telescope. For each particle which traverses these elements, the outputs from the Cerenkov counter and the scintillation counter are recorded. A notation is also made when a telescope event is accompanied by the triggering of more than one counter in the tray or by one of the ring of guard counters. The data are recorded on a continuously moving film with an accurate time base superimposed. These data are then reduced by measuring for each event the pulse height from the scintillation counter and from the Cerenkov counter. The energy calibration is obtained by studying the ionization distribution of highly relativistic alphas or protons (as defined by large pulses from the Cerenkov counter) and measuring the

*The balloon flights from which the data reported here were attained were carried out while the authors were at the State University of Iowa, Department of Physics, Iowa City, Iowa, and were sponsored by the Office of Naval Research.
**Now at the University of Minnesota, Minneapolis, Minnesota.

rate of the most probable energy loss of the alpha particles or protons at minimum ionization, $(E_p)_{min}$. The selected intervals of ionization are then defined in terms of $(E_p)_{min}$. It is necessary to know only the form of the dE/dx vs. energy curve and not its absolute value. The selected intervals of ionization are then related to the corresponding kinetic energy and corrected for energy loss by ionization to the top of the atmosphere.

There are four corrections to be applied to the data in order to deduce an absolute flux at the top of the atmosphere. These are: a general background correction, a correction for the absorption of alpha particles and protons in the telescope and in the atmosphere above the telescope due to nuclear interactions, a delta ray correction, and a correction for the production of alphas in the atmosphere by the fragmentation of primary heavy nuclei. These corrections have been previously described in detail (Reference 1).

With the Cerenkov-scintillator it is observed that charge resolution is maintained independently of particle velocity and the absolute intensity and energy spectrum can be obtained.

The intensity and rigidity spectra of primary protons and alphas have been obtained on a series of Skyhook balloon measurements extending from 1955 to 1959 (References 1, 2, and 3). The measured differential and integral spectra are shown in Figures 1 and 2. The alpha values have been multiplied by a normalizing factor of 6.8. The proton/alpha ratio has been changed from the previously quoted value of 6.5 due to a more complete fragmentation correction. These results were obtained using the Cerenkov-scintillation technique at an average altitude of 5 gm/cm^2.

The results obtained can be summarized as follows:

1. The proton and alphas have the same form of differential rigidity spectrum at solar minimum and maintain the same relative form of rigidity spectrum during the solar cycle.

2. The total intensity is decreased by a factor of approximately 2 from solar minimum to solar maximum and the lower energy particles are affected most but the low energy component is never completely removed.

3. At low energies or rigidities the form of the spectral changes appears to be the same for the 11-year cycle as for the Forbush decreases that we have observed.

In Figures 3 and 4 the differential and integral alpha and proton counting rates have been plotted as a function of Mt. Washington neutron data. Again the alphas have been multiplied by a normalizing factor of 6.8.

These flights occurred under a variety of different conditions including disturbed periods at solar minimum and solar maximum. For a given rigidity, all flux values

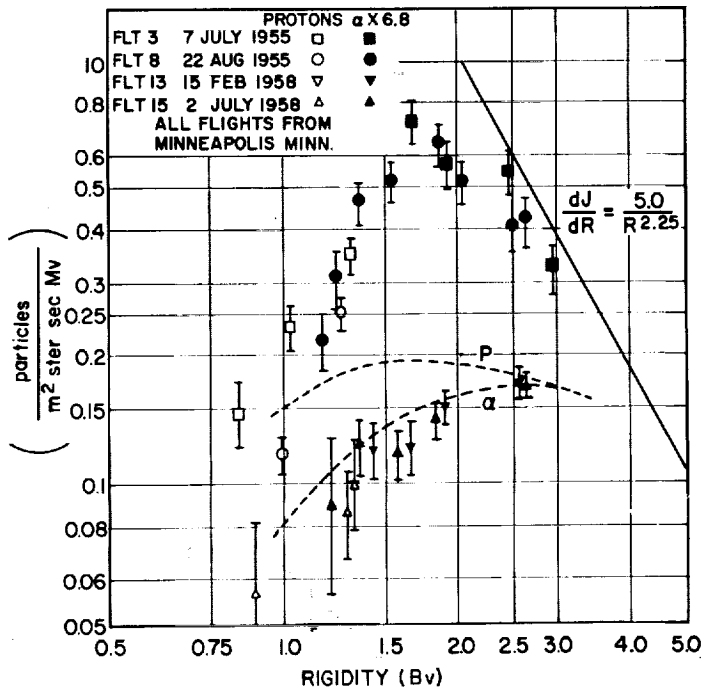

Figure 1 - Proton and alpha differential rigidity spectra. Alpha values have been multiplied by a normalizing factor of 6.8

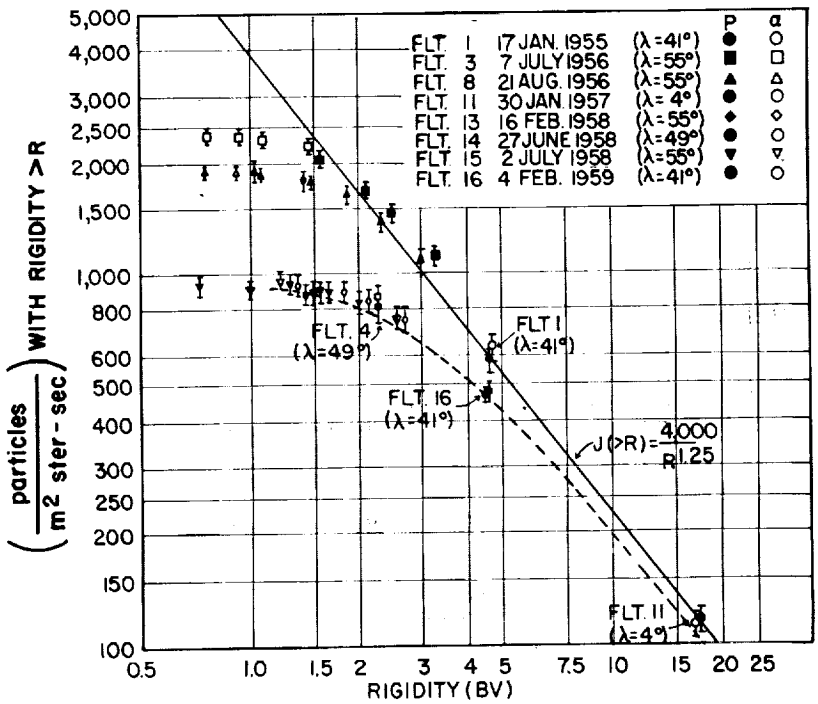

Figure 2 - Integral alpha and proton flux values as a function of rigidity. The alpha values are multiplied by a normalizing factor of 6.8

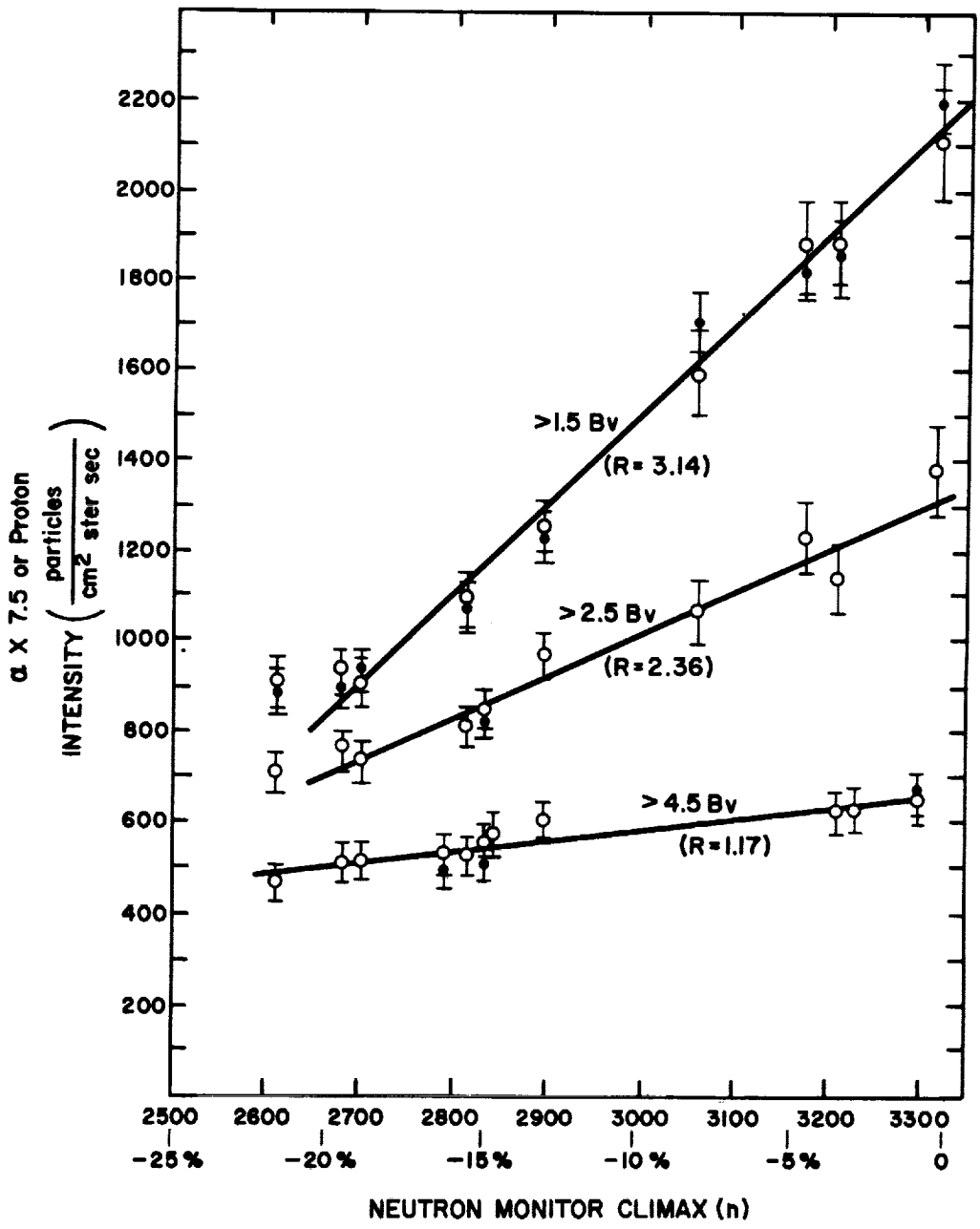

Figure 3 - Integral intensities of protons and alpha particles above 1.5, 2.5, and 4.5 Bv as function of the Mt. Washington Neutron Monitor counting rate. The ratio of changes in the various intensities to those at Mt. Washington are given by R.

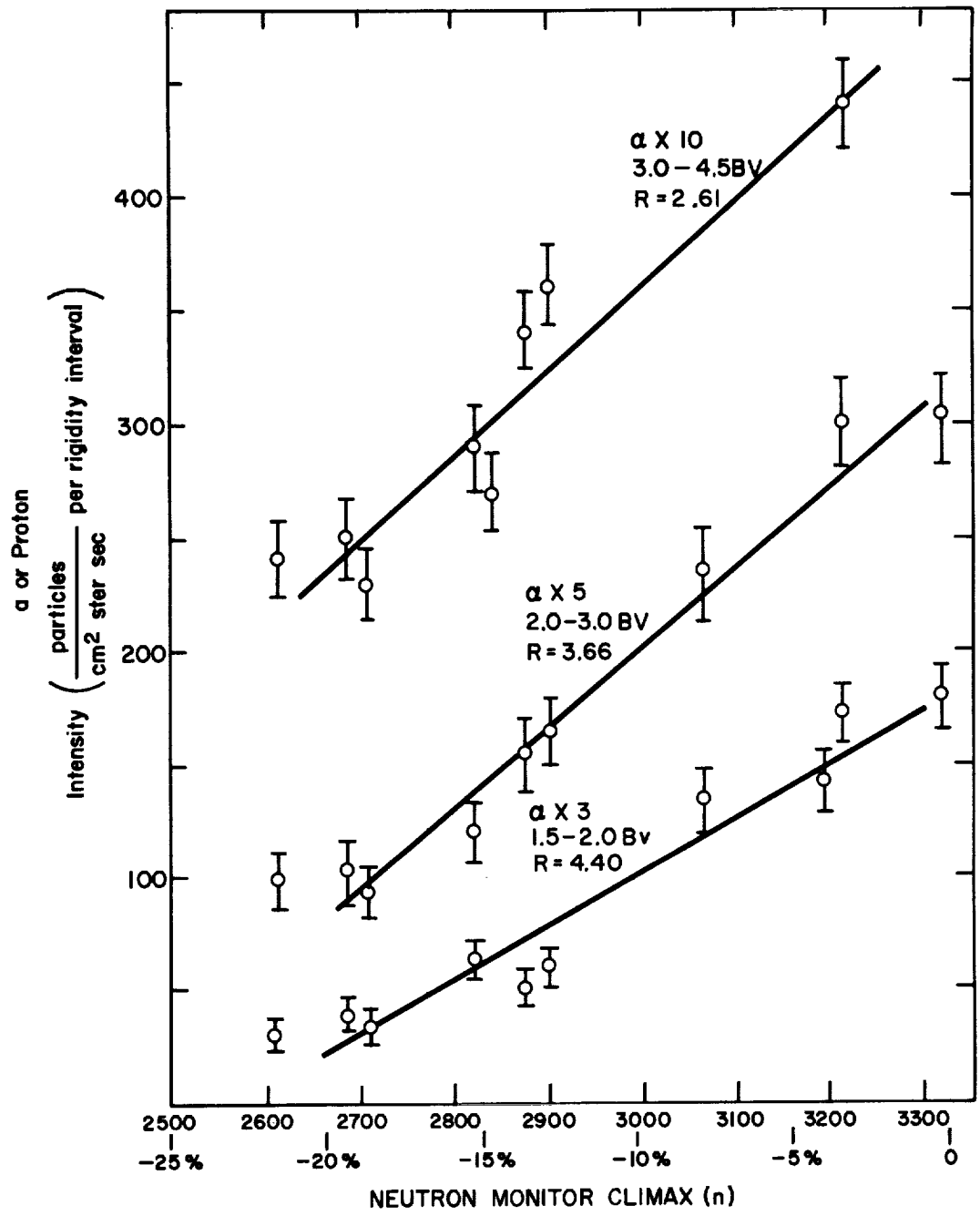

Figure 4 - Differential intensities of protons and alphas from 1.5 to 2.0 Bv and 3.0 to 4.5 Bv plotted as a function of the Mt. Washington Neutron Monitor counting rate. The ratio os changes in the various intensities to that at Mt. Washington are given by R. The α x on each curve indicates the amount both alpha and protons have been displaced for plotting convenience.

appear to be along a single curve. The slope of this curve increases as the rigidity decreases. The fact that the alpha and proton flux values for a given R lie along a single curve strongly reinforces the previous conclusion that the form of the modulation is the same for both the 11-year variation and the Forbush decrease. This type of plot also offers a convenient means of comparing data obtained at different times in the solar cycle by other observers. Such a comparison is given in Figure 5 of the alpha particle data of Frier et al., Meyer, Fichtel, Fowler et al., O'Brien et al., and Duke (References 4 through 11) and Engler (private communication) and the appropriate curve obtained from Figure 4 using the present data. The agreement between all experiments is excellent.

MEASUREMENTS ON LIGHT AND MEDIUM NUCLEI

Measurements on primary cosmic ray nuclei heavier than alpha particles have provided much information helpful in understanding the problem of the acceleration and propagation of the primary cosmic rays to the earth. The flux and energy spectra of the lignt and medium nuclei have been measured on a series of three balloon flights (March 20, 1956, August 17, 1956 and August 1, 1958) extending from a period close to solar minimum to solar maximum. The first two flights employed the Cerenkov-scintillation telescope identical with that used for previously reported proton and alpha measurements (References 1 and 2).

The third flight reported here was made with a somewhat different detector. In this case a second NaI scintillation crystal was used in place of the Geiger counter tray. The two scintillation crystals were then defining elements of the telescope. For each particle three outputs, two scintillation and one Cerenkov were recorded giving in effect a double scintillation Cerenkov detector. A schematic drawing of this detector is shown in Figure 6. The characteristic features of this detector are generally similar to the earlier one; however, the replacement of the Geiger counter tray by the scintillation crystal led to certain notable improvements. These were:

(1) The second scintillator provided a self-consistent check on the charge and energy of the particles, already determined from the relative outputs of the Cerenkov detector and the other scintillation crystal. A comparison of the outputs of the two scintillation crystals gave an additional parameter to check the charge and energy of the particles, namely, the rate of energy loss at two different points on the trajectory.

(2) The second scintillator also reduced the problem of background counts to negligible proportions. Since most of these "confusion" counts were due to interactions or knock-on electrons produced in the material of the detector itself a greater degree of selection for these local events could be made by comparing the two scintillation outputs which reflected ionization loss conditions upon entrance and exit from the detecting system. Only those events which were consistent with single particles traversing the system were used.

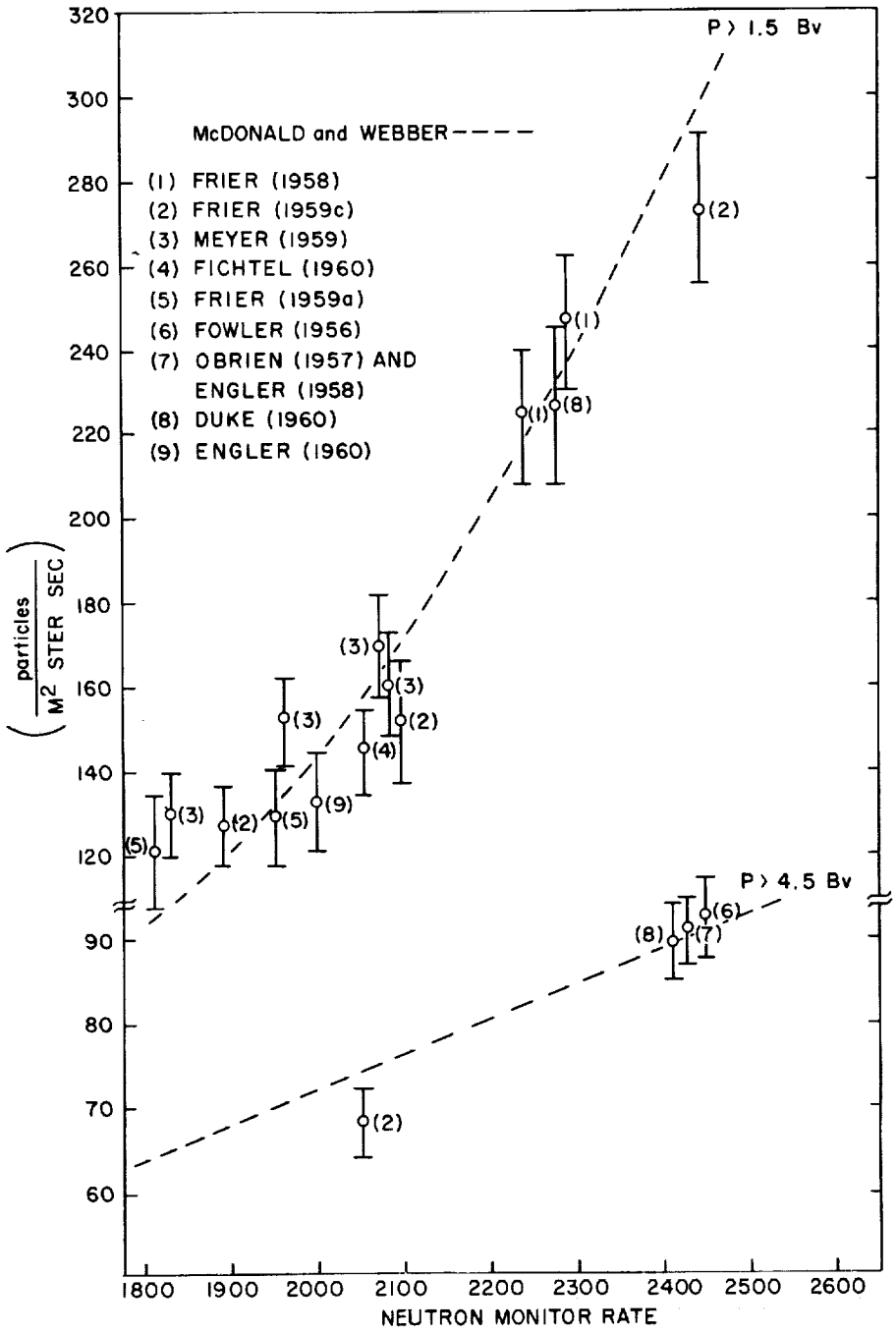

Figure 5 - The variation of integral alpha particle intensities above 1.5 and 4.5 Bv during the period 1954-1959 as measured by various observers. Intensities are shown as a function of the Mt. Washington Neutron Monitor counting rate at the time of the measurement. Results of McDonald and Webber are shown as a dashed curve.

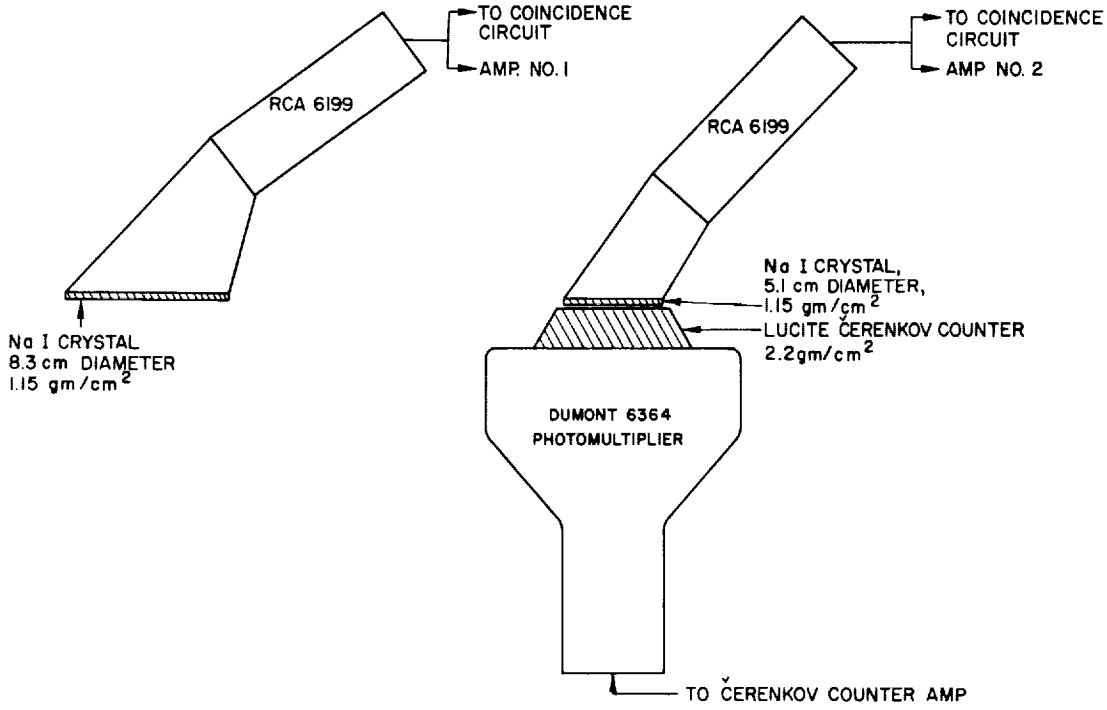

Figure 6 - Double scintillator counter and Cerenkov telescope. For each event the pulse height from all three detectors is recorded

A plot of Cerenkov output vs. ionization loss (Figure 7) indicates the charge resolution which can be obtained with this telescope. The end points of the individual lines represent the two measurements of energy loss of the scintillation counters. The charge resolution achieved here appears to be better than that generally obtained with emulsions.

The absolute flux values, obtained after the corrections for nuclear interactions in the telescope and knock-on electrons, are extrapolated to the top of the atmosphere in the conventional manner using the diffusion equations as introduced by Kaplon, Noon and Racete (Reference 12). The interaction mean free paths and fragmentation probabilities used are those determined by Waddington (Reference 11) in his survey of presently available data on the subject. Energy loss has not been introduced directly into the diffusion equations but instead the energy intervals appropriate to the flight altitude, approximately 6 gm/cm² for each charge group, have been corrected for energy loss to give the equivalent intervals at the top of the atmosphere.

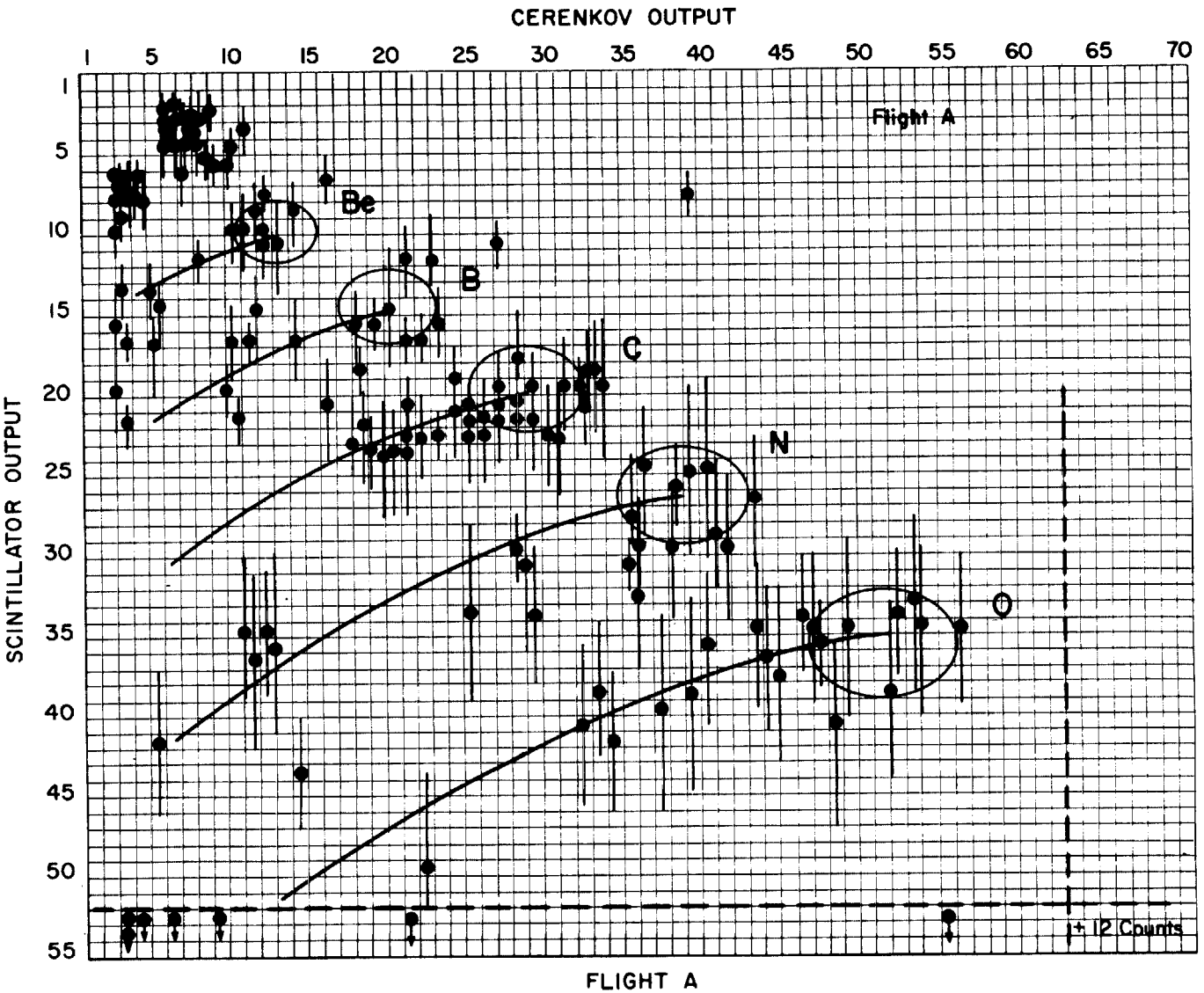

Figure 7 - Plot of Cerenkov pulse heights vs ionization loss in the three element telescope of Figure 6. The end points of the individual lines represent the two measurements of ionization loss. A selection criterion has been applied which demands that the two measurements be within ±20 percent of each other. An appropriate correction for Landau fluctuations is then made.

The relative charge distribution and absolute flux values for the three flights are summarized in Tables 1 and 2. The differential flux values are plotted in Figure 8. In agreement with the previous results obtained for protons and alphas it is concluded that:

(1) The measurements near sunspot minimum established a high degree of similarity in the differential spectra of the various components only when spectra are expressed in terms of the rigidity of the particles.

(2) The solar modulation of intensity appears to be identical for all positively charged particles of the same rigidity.

Table 1

Average Charge Distribution Obtained on Three Balloon Flights

Charge	Counts	Percent of Total Counts
Be	46	6.7
B	70	10.1
C	197	28.6
N	92	13.3
O	123	17.9
Z > 10	114	16.6

The average L/M ratio for the three flights is 0.41 ± 0.06 for particles with energy greater than 1.55 Bev/nuc and 0.43 ± 0.05 for particles with energy greater than 0.41 Bev/nuc. These values are in generally good agreement with those that have been obtained by emulsion techniques. In his survey of all previous determinations using these methods, Waddington (Reference 13) derives a mean L/M ratio of 0.38 ± 0.03 for particles with energy greater than 1.3 Bev/nuc. The more recent L/M determinations of Van Heerden and Judek (Reference 14) of 0.35 ± 0.04 and O'Dell et al. (Reference 15) of 0.36 ± 0.05 for particles with energies greater than 1.5 Bev/nuc, or those of Aizu et al (Reference 16) of 0.41 ± 0.06 and Fichtel (Reference 8) of 0.40 ± 0.08 for particles with energies greater than 0.4 Bev/nuc give a clear indication that there is no longer any substantial uncertainty in this ratio whether it is measured by emulsion techniques or by counter techniques.

A clear difficulty arises, however, in using this ratio to attempt to calculate the amount of interstellar material traversed by the primary radiation. Making the usual assumption that the L nuclei are absent in the source region and that all particles traverse the same amount of interstellar material (one-dimensional diffusion), Hayakawa et al. (Reference 17) have concluded that an L/M ratio of 0.3 implies that the most probable amount of matter traversed was 3 ± 0.5 gm/cm^2. Using more recent values for the

Table 2

Summary of Flux Values

Cosmic Ray Component	Flight 6 - 20 March 1956		Flight 7 - 17 August 1956		Flight 20 - 1 August 1958	
	E > 0.43 Bev/nuc	E > 1.55 Bev/nuc	E > 0.41 Bev/nuc	E > 1.50 Bev/nuc	E > 0.55 Bev/nuc	E > 1.53 Bev/nuc
α	176 ± 6	86 ± 3	225 ± 10	88 ± 5	105 ± 5	12.2 ± 5
L (L, Be, B) $\left(\frac{\text{particles}}{\text{cm}^2\text{-ster-sec}}\right)$	4.8 ± 0.8	2.4 ± 0.5	5.0 ± 0.9	1.5 ± 0.6	2.8 ± 0.5	1.7 ± 0.4
M $\left(\frac{\text{particles}}{\text{cm}^2\text{-ster-sec}}\right)$	10.2 ± 0.9	4.4 ± 0.6	15.3 ± 1.3	6.4 ± 0.9	7.2 ± 0.6	4.1 ± 0.5
$\frac{L}{M}$	0.47 ± 0.07	0.51 ± 0.09	0.31 ± 0.08	0.23 ± 0.06	0.39 ± 0.07	0.42 ± 0.1
$Z \geq 10$ $\left(\frac{\text{particles}}{\text{cm}^2\text{-ster-sec}}\right)$	3.4 ± 0.6		3.8 ± 0.8		1.8 ± 0.4	

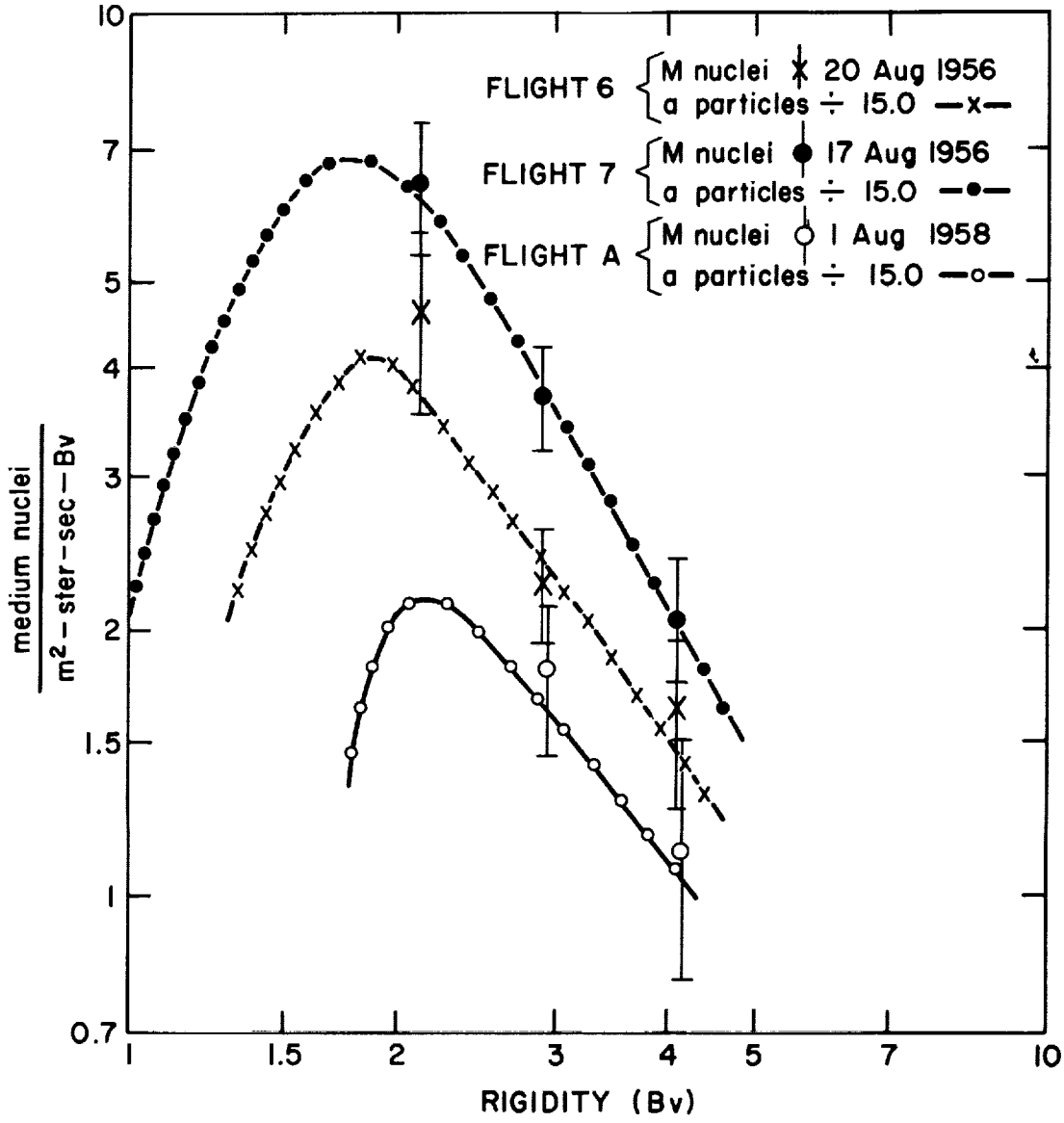

Figure 8 - Measured differential rigidity spectra of medium nuclei. The appropriate alpha particle data divided by 15 are also shown for comparison

fragmentation parameters of the heavier nuclei in hydrogen, Fichtel (Reference 8) arrives at a value of 5 ± 2 gm/cm^2 for a L/M ratio of 0.3. The differences in these values and the uncertainties in the values themselves represent the degree of our uncertainty about the fragmentation parameters for heavy nuclei collisions with interstellar hydrogen.

The flux data on M nuclei from this experiment can be compared with those obtained by others and with the curves obtained here from proton and alpha measurements. Shown in

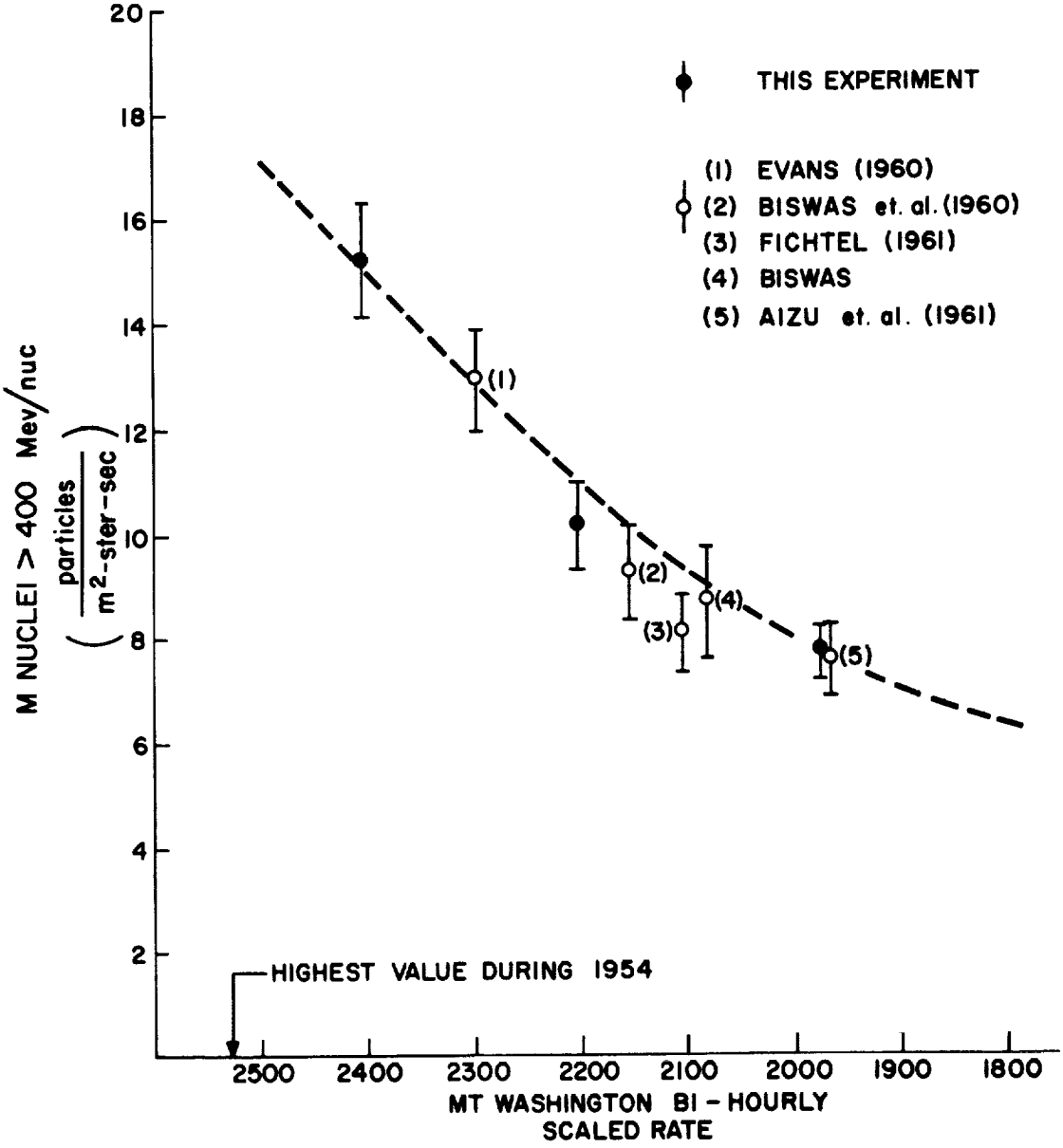

Figure 9 - The variation of integral medium nuclei intensities above 400 Mev/nuc during the period 1956-1959 as measured by various observers. Intensities are shown as a function of the Mt. Washington Neutron Monitor counting rate at the time of the measurements. Alpha particle results of McDonald and Webber divided by 12 are shown as a dotted curve.

Figure 9 are the three integral points (E > 400 Mev/nuc) obtained in this experiment and the emulsion data of Evans (Reference 18), Biswas (References 20 and 21), Fichtel (Reference 8), and Aizu et al. (Reference 16). The dotted line represents the slope of the proton/alpha line shown in the first section of this paper. Again the resulting agreement is excellent.

REFERENCES

1. McDonald, F. B., and Webber, W. R., "Proton Component of the Primary Cosmic Radiation," Phys. Res. 115(1):194-205, July 1, 1959
2. McDonald, F. B., "Primary Cosmic-Ray Intensity near Solar Maximum," Phys. Res. 116(2):462-463, October 15, 1959
3. McDonald, F. B., and Webber, W. R., "Changes in the Low-Rigidity Primary Cosmic Radiation During the Large Forbush Decrease of May 12, 1959," J. Geophys. Res. 65(2):767-770, February 1960
4. Freier, P. S., Ney, E. P., and Fowler, P. H., "Primary α-Particle Intensity at Sunspot Maximum," Nature 181(4619):1319-1321, May 10, 1958
5. Freier, P. S., Ney, E. P., and Winckler, J. R., "Balloon Observation of Solar Cosmic Rays on March 26, 1958," J. Geophys. Res. 64(6):685-688, June 1959
6. Freier, P. S., Ney, E. P., and Waddington, C. J., "Flux and Energy Spectrum of Cosmic-Ray α Particles during Solar Maximum," Phys. Rev. 114(1):365-373, April 1, 1959
7. Meyer, P., "Primary Cosmic-Ray Proton and Alpha-Particle Intensities and Their Variation with Time," Phys. Rev. 115(6):1734-1741, September 15, 1959
8. Fichtel, C. E., "The Multiply Charged Component of the Primary Cosmic Radiation at a Low Energy Cut-Off During Solar Maximum," Ph.D Thesis, Washington Univ., St. Louis, Mo., 1960
9. Fowler, P. H. and Waddington, C. J., "The Energy Distribution of Cosmic Ray Particles over Northern Italy," Phil. Mag. 1(7):637-650, July 1956
10. O'Brien, B. J., and Noon, J. H., "Measurement of the Alpha Particle Flux at 41°N Geomagnetic Latitude Using Nuclear Emulsions," Nuovo Cimento 5(6):1463-1468, June 1, 1957
11. Duke, P. J., "Observations on the Helium Nuclei of the Cosmic Radiation," in: Proc. Internat. Conf. of Cosmic Radiation, Moscow, July 1959, ed. by G. B. Zhdanov, Moscow, 1960, Vol. 3, pp. 89-91
12. Kaplon, M. F., Noon, J. H., and Racette, G. W., "Abundance of Lithium, Beryllium, and Boron in the Primary Cosmic Radiation," Phys. Rev. 96(5):1408-1416, December 1, 1954
13. Waddington, C. J., "The Composition of the Primary Cosmic Radiation," in: Progress in Nuclear Physics, ed. by O. Frisch, New York: Pergamon Press, 1960, Vol. 8, pp. 1-45

14. Van Heerden, I. J., and Judek, B., "The Relative Abundances of Cosmic Ray Nuclei of Charge Z ≥ 3," Can. J. Phys. 38(7):964-967, July 1960

15. O'Dell, F. W., Shapiro, M. M., and Stiller, B., "Abundance Ratio of Lithium, Beryllium, and Boron to the Heavier Primary Nuclei in the Cosmic Radiation," in: Proc. Internat. Conf. of Cosmic Radiation, Moscow, July 1959, ed. by G. B. Zhdanov, Moscow, 1960, Vol. 3, pp. 118-122

16. Aizu, H., Fujimoto, Y., et. al., "Heavy Nuclei in the Primary Cosmic Radiation at Prince Albert, Canada. I. Carbon, Nitrogen, and Oxygen," Phys. Rev. 116(2):436-444, October 15, 1959

_____ "Heavy Nuclei in the Primary Cosmic Radiation at Prince Albert, Canada. II," Phys. Rev. 121(4):1206-1218, February 15, 1961

17. Hayakawa, S., Ito, K., Terrashima, Y., "Origin of Cosmic Rays," Suppl. Prog. Theor. Phys. 6:1-92, 1958

18. Evans, D., "Observations on the Heavy Nuclei of the Cosmic Radiation at Very Low Energies," in: Proc. Internat. Conf. of Cosmic Radiation, Moscow, July 1959, ed. by G. B. Zhdanov, Moscow, 1960, Vol. 3, pp. 92-95

19. Biswas, S., Lavakare, P. J., et al., "The Energy Spectrum of Nuclei with Charge Z ≥ 6 in the Primary Cosmic Radiation," Nuovo Cimento 16(4):644-670, May 16, 1960

20. Biswas, S., "Intensity of Heavy Nuclei (Z ≥ 3) of Cosmic Rays Following a Solar Flare," Bull. Am. Phys. Soc. Ser. II, 5(4):258, April 25, 1960

D-1061

PRESENT STATE OF KNOWLEDGE OF THE COMPOSITION OF THE PRIMARY COSMIC RADIATION

by
C. J. Waddington*

INTRODUCTION

This article summarizes the data on the composition of the primary cosmic radiation reported at this meeting and relates it to that available previously. It is based mainly on a more detailed summary of the earlier data presented at the 1961 Varenna Summer School (Reference 1).

Before considering the experimental data we should discuss, in the most general terms, the significance of the composition to our present concepts of the origins and modes of propagation of the particles of the primary radiation. It is consistent with the experimental evidence to state that among those particles arriving in the vicinity of the earth are examples of all the stable isotopes up to those of iron, and probably those of the heavier elements as well; see, for example, the results reported by Alvial at this conference (Reference 2). The relative abundances of these isotopes are not, in general, well known at this time, and only the crude features of the charge distribution can be discussed with any degree of confidence. However, some attempts have been made to investigate isotopic abundances of a few of the represented elements, and these are discussed by Kaplon in this conference (Reference 2).

The most significant of the general features of the charge distribution appears to be the marked divergence of that observed from that assumed to be typical of the universe as a whole. The reasons for this divergence are thought to be twofold. First, it is assumed that the nuclei which are accelerated in cosmic ray sources are not a representative sample, though it is not clear whether this is due to a preferential acceleration mechanism or to a singularity in the composition of the sources themselves. Second, the nuclei emitted by the sources, from the moment they receive any appreciable suprathermal energies, have to pass through interstellar and source material before they can

*National Academy of Science – NASA Post Doctoral Resident Research Associate; on leave from University of Bristol, Bristol, England

reach the earth. Consequently, because of nuclear interactions, the observed charge distribution is degraded from that existing at or near the source. It is thus of considerable interest to be able to estimate the amount of material traversed and the effect this has had on the charge distribution. Such an estimate can, in principle, be made by looking in the primary cosmic radiation for isotopes or elements which are believed to be extremely rare in the sources. Possible examples are H^2, He^3, the L-nuclei, Li, Be and B, and F. Note, however, that Burbidge and Burbidge have discussed at this conference (Reference 2) evidence that some stars contain an appreciable concentration of He^3 in their atmospheres.

The charge distribution observed in the vicinity of the earth is thus a reflection of the composition of the sources, the mechanism of acceleration, and the traversal of the interstellar and source material.

THE CHARGE DISTRIBUTION ABOVE 4.5 Bv

We shall start by considering the experimental data on the charge distribution of those particles with a rigidity sufficient to permit them to be observed over Texas or Northern Italy, where the geomagnetic threshold is 4.5 Bv.

Hydrogen Nuclei

Intensities of these nuclei have been measured with counters (Reference 3) and emulsions (References 2 and 5) and lead to consistent results. These experiments give a value of the intensity at a time of low solar activity of: $J_{p0} = 610 \pm 30$ hydrogen nuclei/m^2-ster-sec. There is little or no experimental data on the isotopic composition of the hydrogen nuclei, although experiments to investigate this problem have been discussed in the literature (e.g., Reference 6).

Helium Nuclei

The intensity of helium nuclei with $R \geq 4.5$ Bv has been measured by many investigators and the mean value during solar minimum has been calculated to be (Reference 7) $J_{\alpha 0} = 88 \pm 2$ helium nuclei/m^2-ster-sec. It is found (e.g., Reference 8) that the ratio of the intensities of hydrogen and helium nuclei above a given rigidity, $\Gamma_{p\alpha}$ (R), is constant down to at least 1.0 Bv, with a value of 7.0 ± 0.2. It is a result of this constancy that the ratio above a given energy per nucleon, $\Gamma_{p\alpha}$ (E), varies unless $E \gg m_0 c^2$, decreasing with decreasing E. When $E \gg m_0 c^2$, then $\Gamma_{p\alpha}$ (E) = 19.8 ± 1.2, and this is an upper limit to this ratio at any energy.

The ratio above a given *total* kinetic energy, $\Gamma p\alpha$ (U), is derived from $\Gamma_{p\alpha}$ (E) and, when $E \gg m_0 c^2$, has a value 2.48 ± 0.15.

Z ≥ 3 Nuclei

The Ratio of L to S Nuclei, Γ_{LS}

It at last appears that essential agreement has been reached among all major groups working on this problem that there is a finite intensity of L nuclei in the primary cosmic radiation.

The values found in a number of recent experiments performed near the top of the atmosphere for the ratio Γ_{LS} (R,x) of L nuclei to all heavier nuclei, (S nuclei), are shown in Figure 1 as a function of the depth of overlying atmosphere. Included here are the results of O'Dell et al. reported at this conference (Reference 2).* It can be seen that all these experimental results are consistent with a unique growth curve through the atmosphere. This growth curve may be constructed theoretically by using the somewhat uncertain experimental parameters which describe the absorption and production of nuclei in the atmosphere, or directly from the experimental values of Γ_{LS} (x). The first approach is shown on Figure 1 as the dashed curve constructed from the parameters given previously (Reference 7) and arbitrarily normalized to the point W at x = 12 gm/cm^2. This leads to Γ_{LS} (0) = 0.27. The second approach consists of fitting a straight line by the method of least squares and produces the solid line shown in Figure 1. This gives Γ_{LS} (0) = 0.19 ± 0.02. It may be noticed that the difference between these two curves is due almost entirely to one experimental result, that of O'Dell, et al. (Reference 2) and it is therefore entirely reasonable to take as the best value Γ_{LS} (0) = 0.21 ± 0.05, where this error is a 90 percent confidence limit rather than a standard deviation. Results reported by Daniel and Durga Prasad of the Tata Institute at this conference (Reference 2) agree with this conclusion and show that this group also now accept the existence of a finite intensity of L nuclei.

Other experiments bearing on this problem have been reported at this conference by Zhdanov et al. (Reference 2) who used emulsions exposed under 8 to 10 gm/cm^2 of material in a Sputnik and by McDonald and Webber (Reference 2) who flew Cerenkov scintillator arrays at approximately 6 gm/cm^2. In both cases values of Γ_{LS} (x) ≈ 0.3 were reported for R ≳ 4.5 Bv, which, after correction for overlying material, would be quite consistent with the value given above for Γ_{LS} (0).

*The author is indebted to Dr. M. M. Shapiro for communication of these results prior to the conference.

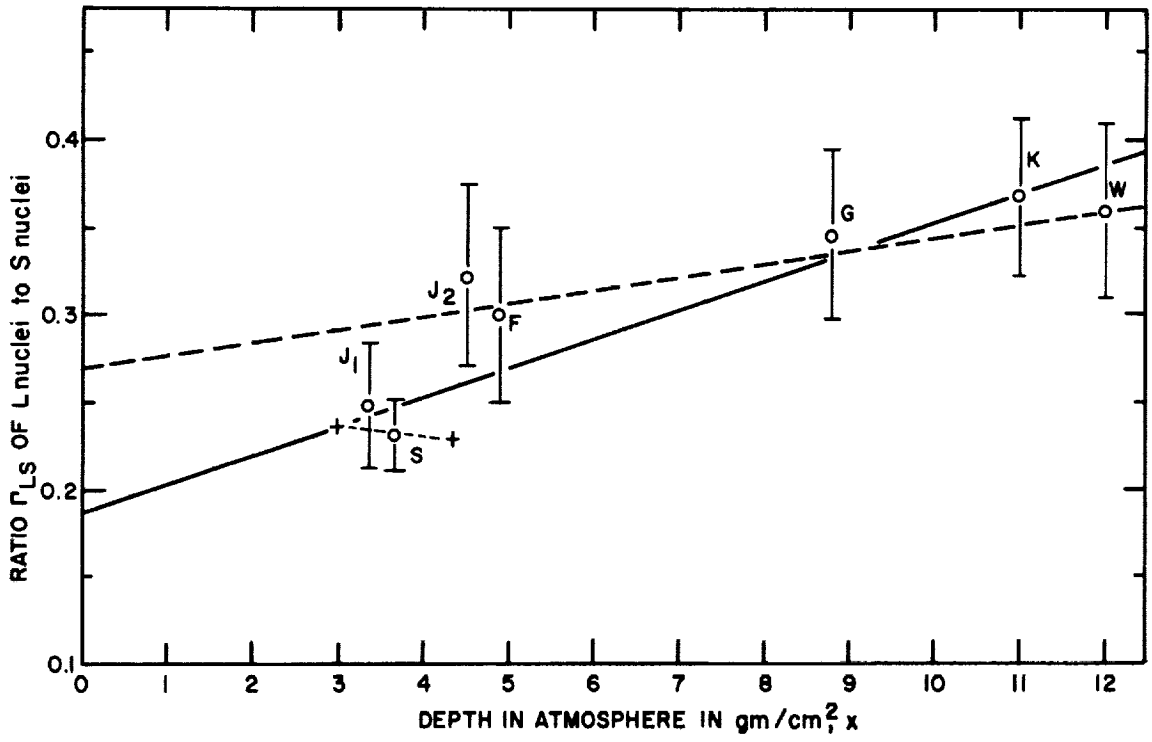

Figure 1 — The ratio of L to S nuclei, Γ_{LS}, as a function of the depth of the atmosphere. Points are: W, Waddington (Reference 9); K, Koshiba et al. (Reference 10); G, Garelli et al. (Reference 11); F, Freier et al. (Reference 12); J_1 ($\theta \leq 30°$) and J_2 ($30° < \theta \leq 60°$), Van Heerden and Judek (Reference 13); and S, O'Dell et al. (Reference 2). Crosses show $\theta \leq 30°$ and $30° < \theta \leq 60°$. The dashed straight line shows the diffusion extrapolation to the top of the atmosphere, normalized to point W; while the solid straight line is the least-squares fit.

Ratio of Heavy to Medium Nuclei, Γ_{HM}

Figure 2 shows results similar to those in Figure 1 but for Γ_{HM} (x), and a similar approach to the determination of Γ_{HM} (0) suggests a best value of 0.34 ± 0.04. This may be compared with the value of 0.30 ± 0.02 reported by Daniel and Durga Prasad at this conference (Reference 2).

Individual Nuclei

The intensities of the individual nuclei are not too well determined at this time, because of the uncertain corrections that must be made for the overlying material. By

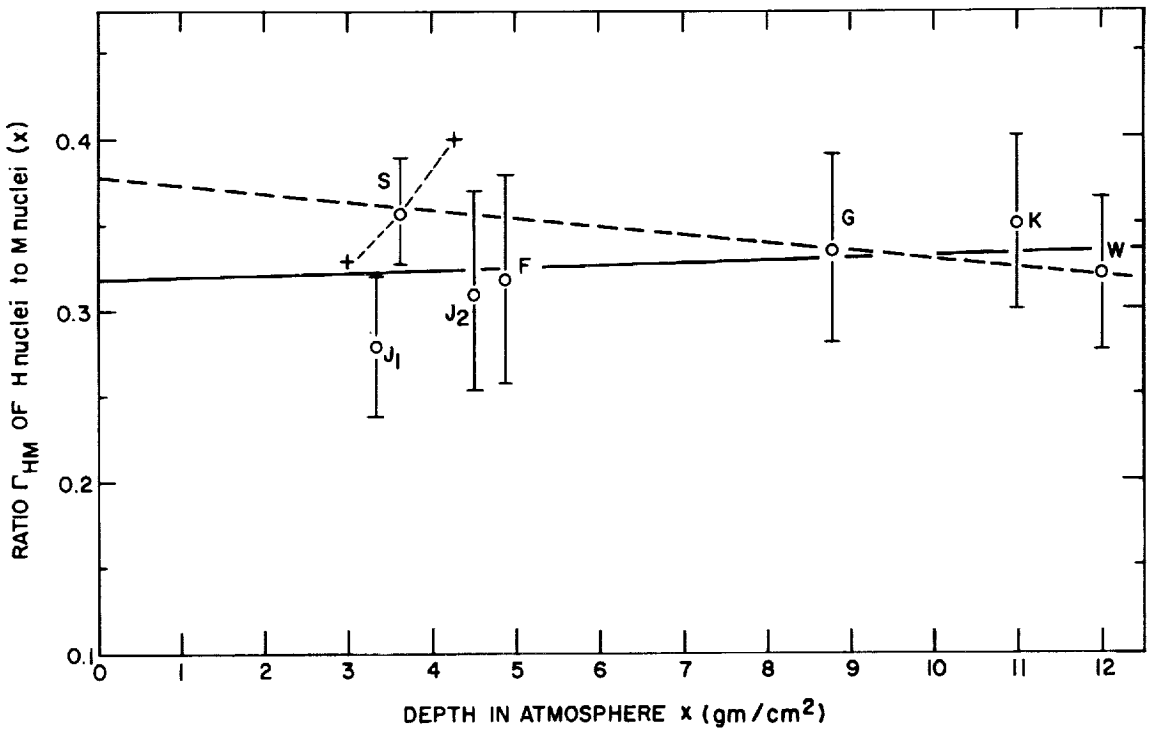

Figure 2 — The ratio of H to M nuclei, Γ_{HM}, as a function of the depth in the atmosphere. Experimental points and lines have the same significance as in Figure 1.

an approach similar to that employed to determine Γ_{LS} and Γ_{HM}, least mean square fits can be obtained for the percentage abundance of individual nuclei (Γ_{iY} values, where Y represents all nuclei with $Z \geq 3$). These values are shown in Table 1 and must have standard errors of between 20 and 30 percent. Also shown in this table are the values reported by McDonald and Webber at this conference (Reference 2) for $R \gtrsim 2$ Bv and $x \approx 6$ gm/cm^2. Apart from the large difference for Be nuclei, which may be due to a rapid production of these nuclei in the atmosphere as is suggested by the least mean squares analysis, the agreement between these two sets of figures is very reasonable. Both illustrate the interesting feature that nitrogen appears to be significantly less abundant than either carbon or oxygen.

For the H nuclei the relative abundances given in Reference 7, while not particularly reliable, do not appear to have been improved on. At this conference the Bombay group

Table 1

Intensities of Individual Nuclei

Element(s)	From Emulsion Data ± 20 - 30% (percentages)	McDonald and Webber (Reference 2) (percentages)
Li	3.9	—
Be	1.7	6.7
B	11.6	10.1
C	26.0	28.6
N	12.4	13.3
O	17.9	17.9
F	2.6	—
$Z \geq 10$	23.9	16.6

have again directed attention to the apparent paucity of elements with $15 \leq Z \leq 19$ which was shown in that review.

Thus, apparently, there begins to be significant evidence for detailed structure in the charge distribution which is hardly compatible with the suggestion that this distribution is the result of fragmentation after a preferential acceleration of heavy nuclei.

Intensities

In order to compare these results with those on the hydrogen and helium nuclei it is necessary to determine the absolute intensities of the various groups. This is made rather difficult by the fact that neither of the two experiments on $Z \geq 3$ nuclei of high statistical weight performed at $x < 5$ gm/cm^2 can be used, because of an uncertainty in the flight time, while the other experiments were performed during different levels of solar activity. However, by using neutron monitor data to establish this level, the published intensity values can be scaled up or down to a standard level. Such a procedure results in values (Reference 1) typical of a period of low solar activity:

$$J_{L^0} = 1.60 \pm 0.40 \text{ nuclei/m}^2\text{-ster-sec},$$

$$J_{M^0} = 5.70 \pm 0.28 \text{ nuclei/m}^2\text{-ster-sec},$$

$$J_{H^0} = 1.94 \pm 0.25 \text{ nuclei/m}^2\text{-ster-sec}.$$

From these intensities, and those given previously for J_{p_0} and J_{α_0}, the various values of $\Gamma_{i\alpha}$ and Γ_{ip} given in Table 2 were calculated. These ratios have been

Table 2

Summary of Calculated Γ Values for the Various Species

Species	$\bar{A}$	$\Gamma_{i\alpha}(R,0)$	$\Gamma_{i\alpha}(E,0)$	$\Gamma_{i\alpha}(U,0)^*$
p	1	7.0 ± 0.2	19.8 ± 1.2*	2.48 ± 0.15
L	9.9	0.018 ± 0.005	0.018 ± 0.005	0.070 ± 0.02
M	14.0	0.065 ± 0.004	0.065 ± 0.004	0.425 ± 0.026
H	30.5	0.022 ± 0.003	0.022 ± 0.003	0.46 ± 0.06
		$\Gamma_{ip}(R,0)$	$\Gamma_{ip}(E,0)$	$\Gamma_{ip}(U,0)^*$
α	4	0.143 ± 0.004	0.050 ± .002	0.45 ± 0.02
L	9.9	0.0026 ± 0.0007	0.00090 ± 0.00003	0.029 ± 0.008
M	14.0	0.0093 ± 0.0006	0.0033 ± 0.0002	0.17 ± 0.01
H	30.5	0.0031 ± 0.0004	0.0011 ± 0.0002	0.19 ± 0.03

*/For $E \gg m_0c^2$

compared in Table 3 with the similar ratios derived for the so-called cosmic abundances of elements in the universe, Φ_{ij}, derived by Suess and Urey (Reference 14), and by Cameron (Reference 15).

CHARGE DISTRIBUTION AT LOW RIGIDITIES

At rigidities below 4.5 Bv, solar modulation of the galactic radiation and solar injection of particles becomes progressively more important. However, it appears that, if injection effects are neglected, $\Gamma_{p\alpha}$ (R) values probably remain constant down to at least R > 1 Bv. Thus a knowledge of the energy spectrum, and hence the rigidity spectrum, of one of these components, permits the calculation of the intensities of the other. In practice, the energy spectrum of the helium nuclei is the best known experimentally. It should be noticed however, that Pomerantz and Witten, as reported at this conference (Reference 2), find that the energy spectrum of the high energy, E > 3.0 Bev/nuc, S nuclei varies quite rapidly over periods of a few weeks. It is not yet established whether the other components show a similar variation, but this observation suggests that it is very dangerous to compare results obtained from experiments made at different times.

At these low rigidities the determination of Γ_{ij} values for $Z \geq 3$ nuclei is experimentally more difficult than at higher rigidities, so that some care is necessary in assessing the value of those experimental results reported thus far. The most extensive results reported are those of the Japanese group, Aizu et al. (Reference 16) and the

Table 3

Comparison of Cosmic Abundances and Cosmic Ray Abundances

Ratios	p	L	M	H	VH
$\Phi_{i\alpha}$ (Suess and Urey)	13.0	$4.7\ 10^{-8}$	$1.03\ 10^{-2}$	$3.6\ 10^{-3}$	$2.3\ 10^{-4}$
$\Phi_{i\alpha}$ (Cameron)	6.6	$3.8\ 10^{-8}$	$9.6\ 10^{-3}$	$8.9\ 10^{-4}$	$4.7\ 10^{-5}$
$\Gamma_{i\alpha}$ (E)	19.8*	$1.8\ 10^{-2}$	$6.5\ 10^{-2}$	$1.6\ 10^{-2}$	$6.0\ 10^{-3}$
	α	L	M	H	VH
Φ_{ip} (Suess and Urey)	$7.7\ 10^{-2}$	$3.6\ 10^{-9}$	$7.9\ 10^{-4}$	$2.8\ 10^{-4}$	$1.8\ 10^{-5}$
Φ_{ip} (Cameron)	$1.5\ 10^{-1}$	$5.7\ 10^{-9}$	$1.5\ 10^{-3}$	$1.3\ 10^{-4}$	$7.1\ 10^{-6}$
Γ_{ip} (E)*	$5.05\ 10^{-2}$	$9.0\ 10^{-4}$	$3.3\ 10^{-3}$	$8.0\ 10^{-4}$	$3.0\ 10^{-4}$

*These values are somewhat doubtful because of the uncertain nature of the proton energy spectrum, and the composition of the α particles, but have been calculated assuming $E \gg m_0 c^2$.

report by Koshiba at this conference (Reference 2). These workers have performed two separate experiments in emulsions flown at very great altitudes, $x \gtrsim 1.5$ gm/cm^2, and have found that Γ_{LM} (E) increases by 20 ± 7 percent for $1.3 \leq R \leq 2.7$ Bv over the value at R > 2.7 Bv, while Γ_{HM} (E) shows an indication of a decrease, although it is hardly statistically significant. They also point out that if the L and M nuclei are assumed to have a distribution of isotopes similar to that in the cosmic abundances (an unlikely assumption) then Γ_{LM} (R) at low rigidities is similar to that at higher values.

These conclusions are supported by the results reported by Zhdanov et al. at this conference (Reference 2) who also find an increase in Γ_{LM} at low rigidities. Further, they are not incompatible with those of McDonald and Webber, who find no difference between Γ_{LM} at R > 4.5 Bv and Γ_{LM} for $2.0 \leq R \leq 4.5$ Bv.

However, it should be noted that the positive evidence for an increase in Γ_{LM} (E) at low energies rests mainly on the results of those experiments reported by Koshiba, and our experience of the controversy on the value of this quantity at higher energies shows that even apparently reliable emulsion experiments can be subject to unsuspected errors. For this reason, it would appear that some caution should be exercised in accepting these results until they have been confirmed by other independent experiments.

Two other components have been detected at these low rigidities which have not been seen at higher rigidities. Meyer and Vogt (Reference 17) and Earl (Reference 18) have both detected evidence for a primary electron flux which is a few percent of the primary nucleon flux above about 0.5 Bev per nucleon. These results were discussed by Meyer at

this conference (Reference 2). Appa Rao (Reference 19) has reported the presence of an appreciable He^3 abundance in the low energy helium nuclei component, finding $He^3/(He^3 + He^4) = 41 \pm 9$ percent for $0.2 \leq E \leq 0.4$ Bev/nuc. Aizu, however, finds evidence that this ratio is only 8 ± 8 percent. The presence of He^3 nuclei to the extent indicated by Appa Rao suggests a traversal of approximately 12 gm/cm^2 of interstellar matter by the producing particles (cf. the 5 gm/cm^2 suggested by the abundance of L nuclei). If this difference is confirmed by further experiments it will provide good evidence for the diffusion model of propagation in interstellar space, in which lighter particles would have a greater average "age."

CHARGE DISTRIBUTION AT HIGH RIGIDITIES

Above 4.5 Bv the experimental data on the chemical distribution are rather sparse, owing principally to the difficulty of obtaining results of significant statistical weight. At $R > 16$ Bv, the Γ_{ij} values appear to be closely similar to those at $R > 4.5$ Bv; see, for example, the work of Neelakantan and Shukla, reported at this conference (Reference 2); while $\Gamma_{p\alpha}$ (R) has been studied up to $R \gtrsim 5.10^3$ Bv and still appears to be constant. Jain et al. (Reference 20) find that the H-nuclei and M-nuclei have the same rigidity spectra at 200 Bv as at lower rigidities. Finally, at very high energies (about 10^{17} ev or more) there is the very interesting observation of the Massachusetts Institute of Technology group, reported here, that the primary particles, judged on a basis of their total kinetic energy, are predominantly lighter or heavier than carbon nuclei; this suggests that the charge distribution has changed appreciably from that observed at lower energies.

REFERENCES

1. Waddington, C. J., "The Primary Cosmic Radiation," Rendiconti della Scuola Internazionale di Fisica "Enrico Fermi" Corso 19, 1961 (To be published)

2. "Proceedings of the International Conference on Cosmic Rays and the Earth Storm," Kyoto, Japan, September 1961, Suppl. J. Phys. Soc. Japan 17, 1962 (To be published)

3. McDonald, F. B., and Webber, W. R., "Proton Component of the Primary Cosmic Radiation," Phys. Rev. 115(1):194-205, July 1, 1959

4. Waddington, C. J., "The Determination of the Flux of Cosmic Ray Protons with Nuclear Emulsions," Phil. Mag. 5(59):1105-1117, November 1960

5. Waddington, C. J., "Hydrogen Nuclei of the Primary Cosmic Radiation," Phil. Mag. 6(68):965-970, August 1961

6. Daniel, R. R., Lavakare, P. J., and Aditya, P. K., "A Method for Detecting the Possible Existence of High Energy Deuterons in the Primary Cosmic Radiation," Nuovo Cimento 17(6):837-844, September 16, 1960

7. Waddington, C. J., "The Composition of the Primary Cosmic Radiation," in: Progress in Nuclear Physics, ed. by O. Frisch, New York: Pergamon Press, 1960, Vol. 8, pp. 1-45

8. Webber, W. R., "Primary Cosmic Radiation," in: Progress in Cosmic Ray Physics, Amsterdam: North-Holland Publ. Co., Vol. 6 (To be published)

9. Waddington, C. J., "The Charge Distribution of Multiply Charged Nuclei in the Primary Cosmic Radiation. Part I: The Light and Medium Nuclei," Phil. Mag. 2(21):1059-1078, September 1957

10. Koshiba, M., Schultz, G., and Schein, M., "The Charge Spectrum of the Cosmic Radiation at 41° N," Nuovo Cimento 9(1):1-16, July 1, 1958

11. Garelli, C. M., Quassiati, B., and Vigone, M., "On the Relative Abundances of Cosmic Ray Nuclei of Charge $Z \geq 3$," Nuovo Cimento 15(1):121-129, January 1, 1960

12. Freier, P. S., Ney, E. P., and Waddington, C. J., "Lithium, Beryllium, and Boron in the Primary Cosmic Radiation," Phys. Rev. 113(3):921-927, February 1, 1959

13. Van Heerden, I. J., and Judek, B., "The Relative Abundances of Cosmic Ray Nuclei of Charge $Z \geq 3$," Can. J. Phys. 38(7):964-967, July 1960

14. Appa Rao, M. V. K., "Isotopic Composition of the Low-Energy Helium Nuclei in the Primary Cosmic Radiation," Phys. Rev. 123(1):295-300, July 1, 1961

15. Cameron, A. G. W., "A Revised Table of Abundances of the Elements," Astrophys. J. 129(3):676-699, May 1959

16. Aizu, H., Fujimoto, Y., et al., "Heavy Nuclei in the Primary Cosmic Radiation at Prince Albert, Canada. II. Phys. Rev. 121(4):1206-1218, February 15, 1961

17. Meyer, P., and Vogt, R., "Electrons in the Primary Cosmic Radiation," Phys. Rev. Letters 6(4):193-196, February 15, 1961

18. Earl, J. A., "Cloud-Chamber Observations of Primary Cosmic-Ray Electrons," Phys. Rev. Letters 6(3):125-128, February 1, 1961

19. Suess, H. E., and Urey, H. C., "Abundances of the Elements," Rev. Mod. Phys. 28(1):53-74, January 1956

20. Jain, P. L., Lohrmann, E., and Teucher, M. W., "Energy Spectrum of the Heavy Nuclei in the Cosmic Radiation between 7- and 100-Bev/Nucleon," Phys. Rev. 115(3):654-659, August 1, 1959

NASA TN D-1061
National Aeronautics and Space Administration.
GODDARD SPACE FLIGHT CENTER CONTRIBUTIONS TO THE 1961 KYOTO CONFERENCE ON COSMIC RAYS AND THE EARTH STORM. June 1962. 98p. OTS price, $2.25.
(NASA TECHNICAL NOTE D-1061)

The international conference on cosmic rays and the earth storm was held at Kyoto, Japan, on September 4-15, 1961. This volume is a compilation of papers presented at this conference by members of the fields and particles group of NASA's Goddard Space Flight Center.

I. NASA TN D-1061

(Initial NASA distribution:
15, Chemistry, physical;
16, Cosmochemistry;
21, Geophysics and geodesy;
30, Physics, atomic and molecular; 31, Physics, nuclear and particle;
33, Physics, theoretical.)

NASA

NASA TN D-1061
National Aeronautics and Space Administration.
GODDARD SPACE FLIGHT CENTER CONTRIBUTIONS TO THE 1961 KYOTO CONFERENCE ON COSMIC RAYS AND THE EARTH STORM. June 1962. 98p. OTS price, $2.25.
(NASA TECHNICAL NOTE D-1061)

The international conference on cosmic rays and the earth storm was held at Kyoto, Japan, on September 4-15, 1961. This volume is a compilation of papers presented at this conference by members of the fields and particles group of NASA's Goddard Space Flight Center.

I. NASA TN D-1061

(Initial NASA distribution:
15, Chemistry, physical;
16, Cosmochemistry;
21, Geophysics and geodesy;
30, Physics, atomic and molecular; 31, Physics, nuclear and particle;
33, Physics, theoretical.)

NASA

NASA TN D-1061
National Aeronautics and Space Administration.
GODDARD SPACE FLIGHT CENTER CONTRIBUTIONS TO THE 1961 KYOTO CONFERENCE ON COSMIC RAYS AND THE EARTH STORM. June 1962. 98p. OTS price, $2.25.
(NASA TECHNICAL NOTE D-1061)

The international conference on cosmic rays and the earth storm was held at Kyoto, Japan, on September 4-15, 1961. This volume is a compilation of papers presented at this conference by members of the fields and particles group of NASA's Goddard Space Flight Center.

I. NASA TN D-1061

(Initial NASA distribution:
15, Chemistry, physical;
16, Cosmochemistry;
21, Geophysics and geodesy;
30, Physics, atomic and molecular; 31, Physics, nuclear and particle;
33, Physics, theoretical.)

NASA

NASA TN D-1061
National Aeronautics and Space Administration.
GODDARD SPACE FLIGHT CENTER CONTRIBUTIONS TO THE 1961 KYOTO CONFERENCE ON COSMIC RAYS AND THE EARTH STORM. June 1962. 98p. OTS price, $2.25.
(NASA TECHNICAL NOTE D-1061)

The international conference on cosmic rays and the earth storm was held at Kyoto, Japan, on September 4-15, 1961. This volume is a compilation of papers presented at this conference by members of the fields and particles group of NASA's Goddard Space Flight Center.

I. NASA TN D-1061

(Initial NASA distribution:
15, Chemistry, physical;
16, Cosmochemistry;
21, Geophysics and geodesy;
30, Physics, atomic and molecular; 31, Physics, nuclear and particle;
33, Physics, theoretical.)

NASA